AFFDL-TR-77-2

VOLUME I

EFFECTS OF UNDERLOADS ON FATIGUE CRACK GROWTH; TECHNICAL SUMMARY

LOCKHEED–GEORGIA COMPANY
MARIETTA, GEORGIA 30063

MARCH 1977

FINAL REPORT JUNE 1975 – MARCH 1977

AIR FORCE FLIGHT DYNAMICS LABORATORY
AIR FORCE WRIGHT AERONAUTICAL LABORATORIES
AIR FORCE SYSTEMS COMMAND
WRIGHT PATTERSON AIR FORCE BASE, OHIO 45433

NOTICE

When Government drawings, specifications, or other data are used for any purpose other than in connection with a definitely related Government procurement operation, the United States Government thereby incurs no responsibility nor any obligation whatsoever; and the fact that the Government may have formulated, furnished, or in any way supplied the said drawings, specifications, or other data, is not to be regarded by implication or otherwise as in any manner licensing the holder or any other person or corporation, or conveying any rights or permission to manufacture, use, or sell any patented invention that may in any way be related thereto.

This report has been reviewed by the Information Office (OI) and is releasable to the National Technical Information Service (NTIS). At NTIS, it will be available to the general public, including foreign nations.

This technical report has been reviewed and is approved for publication.

ROBERT M. ENGLE,
Project Engineer

ROBERT M. BADER, Chief
Structural Integrity Br

FOR THE COMMANDER

HOWARD L. FARMER, Colonel, USAF
Chief, Structural Mechanics Division

Copies of this report should not be returned unless return is required by security considerations, contractual obligations, or notice on a specific document.

SECURITY CLASSIFICATION OF THIS PAGE *(When Data Entered)*

REPORT DOCUMENTATION PAGE		READ INSTRUCTIONS BEFORE COMPLETING FORM
1. REPORT NUMBER AFFDL-TR-77-2, VOLUME I	2. GOVT ACCESSION NO.	3. RECIPIENT'S CATALOG NUMBER
4. TITLE *(and Subtitle)* EFFECTS OF UNDERLOADS ON FATIGUE CRACK GROWTH; Technical Summary		5. TYPE OF REPORT & PERIOD COVERED Final report 20 June 1975 - 20 March 1977 6. PERFORMING ORG. REPORT NUMBER LG77ER0070
7. AUTHOR(s) W. M. McGee, T. M. Hsu		8. CONTRACT OR GRANT NUMBER(s) F33615-75-C-3111
9. PERFORMING ORGANIZATION NAME AND ADDRESS Lockheed-Georgia Company A Division of Lockheed Aircraft Corporation Marietta, Georgia 30063		10. PROGRAM ELEMENT, PROJECT, TASK AREA & WORK UNIT NUMBERS Project No: 486U Task No: 486U02 Work Unit No: 486U0211
11. CONTROLLING OFFICE NAME AND ADDRESS Air Force Flight Dynamics Laboratory (AFFDL/FBE) Wright-Patterson AFB, Ohio 45433		12. REPORT DATE March 1977 13. NUMBER OF PAGES 156
14. MONITORING AGENCY NAME & ADDRESS*(if different from Controlling Office)*		15. SECURITY CLASS. *(of this report)* Unclassified 15a. DECLASSIFICATION/DOWNGRADING SCHEDULE

16. DISTRIBUTION STATEMENT *(of this Report)*

Approved for public release; distribution unlimited.

17. DISTRIBUTION STATEMENT *(of the abstract entered in Block 20, if different from Report)*

18. SUPPLEMENTARY NOTES

19. KEY WORDS *(Continue on reverse side if necessary and identify by block number)*

Fatigue
Crack propagation
Mathematical models
Delay
Overload
Underload
2219-T851 Aluminum

20. ABSTRACT *(Continue on reverse side if necessary and identify by block number)*

The effects of single overload-underload interaction on constant amplitude crack growth in 2219-T851 aluminum alloy are characterized in terms of delay cycles, affected zone sizes and overload shut-off ratios. Data are presented showing the effects of overload-underload/underload-overload sequences, overload magnitude, underload magnitude, and the constant amplitude maximum and minimum. The effects of hold periods in both tension and compression are also experimentally investigated. Delay cycle data are correlated with predictions from three different crack growth retardation models; namely

DD FORM 1 JAN 73 1473 EDITION OF 1 NOV 65 IS OBSOLETE

UNCLASSIFIED

SECURITY CLASSIFICATION OF THIS PAGE *(When Data Entered)*

20. ABSTRACT (Cont'd)

the generalized Wheeler model, the generalized Willenborg model and the Grumman closure model. For each model, predictions are made using an assumed plastic zone radius and diameter for both plane stress and plane strain conditions and model comparisons are made. Correlations of measured affected zone sizes with the four different assumed plastic zone sizes are also presented. Sensitivities of the generalized Wheeler and generalized Willenborg models to overload shut-off ratio and threshold stress intensity factor are determined. Prediction sensitivity to three different crack growth equations for the 2219-T851 aluminum alloy is also evaluated. Recommendations for future work in development of crack growth retardation models are presented.

FOREWORD

Reported herein are results of work performed by the Lockheed-Georgia Company on Contract No. F33615-75-C-3111, "Underload Effects on Spectrum Crack Growth". The effort was sponsored by the Air Force Flight Dynamics Laboratory as part of the "Advanced Metallic Structures - Advanced Development Program" (AMS-ADP), Project No. 486U. Mr. Robert Engle of AFFDL/FBE was the Air Force Project Engineer.

The Lockheed Project Engineer was W. M. McGee of the Structures and Materials Laboratory. Analytical work was performed by Dr. T. M. Hsu. The experimental evaluations were accomplished by F. L. Amend who was assisted by R. I. Prescott and L. T. Reynolds. This is Volume I of the final technical report which summarizes results of the experimental and analytical investigations performed over the period of June 1975 - March 1976.

A second volume, Volume II contains tabulations of experimental data collected on this program and is available on request. Send requests to:

AFFDL/FBE
Attn: R. M. Engle
Wright-Patterson AFB, Ohio 45433

TABLE OF CONTENTS

TABLE OF CONTENTS (Continued)

LIST OF ILLUSTRATIONS

LIST OF ILLUSTRATIONS (Continued)

LIST OF ILLUSTRATIONS (Continued)

LIST OF TABLES

LIST OF TABLES (Continued)

LIST OF SYMBOLS

a	Half crack length for center crack plate, inch.
a^*	Overload affected zone size, inch.
α	Factor in overload interaction zone equation.
B	Specimen thickness, inch.
c	Empirical constants in Grumman equation and Wheeler model.
C_f	Closure factor.
C_H	Empirical constant in Hall equation.
C_w	Empirical constant in Walker equation.
Δa	Increment of crack growth, inch.
ΔK	Constant amplitude stress intensity factor range, KSI $\sqrt{\text{in.}}$
ΔN	Cycle increment.
K	Stress intensity factor, KSI$\sqrt{\text{in.}}$
K_1	Maximum stress intensity factor for tensile overload, KSI$\sqrt{\text{in.}}$
K_2	Stress intensity factor for the constant amplitude maximum, KSI$\sqrt{\text{in.}}$
K_3	Stress intensity factor for the constant amplitude minimum, KSI$\sqrt{\text{in.}}$
K_4	Stress intensity factor for the tensile underload, KSI$\sqrt{\text{in.}}$
K_5	Stress intensity factor for the compressive underload, KSI$\sqrt{\text{in.}}$
K_{max}	Current maximum stress intensity factor, KSI $\sqrt{\text{in.}}$
K_{th}	Threshold stress intensity factor, KSI$\sqrt{\text{in.}}$
K_{max}^{OL}	Stress intensity factor for overload, KSI $\sqrt{\text{in.}}$
K_{max}^*	Stress intensity factor for any given load, KSI $\sqrt{\text{in.}}$
K_c	Closure stress intensity factor, KSI $\sqrt{\text{in.}}$
K_{c2}	Closure stress intensity factor for constant amplitude, KSI $\sqrt{\text{in.}}$
m_H	Empirical constant in Hall equation.
m_W	Empirical constant in Walker equation.
N_D	Number of delay cycles.
n	Empirical constants in Grumman equation and Wheeler model.
n_H	Empirical constant in Hall equation.
n_W	Empirical constant in Walker equation.
P	Applied load, pounds.
q	Empirical constant in Grumman equation.

R	Constant amplitude stress intensity factor ratio.
R_c	Stress ratio cut off value.
S	Overload stress intensity factor ratio.
S_{so}	Overload shut-off ratio.
σ_{ys}	Tensile yield strength, KSI.
t	Hold time, hours.
U	Underload stress intensity factor ratio, K_1/K_4.
U_c	Compressive stress intensity factor ratio, K_1/K_5.
W	Specimen width, inch.
X	Factor designating plane stress or plane strain in overload interaction zone equation.
Y	Factor designating radius or diameter in overload interaction zone equation.
Z_{OL}	Load interaction zone size created by an overload, inch.

SUMMARY

An experimental and analytical investigation was performed to characterize the effects of underloads on crack growth and to evaluate current crack growth retardation models for predicting underload effects. Experimental data in the form of delay cycles and overload affected zone sizes resulting from applications of a single overload and overload combined with underload were obtained for approximately 200 different cases. The cases evaluated represented combinations of load profile classes, stress intensity factor parameters, and stress intensity factor levels. Limited evaluations were also performed to determine effects of hold periods in tension and compression. All experimental work was performed on specimens from a single heat of 2219-T851 aluminum alloy plate.

It was found that underloads following overloads decreased delay cycles and increased the overload shut-off ratio. The decrease was most pronounced for compressive underloads, and when the constant amplitude stress intensity factor ratio, R, was high. Underloads preceeding overloads produced essentially the same results as the equivalent tension-tension loading with the underload truncated. Delay cycles increased as the overload increased and as the constant amplitude minimum increased.

The overload affected zone size also increased as the overload increased, but decreased as the constant amplitude minimum increased. Measured overload affected zone sizes were correlated with overload interaction zone sizes calculated using the radius and diameter assumptions for both plane strain and plane stress conditions. Most of the measured values were between the values computed using the plane strain plastic zone radius and plane stress plastic zone radius.

Delay cycles increased with hold time in tension for times up to 24 hours which represented the longest period evaluated. It was also indicated that holding in tension may decrease the overload shut-off ratio for certain cases. Holding in compression produced a small reduction in delay cycles.

Analytical predictions of delay cycles were made for all cases evaluated experimentally. Predictions were made using three current crack growth retardation models in generalized form; namely the Wheeler model, Willenborg model and the Grumman closure model. For each model, predictions were made using an assumed plastic zone radius and diameter for both plane stress and plane strain conditions. Based on correlations of measured and predicted values, it was found that the best results were achieved by pairing models and overload affected zones as follows:

1) The generalized Wheeler model and the plane strain plastic zone radius.
2) The generalized Willenborg model and the plane stress plastic zone diameter.
3) The closure model and the plane stress plastic zone radius.

A comparison of the three models as paired above revealed that at high overload ratios both the generalized Wheeler and closure models were unconservative while most of the generalized Willenborg model predictions were within a factor of two of measured delay cycles. At low overload ratios, all three models provided reasonable predictions except for the tension-compression load class having high compression load for which the closure model gave the best predictions.

Both the generalized Wheeler and generalized Willenborg models require overload shut-off ratios and threshold stress intensity factor for predictions. Sensitivity of the models to these parameters was evaluated. Sensitivity to threshold was found to increase as overload ratio increased, and sensitivity to shut-off ratio increased as overload ratio decreased. The generalized Willenborg model exhibited the least sensitivity to variances in both parameters. Predictions were also made using three different crack growth rate equations for 2219-T851 aluminum alloy. Generally, there was little difference between predictions for the different equations.

SECTION I
INTRODUCTION

Analytical methodology to predict subcritical crack growth in aerospace structures subjected to complex loading is an essential element in the overall fracture control program currently being applied on fracture critical structures. Current analytical methods for complex loading are not precise; however, considerable effort has, and is, being directed toward a better understanding of the crack growth process. From such efforts will evolve improved analytical modeling of fatigue crack behavior. Within the current state of technology, an unconservative or conservative crack growth prediction is possible depending upon the analysis methodology selected for a particular load profile. Consequently, current methods must be judiciously applied and substantiated by adequate testing. Eventually, unconservatism must be eliminated for reasons of safety and structural life, and over-conservatism must be eliminated since it integrates throughout the entire design process to adversely effect total performance.

It is generally agreed that linear analysis produces acceptable crack growth predictions for constant amplitude loading provided an adequate data base is available, a valid stress intensity factor solution is available, and environmental variations are excluded. The introduction of a high load, however, retards subsequent crack growth to the extent that use of linear analysis without considering load interaction effects is precluded. Considerable data are available characterizing this retardation effect, and several retardation models have been developed for predicting the overload effects on subsequent crack growth rate. Limited data are available which show that this retardation effect is reduced when the high load is followed by a compressive load or underload. The current retardation models account for the beneficial effects produced by overload conditions, but most models do not consider a reduction in these beneficial effects when underloads are included. Further characterization of the underload effect and its interaction with overloads is necessary to identify controlling parameters which will guide future development of analytical methods to more accurately predict crack growth under complex loading.

This program represents an experimental and analytical investigation to characterize crack growth behavior associated with underloads and their interaction with over-

loads. The experimental effort encompassed approximately 200 variables which represented combinations of load profile classes and stress intensity factor parameters. All experimental evaluations were performed on specimens from a single heat of 2219-T851 aluminum alloy plate. Analytical predictions were made for all variables evaluated experimentally. Predictions were made using three current retardation models in generalized form, and these predictions were correlated with the experimental data. Sensitivities of the models to such parameters as overload shut-off ratio, stress intensity factor threshold and overload affected zone size formulations were evaluated.

SECTION II
SCOPE

1. LOAD PROFILES

An experimental program was performed to characterize effects of underloads on crack growth and to provide data with which to correlate retardation model predictions. Experimental data in the form of delay cycles and overload affected zone sizes resulting from application of a single overload, underload, and overload combined with underload were obtained for approximately 200 different cases. The cases evaluated represented combinations of load profile classes, stress intensity factor parameters, and stress intensity factor levels. The load profile classes evaluated are defined in Figure 1 and include (a) tension-tension; (b) tension-zero; (c) zero-tension; (d) tension-compression; and (e) compression-tension. Although the retardation models currently do not account for hold time effects, classes (f) and (g) were included to experimentally evaluate the significance of hold periods. These load classes were illustrated in terms of stress intensity factor, K, since the experimental evaluations were performed under quasi-constant K conditions as described in a subsequent section.

2. STRESS INTENSITY FACTOR PARAMETERS

Generally, the program was designed to systematically determine the effects of the following parameters on subsequent crack growth for each of the load profile classes: (a) the overload stress intensity factor ratio, $S=K_1/K_2$; (b) the constant amplitude stress intensity factor ratio, $R=K_3/K_2$; (c) the maximum of the constant amplitude cycle, K_2; (d) the underload minimum, K_4 or K_5; and (e) the overload-underload and underload-overload sequences. The program was also structured to determine overload shut-off ratios and the effect of underload on shut-off ratio. The stress intensity factor parameters and levels referenced above are defined in Figure 2.

3. BASIC PROGRAM

The basic experimental program was established to provide data for all parameters of interest except variations in K_2 and hold time effects. As shown in Table I all five load profile classes were included which allowed evaluations of underload magnitude effects as well as the overload-underload and underload-overload sequences. K_2 was held constant at 10 KSI$\sqrt{\text{in.}}$ for the basic program, and that value was selected to pro-

vide growth rates in the 10^{-5} to 10^{-6} inch per cycle range for the constant amplitude conditions contained in the basic program. Several values of overload stress intensity factor ratio, S, were included for each of three different constant amplitude stress intensity factor ratios, R=0.1, 0.3 and 0.5. The number of S values for each combination of load profile class and R depended upon the overload shut-off ratio as later discussed under TESTING PROCEDURES. With K_2 constant, the different R values provided variations in ΔK and K_3. Conditions ranging from overload without underload to overload coupled with high compressive underload were provided by varying the underload ratio, U, and compressive underload ratio, U_c.

4. SUPPLEMENTARY PROGRAM

In order to determine K_2 effects, the basic program was supplemented by the K_2=7.78 and 14 KSI$\sqrt{\text{in.}}$ evaluations defined in Tables II and III, respectively. A different R value was assigned to each K_2 such that ΔK was constant at 7 KSI$\sqrt{\text{in.}}$ When combined with the K_2=10 KSI$\sqrt{\text{in.}}$ cases for R=0.3 in the basic program, three different values of K_2 resulted for ΔK constant at 7 KSI$\sqrt{\text{in.}}$ Several values of overload stress intensity factor ratio were included as was done in the basic program. Only four of the five load profile classes were included. The zero-tension class was eliminated since results from the basic program were essentially the same for tension-tension without underload, zero-tension and compression-tension. The more severe compression-tension load profile class, however, was retained to evaluate underload preceeding overload for the different values of K_2.

5. HOLD PERIOD PROGRAM

As shown in Table IV, the tension-tension load profile class was employed to evaluate effects of hold periods in tension at K_1 for times up to 24 hours. Similarly, the tension-compression load profile class was employed to evaluate effects of holding in compression at K_5. The stress intensity factor parameters for each load profile class were selected to provide two different values for each stress intensity factor, K, and to represent cases below the overload shut-off ratio without hold time effects.

SECTION III
EXPERIMENTAL PROGRAM

1. MATERIAL AND SPECIMENS

All experimental evaluations were performed on plates from a single heat of 2219-T851 aluminum alloy. The plates were from the same heat as those used on a previous program, Reference 1, to evaluate crack growth for arbitrary spectrum loading. Basic material characterization tests were performed as part of the previous program, and the results are documented in Reference 1. The plates were 48 inches wide by 72 inches long and had a nominal thickness of 5/8-inch.

Test specimen blanks were machined from six plates, and each blank was uniquely serialized to identify the plate from which it came and its location within the plate as shown in Figure 3. The blanks were then machined to produce six inch wide center crack specimens of the configuration shown in Figure 4. All test section thicknesses were 0.250 inch, and the longitudinal grain was oriented parallel to the loading direction. A 0.5 inch long crack starter slot was placed in the center of each specimen by electrical-discharge-machining (EDM).

2. TESTING PROCEDURES

All testing was performed in two identical electrohydraulic servo controlled test systems. Each system contained the necessary electronic elements properly integrated to provide control of the servo loop, monitor loads and perform failsafe functions. Additionally, each system was interfaced to a digital computer which was used to program the tests as well as store and reduce data. For tests requiring compressive loads, the specimens were fitted with Teflon lined support bars to prevent buckling.

Crack length measurements were made on one surface of the specimens using an optical technique. Measurements were made to within $\pm$ 0.001 inch by microscopically observing the crack tip against a reference grill lightly engraved on the specimen surface. Measurements were made while holding at the constant amplitude mean for the particular test being performed.

Load form was sine wave in all cases, and all constant amplitude cycles were applied at a rate of 12 cycles per second. Overloads were applied at one-quarter cycle per second as well as were underloads. The test area of each specimen was enclosed in a clear acrylic chamber containing dessicant, and testing was subsequently performed at ambient temperature, 70-80 degrees F.

The EDM crack starter slot in each specimen was precracked to produce an initial crack length, 2a, of 1.0 inch. Loads were continually reduced during precracking, and the final loads represented the constant amplitude condition for the particular test to be performed.

3. TEST SYSTEM COMPUTER PROGRAM

Each test system computer was programmed to accept desired stress intensity factor values as input, compute corresponding loads using the stress intensity factor equation for a finite width center cracked plate, and then apply these loads to the specimen. Periodically during test, crack length measurements were made and input to the computer which automatically reduced loads in accordance with the stress intensity factor equation defined as

$$K = \frac{P}{wB}\sqrt{\pi a}\sqrt{\sec\frac{\pi a}{w}} \qquad (1)$$

where P is the far-field applied load; w and B are the specimen width and thickness, respectively; and a is one-half the total crack length. In this manner testing was accomplished under quasi-constant K conditions, and crack length data were updated at intervals necessary to prevent desired K values varying more than one percent.

In addition to controlling the tests, the computers were also used to store, reduce and output data. In performing a particular test, constant amplitude cycling was initially performed using the appropriate R and K_2 values. This was continued while collecting data until it was assured that a constant growth rate had been reached. The desired overload and/or underload cycle was then applied followed by the previously applied constant amplitude condition. During this latter constant amplitude cycling, crack length and cycle data were collected, examined and stored until it was assured that the previous constant amplitude growth rate had been reached. Except for cases producing a large

number of delay cycles and hold time evaluations, at least three repeated tests were usually performed. For these repeated tests, crack length measurements were made at the same cycle increments which allowed crack length data to be averaged. Upon test completion, the stored data were reduced and tabulated by the computer as detailed in Volume II.

For approximately 50 percent of the tests producing delay cycles in excess of 10^5, both crack tips did not always recover at the same rate and an eccentric crack resulted. When this occurred, testing was terminated before the difference in finite width correction factors for the symmetric crack and eccentric crack invalidated quasi-constant K conditions. The resulting data reflect growth history of the one crack tip that had attained constant growth rate. All other data represent the average of both crack tips.

4. RETARDATION PARAMETER DETERMINATION

The experimental data were used to determine the number of delay cycles, N_D, produced by the overload and/or underload cycle and the associated overload affected zone size, a*, defined in Figure 5. Data for a selected case are in Figure 6 which shows change in crack length after overload versus number of cycles after overload for each of three repetitive tests. Also shown in the figure are average data for the three tests. Figure 7 shows incremental $\Delta a/\Delta N$ versus number of cycles after overload derived from the basic data shown in Figure 6. The average $\Delta a/\Delta N$ data were used as an index for determining the retardation parameters, and for the case illustrated N_D was 56,000 cycles. Generally, N_D could be determined from the average data to plus or minus one data interval which was usually either 1000 or 2000 cycles. Figure 8 shows $\Delta a/\Delta N$ versus change in crack length after overload and an a* of 0.014 inch corresponding to the 56,000 delay cycles from Figure 7. Retardation parameter data obtained in this manner are listed in Tables V through XVI for the various load classes and stress intensity factor parameters evaluated during the experimental program. These data are illustrated in Section IV to show effects of the various load classes and stress intensity factor parameters.

5. SHUT-OFF RATIO DETERMINATION

In performing the experimental evaluations, delay cycle and overload affected

zone size data were collected at 0.5 increasing increments of overload ratio. This was continued until crack arrest occurred. Additional tests were then performed at overload ratios within the last 0.5 increment to zero-in on the overload shut-off ratio, S_{so}, to within $\pm$ 0.1. In determining overload shut-off ratio, cycling was performed until it was assured that crack growth rate was less than 10^{-9} inch per cycle which corresponds to threshold growth rate from basic da/dN data[2].

SECTION IV
SUMMARY OF EXPERIMENTAL DATA

1. EFFECTS OF OVERLOADS

In order to provide baseline data for determining underload effects, several tests were performed involving tensile overloads without underloads. The effect of overload on crack growth history is illustrated by the family of curves in Figure 9. These curves show crack extension after overload versus cycles after overload for different values of overload ratio with R constant at 0.1 and K_2 constant at 10 KSI$\sqrt{in.}$ Delay cycles obtained from these data and similar data for R=0.3 and 0.5 are summarized in Figure 10. Delay cycles increased with an increase in overload ratio, S, and also increased as K_3 increased which was equivalent to an increase in the constant amplitude stress intensity ratio, R, and a decrease in ΔK. The overload shut-off ratio, S_{so}, decreased as ΔK became smaller or as R became larger. In this figure, and similar ones to follow, the curves have been drawn to project toward zero delay cycles at S=1.0; however, it is recognized that delay may not exist at an overload ratio greater than one. The overload shut-off ratio points were plotted on the 10^6 cycle line since cycles in the range of 5×10^5 and 10^6 were applied in determining shut-off ratio. Similar data showing the effects of K_2 are summarized in Figure 11 for ΔK constant at 7 KSI$\sqrt{in.}$ Delay cycles increased with an increase in overload ratio, but decreased as K_2 increased. The shut-off ratio increased as K_2 decreased.

2. EFFECTS OF UNDERLOADS

A limited number of tests were performed to determine the effect of a single underload without overload. All tests were performed using tension-tension constant amplitude cycles with tension, zero and compression underloads. No effect on crack growth rate was observed for the cases evaluated. Data obtained for a high compression underload are illustrated in Figure 12 which shows change in crack length after underload versus cycles after underload. Figure 13 shows corresponding $\Delta a/\Delta N$ versus cycles after underload. Growth rate remained essentially constant which was typical for all underload without overload tests.

3. EFFECTS OF UNDERLOAD FOLLOWING OVERLOAD

The effect of underload on decay of retardation due to overload is illustrated

by the family of curves in Figure 14 which shows change in crack length and cycles after overload for K_1, K_2 and K_3 held constant with varying underload. Delay cycles derived from such data are shown in Figure 15 for R constant at 0.1 and K_2 constant at 10 KSI$\sqrt{in.}$ The lower curve represents no underload. A small underload produced no marked effect on delay cycles or shut-off ratio. Underloading into compression produced a relative decrease in delay cycles and an increase in shut-off ratio. Note also that no significant underload effect was shown below an overload ratio of two. Similar data for R constant at 0.3 are shown in Figure 16. There was a trend that tensile and zero underloads decreased delay cycles and increased shut-off ratio, but it could only be positively concluded for the compressive underload. As was observed for the R=0.1 data, there was no positive underload effect at S=2 and below. Data for R constant at 0.5 are shown in Figure 17. At the higher R or lower ΔK, the effect of underloads in reducing delay cycles and increasing overload shut-off ratio was more positive. Also, the effect was evident at lower values of overload ratio. These same trends were observed for K_2=7.78 and 14 KSI$\sqrt{in.}$ data shown in Figures 18 and 19. These two respective figures represent two different R values, 0.1 and 0.5, but a constant ΔK of 7 KSI$\sqrt{in.}$ Data for K_4=0 from these figures along with similar data for K_2=10 are shown in Figure 20 in terms of K_1 and delay cycles. Here the influence of an increasing K_2 coupled with an increasing $K_3 - K_4$ is shown to dramatically decrease delay cycles and increase shut-off ratio. These same data are shown in Figure 21 in terms of overload ratio to demonstrate the ability of overload ratio to normalize the K_2 effect at constant ΔK.

In Figures 18 and 19, the compressive underloads were shown to be approximate values because the tension-compression load class was evaluated in terms of underload ratio, $U_c = K_1/K_5$; consequently, K_5 varied with overload ratio, S. It was found, however, that number of delay cycles was relatively insensitive to magnitude of K_5. This is illustrated in Figure 22 which shows delay cycle variance with overload and underload ratios for K_2=7.78 KSI$\sqrt{in.}$ Similar data are presented in Figure 23 for K_2=14 KSI$\sqrt{in.}$ Shut-off ratio data were not obtained for K_2=14 KSI$\sqrt{in.}$ since K_1 reached K critical before shut-off occurred. The same general results were obtained for tension-compression evaluations in terms of underload ratio at K_2=10 KSI$\sqrt{in.}$ Also, these tension-compression evaluations resulted in K_1 values greater than 30 KSI$\sqrt{in.}$ which produced stable tear and in some cases severe tunneling during the overload cycle. This is subsequently discussed

under FRACTOGRAPHIC EVALUATIONS. Because of those problems evaluations were performed with K_5 constant at -7.5 KSI$\sqrt{in.}$ for the K_2=10 KSI$\sqrt{in.}$ tension-compression load class.

4. EFFECTS OF UNDERLOAD PRECEEDING OVERLOAD

In addition to evaluating underloads following overloads, underloads preceeding overloads as represented by the zero-tension and compression-tension load classes in Figure 1 were also evaluated. Figure 24 shows the compression-tension data along with the overload-underload data for K_2=10 KSI$\sqrt{in.}$ and R=0.1. Delay cycles and shut-off ratio were essentially the same as were obtained for the tension-tension without underload and tension-zero load classes. Only the tension-compression load class showed a significant effect. Similar data for R=0.3, but including the zero-tension load class, are shown in Figure 25. Again no definite difference was observed between tension-tension, tension-zero, zero-tension and compression-tension. A wider variance in shut-off ratio, however, was observed. Figure 26 shows data for R=0.5. At the higher R or lower ΔK; the underload effect of the tension-zero load class became evident, but a positive difference between zero-tension, compression-tension and tension-tension without underload was not present.

Data for K_2=7.78 KSI$\sqrt{in.}$ and R=0.1 are shown in Figure 27. Again the tension-compression effect was apparent, and tension-zero showed a reduction in delay cycles above S=2.5 and an increase in shut-off ratio. The difference between tension-tension without underload and compression tension was not positive. Similar data for K_2=14 KSI $\sqrt{in.}$ and R=0.5 are shown in Figure 28. The same trends were observed, but underload effects associated with tension-zero were evidenced at lower overload ratios. From all data, it was evident that single underloads preceeding overloads produced the same results as the equivalent tension-tension case without underload.

5. OVERLOAD SHUT-OFF RATIO

A summary of the overload shut-off ratio data presented in the previous discussions is presented in Figures 29 and 30. Shut-off ratio variance with K_4 or K_5 are presented in Figure 29 for tension-tension, tension-zero, and tension-compression load profiles. S_{so} is shown to increase as the underload magnitude increases. It is also indicated that S_{so} increases as R decreases. Shut-off was not achieved for K_2=10

and 14 KSI$\sqrt{\text{in.}}$ when followed by high compressive underloads even for values of K_1 exceeding the stable tear threshold.

Similar data are shown in Figure 30 for tension-tension without underload, zero-tension and compression-tension load profiles. Underload preceeding overload produced essentially the same results as tension-tension without underload; however, S_{so} increased as R decreased. In both Figures 29 and 30 there was no distinguishable effect of K_2 variance on overload shut-off ratio. This supports the position of Hillberry[3] that shut-off ratio is independent of K_2.

6. OVERLOAD AFFECTED ZONE SIZE

While effects of the different load classes and stress intensity parameters on delay cycles were of primary interest, the overload affected zone size, a*, was also of interest since the models require an a* definition for delay cycle predictions. It was previously shown that delay cycles increased with an increase in overload ratio for any particular set of conditions. Also, delay cycles increased as R increased corresponding to a decrease in ΔK. The overload affected zone size also increased as overload ratio increased, but decreased as R increased. Figure 31 shows overload affected zone size data and delay cycle data for tension-tension without underload and K_2 constant at 10 KSI$\sqrt{\text{in.}}$ Both N_D and a* increased as overload ratio increased. With overload ratio constant, delay cycles increased as K_3 increased, but a* decreased. Data showing these same trends are shown in Figure 32 for underloading to zero following overload, and in Figure 33 for compressive underload. This K_3 effect on overload affected zone size was the trend throughout the data for all load profile classes and stress intensity factor parameters. A positive influence of underload magnitude on overload affected zone size could not be identified, and there was no significant difference in zone size data for underload preceeding overload and tension-tension without underload. Correlation of overload affected zone size data with values calculated based on different assumptions are contained in a subsequent section.

7. EFFECTS OF HOLD PERIODS

Evaluations were performed to determine the effects of hold times in tension and compression on delay cycles. Two different values for each stress intensity factor: K_1, K_2, K_3, K_4 or K_5, were evaluated for hold times up to 24 hours. Values

for each stress intensity factor were selected to provide delay rather than shut-off based on data for no hold time. The family of growth history curves in Figure 34 illustrates the increase in retardation associated with increasing hold time in tension at K_1. Delay cycle data obtained for hold times in tension are summarized in Figures 35 through 38. In every case a significant increase in delay cycles was observed as hold time at K_1 was increased. There was no indication that stable conditions had been reached at the 24 hours hold period; consequently, a further increase in delay cycles could be expected for longer hold periods. The data in Figure 38 for K_4=5 KSI$\sqrt{\text{in.}}$ indicate that the overload shut-off ratio was being approached at the 24 hour hold time. Delay cycles for K_1=25 KSI$\sqrt{\text{in.}}$ in Figure 35 and for K_2=7.78 KSI$\sqrt{\text{in.}}$ in Figure 36 were also approaching the shut-off range at 24 hours. It would be reasonable to assume that shut-off would have been reached for these cases with a short extension in hold time. Approximately paralleling results were obtained for each value of the same stress intensity factor. The paralleling results in Figure 38 for K_4=5 KSI$\sqrt{\text{in.}}$ or overload without underload and for K_4=1 KSI$\sqrt{\text{in.}}$ representing underloading in tension indicated that underloading after holding in tension had no effect. Although delay cycles increased significantly with hold time, there was no distinguishable effect on overload affected zone size as evidenced by data in Table XV.

Data for hold time in compression are illustrated by the family of crack length versus cycle curves shown in Figure 39. The data indicate a small decrease in delay cycles, and that stable conditions were essentially reached within the first hour. These results were typical for all cases evaluated as shown by the delay cycle versus hold time data in Figures 40 through 43.

8. FRACTOGRAPHIC EVALUATIONS

When evaluating the tension-compression load class for constant values of U_c, K_1/K_5, it was necessary to exceed a K_1 of 30 KSI$\sqrt{\text{in.}}$ Even then the overload shut-off ratio was not obtained for many cases because K_1 was incremented upward until it reached K critical during the overload cycle. As K_1 was increased above 30 KSI$\sqrt{\text{in.}}$ relatively large plastic zones were first observed at the crack tip and branching or deviation from the original crack path during recovery was also observed. These conditions became more severe when K_1 exceeded 35 KSI$\sqrt{\text{in.}}$, and in many cases overload affected zone sizes determined from the crack growth data were considerably larger than the specimen thickness.

The fracture surfaces of several specimens from the tension-compression load class were microscopically examined to classify the crack front geometry for several values of K_I. The photographs in Figure 44 show fracture surfaces containing overloads of 25 and 30 KSI$\sqrt{in.}$ At 10X magnification the 25 KSI$\sqrt{in.}$ overload produced arrest marks on the fracture surface which were hardly detectable. The 30 KSI$\sqrt{in.}$ mark was more pronounced and both crack fronts exhibited a slight curvature.

In Figure 45 similar photographs are shown for K_I=35 and 40 KSI$\sqrt{in.}$ At the 35 KSI$\sqrt{in.}$ overload, the mark was even more pronounced. The 40 KSI$\sqrt{in.}$ overload, however, caused considerable crack extension and the onset of tunneling was evident. Sizeable shear lips were also observed at the specimen surfaces. The tunneling and shear lips are very evident for the K_I=49 KSI$\sqrt{in.}$ case shown in Figure 46. The specimen surface is also shown in this figure to illustrate the deviation of crack path observed. The lines on the specimen surface represent the previously described grill against which crack growth measurements were made. Based on crack growth rate measurements the case illustrated in Figure 46 produced an overload affected zone size of 0.490 inch or approximately twice the specimen thickness.

Based on the fracture surface observations, delay cycle and overload affected zone size data reported for K_I values greater than 35 KSI$\sqrt{in.}$ are considered invalid and of questionable value from a linear elastic fracture mechanics point of view. The questionable cases are limited to data in Tables XII and XIII where K_I exceeded 35 KSI$\sqrt{in.}$ Rather than rationalize data for these cases, additional data were collected with K_5 constant at -7.5 KSI$\sqrt{in.}$ in order to evaluate the tension-compression load class. These data are reported in Table XIV and were contained in several of the previous data illustrations.

SECTION V

ANALYTICAL METHODS

1. SUMMARY

Analytical predictions of delay cycles were made for the same cases evaluated experimentally. In making these predictions four basic elements were required. They were (1) baseline crack growth rate data or crack growth rate equation, (2) stress intensity factor solution, (3) applied load spectrum, and (4) the load-interaction models and their assumed overload affected zones. The accuracy of the fatigue crack growth prediction depends upon the accuracy of all individual elements. A good crack growth retardation model alone does not necessarily guarantee a good prediction. Since we have high confidence in the stress intensity factor solution, Equation (1), for a center cracked specimen; and high precision of load spectrum control, these two parameters offer minimal uncertainty in the predictions. The other two parameters, namely the baseline crack growth equation and the crack growth retardation models and their assumed overload affected zones, play very important roles in prediction of delay cycles. In this section, the crack growth rate equations, retardation model formulations and overload affected zones used in subsequent delay cycle predictions are discussed.

2. CRACK GROWTH RATE EQUATIONS

Three different crack growth rate equations from the literature were employed in making delay cycle predictions with each of the three retardation models. The equations were independently developed for 2219-T851 aluminum alloy and were the Hall[4], Grumman [1] and Walker [5] equations. Each represented slightly different mathematical formulations fitted to basic da/dN versus ΔK data. The specific mathematical formulations employed were as follows:

(1) Hall Crack Growth Rate Equation

Crack growth rate data generated using three stress ratios (R=0.1, 0.3 and 0.5) were fitted using the following equation:

$$\frac{da}{dN} = c_H(K_{max} - K_{th})^{mH}(\Delta K)^{nH} \qquad (2)$$

Values of c_H, m_H and n_H were determined by least square fitting the data by assuming K_{th}=1.5 KSI$\sqrt{in.}$ The computed values were

$$c_H = 0.34 \times 10^{-8}$$
$$m_H = 0.84$$
$$n_H = 2.40$$

(2) Grumman Crack Growth Rate Equation

The data generated for various R ratios were fitted to a modified Elber equation of the form:

$$\frac{da}{dN} = c\left[(1 + q\,R)\,\Delta K\right]^n \qquad (3)$$

A least squares procedure was used to fit the data to the above equation, and the best curve fit produced the following constants:

$$c = 1.96 \times 10^{-9}$$
$$n = 3.34$$
$$q = 0.6$$
$$R_c = 0.5$$

where R_c is the stress ratio cutoff value, i.e., if $R > R_c$, $R = R_c$.

(3) Walker Crack Growth Rate Equation

The Walker equation has the following general form:

$$\frac{da}{dN} = c_W\left[K_{max}(1-R)^{m_W}\right]^{n_W} \qquad (4)$$

When the data were fitted to this equation the following constants were obtained:

$$c_W = 1.72 \times 10^{-9}$$
$$m_W = 0.3014$$
$$n_W = 3.415$$

The unit for the stress intensity factor is KSI$\sqrt{in.}$, and the crack growth rate is inch/cycle.

In order to understand the trends those equations predicted, the da/dN vs. ΔK computed using the three equations were plotted in Figures 47 to 49 for R=0.1, 0.3 and 0.5, respectively. As seen from those figures, for $\Delta K > 3$ KSI$\sqrt{in.}$, the

difference in growth rate between the Hall and Grumman equations was negligible for all three R values. But, when ΔK is less than 3 KSI $\sqrt{in.}$, such difference becomes more significant. The smaller the ΔK, the larger the difference in growth rate, and the difference decreases as R increases. The primary reason for the difference is that the Hall equation is anchored by a threshold value. The Walker equation matched the Grumman equation very well for R=0.1; however, when R increases, the growth rate predicted by the Walker equation becomes much higher than that of the Grumman. However, when R ratio is less than 0.1, the rate computed using the Hall equation becomes larger than those computed using the Grumman and Walker equations. Figure 50 shows the relationship between da/dN and ΔK for R= -0.3. As seen from this figure, when ΔK is greater than 3 KSI $\sqrt{in.}$, the growth rate computed using the Hall equation is higher than those computed using the Grumman and Walker equations.

3. RETARDATION MODELS

It is well known that normal crack growth rate under constant amplitude loading changes if the load application is preceded by a loading of different amplitude. A tensile overload produces permanent plastic deformation at the crack tip which delays the crack growth of subsequent low load cycles. The beneficial effect of tensile overloads in extending crack life, however, may be altered if overloads are coupled with underloads. Current analytical models deal with the decay of this beneficial effect as a function of crack tip progress through an "overload affected zone". In order to evaluate the ability of current models to predict underload effects, delay cycle predictions were made for the same cases evaluated experimentally. Predictions were made using three different retardation models: (1) generalized Wheeler model[6], (2) generalized Willenborg model[7], and (3) Grumman closure model[1]. Formulations of the three aforementioned crack growth retardation models are presented and discussed in Appendix A.

4. OVERLOAD AFFECTED ZONE

The overload affected zone, a*, due to the application of the overload is defined as the distance ahead of the crack tip, over which the reduction in fatigue crack growth rate from that of constant amplitude loading is observed. To date,

this zone has been characterized by the plastic zone size created by the overload cycle. The Wheeler model relates a* to the plane strain plastic zone radius while the Willenborg and closure models estimate a* as a function of the plane stress plastic zone radius. Some other investigators, e.g., Probst[3], Von Euw[8], utilized variations of the overload created plastic zone diameter (depending upon the fraction of the cross section exhibiting shear lips) to achieve good correlation with measured overload affected zone.

All three retardation models predict a return to steady state (constant amplitude) crack growth rate subsequent to the application of the overload as soon as the total crack growth increment since the application of the overload equals the overload affected zone, i.e., $\Delta a=a^*$. If the condition is expressed in terms of the stress intensity factor, then the generalized Wheeler and Willenborg models predict the termination of retardation effect due to overload when K^*_{max} and K_{max} are equal. K^*_{max} is the effective stress intensity factor after overload and K_{max} is the stress intensity factor of the constant amplitude maximum. The generalized closure model will predict the same thing when K_{c2} and K_c are equal. K_{c2} being closure stress intensity factor for constant amplitude and K_c is the effective closure stress intensity factor after overload. The overload affected crack length can be determined from the condition $K^*_{max}=K_{max}$ which results in the following equation[9]

$$a^* = z_{OL}\left[1-\left(\frac{K_{max}}{K^{OL}_{max}}\right)^2\right] \qquad (5)$$

For the generalized closure model

$$a^* = z_{OL} \qquad (6)$$

where z_{OL}, defined earlier as the overload created load interaction zone, has the following general form[9]:

$$z_{OL} = \alpha\left(\frac{K^{OL}_{max}}{\sigma_{ys}}\right)^2 \qquad (7)$$

The factor α can be expressed in the following general form[3]:

$$\alpha = \frac{1}{2X + 4\sqrt{2}\ (1 - X)} \cdot \frac{Y}{\pi} \qquad (8)$$

where X represents the fraction of the cross section exhibiting shear lips, and Y equals 1 or 2 depending upon use of the overload plastic zone radius or diameter.

Figures 51, 52 and 53 show a comparison between the measured overload affected crack length, and the computed a* using Equation (5) and various factors for the different overload classes. The factor α used in computing a* ranged from 0.0563 representing the plane strain plastic zone radius to 0.3183 representing the plane stress plastic zone diameter. As seen from these figures, the majority of data indicates that the measured overload affected zone decreases with the increase of the stress intensity factor ratio, R. This suggests that the a* may depend not only on the maxima of the overload and constant amplitude stress intensity factors (K_1 and K_2), but also the minimum of the constant amplitude stress intensity factor, K_3.

SECTION VI
MODEL EVALUATIONS

1. COMPUTER PROGRAM

A computer program was prepared for the purpose of predicting delay cycles due to the application of a single overload and/or underload. The delay cycles to be predicted depend not only upon the model, but also upon the crack growth rate equation and the overload affected zone. For fairness of model evaluations, the program was prepared to predict delay cycles for each of the three models combined with each of the three crack growth equations. Also, the program allowed predictions using the plastic zone radius and diameter for both plane strain and plane stress conditions.

A numerical integration approach similar to the one used by Gallagher and Hughes[7] was employed to estimate the number of applied load cycles required to propagate the crack from the position right after the application of overload to a position one overload affected zone ahead of the crack tip. Four different increments, ranging from 1/25 to 1/250 of a* were used in the numerical integration to study the rate of convergence of integration, and results are tabulated in Table XVII for a case where K_1=15, K_2=10, K_3=1 and K_4=1, all units in KSI$\sqrt{\text{in.}}$ The delay cycles were computed using the Grumman growth rate equation and the plane stress plastic zone radius as the overload affected zone. As can be seen from the table, the rate of convergence was very rapid. Since the computer time required to execute the program was small, 100 integration steps were used in the subsequent predictions.

2. MODEL SENSITIVITY TO SHUT-OFF RATIO

The only parameter capable to account for the underload effect in the mathematic formulation of the generalized Wheeler and Willenborg models is the overload shut-off ratio, S_{so}. For a given constant amplitude stress intensity factor ratio, experimental results indicate that the overload shut-off ratio is dependent upon the magnitude of underload or compressive load. The larger the magnitude of compressive load, the higher the overload shut-off ratio.

For a high compressive load immediately following the tensile overload, there

may not be a shut-off in crack growth. Even if there is a shut-off, the shut-off overload may be much higher than stable tear threshold value or the net section stress (in the plane containing the crack surface) may exceed the yield strength of the material. In this case the value of shut-off ratio may not be too meaningful from linear elastic fracture mechanics point of view.

Since the overload shut-off ratio is required in the generalized Wheeler and Willenborg models and generation of such ratios for all levels of underloads is impractical, a study was conducted to determine the effect of the overload shut-off ratio on predicted delay cycles. It was found that the predicted delay cycles is fairly insensitive to the overload shut-off ratio if the overload cycle minimum is close to the constant amplitude cycle minimum. However, for a tension-compression overload, such effect is more pronounced. Figure 54 shows the predicted delay cycles normalized by the measured delay cycles as a function of assumed overload shut-off ratios for K_1=20, K_2=10, K_4= -K_1 and various K_3. As can be seen from the figure, the effect of S_{so} on the predicted delay cycles is more significant in the generalized Wheeler model than the generalized Willenborg model. This effect remains fairly constant for various constant amplitude stress intensity factor ratios, R. The important thing to be pointed out is that if the lower overload shut-off ratio is used in the prediction, the delay cycles may be over estimated. For the purpose of predicting delay cycles due to overload and/or underload, the curves representing the overload shut-off ratios as shown in Figures 29 and 30 were used. These were obtained by fitting the curves through data generated for each R ratio.

The generalized closure model does not depend upon the overload shut-off ratio. It accounts for the underload or compressive load effect through the closure factor, C_f, of the overload cycle.

3. MODEL SENSITIVITY TO THRESHOLD STRESS INTENSITY RANGE

Other than the overload shut-off ratio, both the generalized Wheeler and generalized Willenborg models also require the value of threshold stress intensity factor range, ΔK_{th}. Since experimental scatter has been observed in data for determining ΔK_{th}, a study was conducted to determine the sensitivity of the models to this parameter. The predicted delay cycles using the generalized Wheeler and generalized Willenborg

models are presented as a function of threshold ΔK in Figure 55 for both tension-tension and tension-compression overloads. The compressive load chosen was the one-half of the tension overload. Two levels of overload (S=1.5 and 3.0) and the Grumman crack growth rate equation were used in the prediction. In each overload case, the prediction was made by holding the overload shut-off ratio constant at measured value and varying threshold ΔK from 1.1 and 1.9. As seen from this figure, the effect of threshold ΔK on predicted delay cycles increases with the increase of overload ratio. The generalized Willenborg model exhibited a low sensitivity to the threshold value while the generalized Wheeler model is more sensitive to the threshold value. The average threshold K_{max} obtained in Reference 2 is about 1.5 for R=0 and was used in the analytical predictions of delay cycles. For applied load ratio, R, different from zero; threshold ΔK was set equal to 1.5 (1-R).

4. EVALUATION OF THE GENERALIZED WHEELER MODEL

As discussed in Section V, the predicted delay cycles due to the application of overload does not depend only on the model and the crack growth rate equation, but also on the overload affected zone, a*. For any given constant amplitude and overload stress intensity factors, the a* is directly proportional to the load interaction zone created by the overload, z_{OL}. Both the original and generalized Wheeler model assumed that the z_{OL} was equal to the overload created plane strain plastic zone radius. Although most of the measured overload affected crack lengths were larger than the corresponding ones computed using Equation (5) by assigning z_{OL} as the overload created plane strain plastic zone radius, these computed a*'s were used in the prediction of delay cycles due to various types of overloads.

The correlations of measured and predicted delay cycles using the generalized Wheeler model and the three different crack growth rate equations are presented in Figures 56 through 61 for 2219-T851 aluminum plates subjected to various types of overload and/or underload. In all figures, an arrow connected to the symbol indicates that the predicted delay cycles is outside the range of the graphic scale. The solid line in all these figures represents perfect correlation, and the broken lines represent a scatter factor of two. The data used in correlations include three different constant amplitude

stress intensity factor ratios (R=0.1, 0.3 and 0.5) and three different constant amplitude stress intensity maxima (K_2=10, 7.78 and 14 KSI$\sqrt{in.}$). The overload ratio, S, ranges from 1.5 to 3.0 for all load classes except tension-compression in which S ranged from 1.5 to 4.5. In general the higher the overload ratio, the larger the delay cycles.

Figure 56 shows the correlations of measured and predicted delay cycles due to tension-tension overloads. When the generalized Wheeler model is used, the predicted delay cycles using the Hall growth rate equation is smaller than the corresponding one predicted using the Grumman or Walker equations. Except for a smaller overload ratio (S=1.5), the predicted delay cycles is larger than the actual measured delay cycles, especially for a high overload ratio even though a smaller than measured overload affected zone was used in predictions. If a larger overload affected zone (as the one measured) is used, then the predicted delay cycles will be even higher than the current predictions. Figure 57 shows similar correlations of delay cycles due to tension-zero overloads for K_2=7.78, 10 and 14 KSI$\sqrt{in.}$ Figures 58 and 59 present the delay cycles due to the application of tension-compression overload cycles for K_2=10 and K_2=7.78 and 14 KSI$\sqrt{in.}$, respectively. By comparing the results shown in Figures 57 through 59 with that of 56, one can see that the presence of underload or compressive load immediately after the overload, does not alter the trend of the prediction on delay cycles. When the sequence of the overload cycle is reversed, i.e. the overload cycle is applied in an order of zero-tension or compressive-tension, the retarded crack growth behavior observed is very similar to those of tension-tension overloads. The generalized Wheeler model does not account for the sequence of overload cycle. Nevertheless, the generalized Wheeler model was used to predict the delay cycles due to zero-tension and compression-tension overloads, and the results are presented in Figures 60 and 61. As was shown for the other overload classes, the generalized Wheeler model overestimates the delay cycles for all cases where the overload ratio is higher than 1.5.

In general, the predicted delay cycles by the generalized Wheeler model together with the usage of the overload created plane strain plastic zone radius in computing the overload affected zone, is significantly higher than the measured delay cycles whenever the overload stress intensity factor exceeds 1.5 times the constant amplitude stress intensity factor maximum. At an overload ratio of 1.5, most of the predicted delay cycles

are within a factor of two of the actual measured values.

5. EVALUATION OF THE GENERALIZED WILLENBORG MODEL

As mentioned earlier, the generalized Willenborg model assumes that the overload created interaction zone, z_{OL}, is equal to the overload created plane stress plastic zone radius. The computed overload affected zone, a*, using the overload created plane stress plastic zone radius correlates better with the data than the one computed using the overload created plane strain plastic zone radius as noted in Figures 51 through 53. For the purpose of evaluating the generalized Willenborg model, the overload affected crack length, a*, computed using the overload created plane stress plastic zone radius together with three crack growth rate equations discussed in Section V were used in predicting the delay cycles due to various types of overloads. Based upon the current study, the predicted delay cycles, using the generalized Willenborg model and the computed a* using the overload created plane stress plastic zone radius is significantly lower than the measured delay cycles. In most cases, the predictions are too conservative. A better correlation was observed when the plane stress plastic zone diameter was used to compute the overload affected crack length. Therefore, the correlations of predicted and measured delay cycles using the generalized Willenborg model are presented for both the a* computed using the overload created plane stress plastic zone radius and diameter. Figures 62 through 67 show correlations of measured delay cycles and delay cycles predicted using Z_{OL} as the plane stress plastic zone radius. In these figures, the solid line represents perfect correlation, and the broken lines represent a scatter factor of two. Examination of these figures show that predictions were generally unconservative for all load profiles.

Similar correlations are shown in Figures 68 through 73 using Z_{OL} as the plane stress plastic zone diameter. Figure 68 shows the correlations of predicted and measured delay cycles using the generalized Willenborg model and three different crack growth rate equations for 2219-T851 aluminum alloy plate subjected to tension-tension overloads. Similar results on delay cycles due to tension-zero overloads are shown in Figure 69. As seen from these two figures compared with Figures 62 and 63, a better correlation will be achieved if the overload affected zone is approximated by the overload created plane stress plastic zone diameter. All predictions are within a factor of two of the

measured values, regardless of which crack growth rate equation is employed. Figure 70 shows correlations of measured and computed delay cycles due to tension-compression overloads. Although the correlation is not as good as that of tension-tension and tension-zero overload cases, the overall correlation is still good. As discussed earlier in this section, one of the main problems in predicting the delay cycles due to tension-compression overloads is the selection of a proper overload shut-off ratios. The overload shut-off ratios shown in Figures 29 and 30 were the best estimations based upon the available data. For high compressive load, the shut-off overload is much higher than stable tear threshold value. In order to enhance the evaluation of the model in predicting delay cycles due to tension-compressive overloads, additional data including the overload shut-off ratio were generated for K_2=10 and K_5= -7.5 KSI$\sqrt{in}$. The correlations of measured and predicted delay cycles using the generalized Willenborg model for these additional cases is shown in Figure 71. Again, good correlation was obtained if the a* was computed using the plane stress plastic zone diameter. When the application of underload or compressive load precedes the overload, the observed overload shut-off ratio does not change significantly with the increase in magnitude of compressive load as seen in Figure 30. Therefore, one could anticipate that the retarded crack growth behavior due to compression-tension overload might be close to that of tension-tension overload. This is confirmed by the results presented in Figures 72 and 73 which show the correlations of measured and predicted delay cycles due to zero-tension and compressive-tension overloads, respectively.

In general, if the overload created load interaction zone, z_{OL}, is assumed equal to the overload created plane stress plastic zone radius as proposed by the Willenborg model, then the delay cycles predicted by the generalized Willenborg is almost always less than the actual measured delay cycles, except for some of the tension-compression overload cases. The crack growth rate equations, proposed by Hall, Bell and Walker for 2219-T851 aluminum alloy plate, do not show a consistent trend in the predicted delay cycles due to various overloads and/or underloads. It is almost impossible to rank one equation to the others. In general, any one of these three equations may be used alone to evaluate the models.

When the overload affected zone was computed using the overload created plane

stress plastic zone diameter, almost all the predicted delay cycles using the generalized Willenborg model were within a factor of two of the actual measured delay cycles.

6. EVALUATION OF THE CLOSURE MODEL

The closure model assumes that the overload affected zone, a^*, is equal to the overload created plane stress plastic zone radius. Unlike the generalized Wheeler and generalized Willenborg models, the closure model does not depend upon the overload shut-off ratio to account for the underload or compressive load effect. Such effect was accounted for through the closure factor, C_f, from which the closure stress intensity factor, K_c, was determined. Upon application of the overload, if the computed K_c is larger than the constant amplitude stress intensity factor maximum, then the closure model predicts that the crack arrest occurs.

The correlations of measured and predicted delay cycles using the closure model and various crack growth rate equations for 2219-T851 aluminum alloy plates subjected to various types of overloads and/or underloads are shown in Figures 74 through 79. Figure 74 presents delay cycle correlations due to tension-tension overloads. As seen from this figure, the predicted delay cycles using the Hall equation are always less than the corresponding ones predicted by the Grumman and Walker equations. Predictions using the Grumman and Walker equations show almost no difference. For an overload ratio, S, less than or equal to 2.0, the predicted delay cycles using the closure model, and the Hall crack growth rate equation, are within a factor of two of the measured delay cycles. However, for $S>2.0$, the predicted delay cycles are much higher than the measured values, and crack arrest is predicted regardless of which crack growth rate equation is used whenever $S>2.5$. Similar results were observed for tension-zero overload cases which are shown in Figure 75. Figures 76 and 77 show the correlations of measured and predicted delay cycles due to tension-compression overloads for K_2=10 KSI$\sqrt{\text{in.}}$ and K_2=7.78 and 14 KSI$\sqrt{\text{in.}}$, respectively. Figures 78 and 79 present similar results on delay cycles due to zero-tension and compression-tension overloads, respectively. Except for compression-tension overload cases, the trend of delay cycle predictions by the closure model is the same as that for tension-tension overload cases. The predicted delay cycles due to compression-tension overloads are less than that of measured values.

In general, when the closure model (together with the assumption that the over-

load affected zone equals the overload created plane stress plastic zone radius) is used to predict the delay cycles due to any type of overload and/or underload, the best results will be achieved if the Hall crack growth rate equation is employed. If the overload ratio is less than or equal to two, the predicted delay cycles are within a factor of two of the measured delay cycles. If the Grumman or Walker crack growth rate equation is used, together with the closure model, to predict the delay cycles due to overloads, the predicted delay cycles will consistently be higher than the measured values. When the overload stress intensity factor exceeds 2.5 times the constant amplitude stress intensity factor maximum, the closure model will predict that the crack arrest occurs, while there are finite delay cycles (less than half million cycles) measured.

7. COMPARISON OF MODELS

As discussed during the evaluation of each model, the predicted delay cycles due to overload and/or underload is dependent upon the overload affected zone size chosen in the prediction. It was found that the best results will be achieved by pairing the model and the overload affected zone as follows:

1) the generalized Wheeler model and the plane strain plastic zone radius,
2) the generalized Willenborg model and the plane stress plastic zone diameter,
3) the closure model and the plane stress plastic zone radius

In order to have a direct comparison between models, the predictions using the Hall crack growth rate equation and the above pairings of the model and overload affected zone, are tabulated in Tables XVIII through XXVII for various types of overload and/or underload conditions. Those results are also presented in Figures 80 through 86. The reason the Hall equation was chosen is that it correlates with available data better than the Grumman and Walker equations in the region where ΔK is less than 3 KSI$\sqrt{\text{in.}}$ When ΔK is higher than 3 KSI$\sqrt{\text{in.}}$, the difference in growth rate predicted by three equations is practically negligible.

Figure 80 shows the correlations of measured and predicted delay cycles using the Hall crack growth rate equation and three aforementioned retardation models for 2219-T851 aluminum alloy plates subjected to tension-tension overloads. The data in-

cludes three constant amplitude stress intensity factor maxima (K_2=7.78, 10 and 14 KSI$\sqrt{in.}$) and three applied load ratios (R=0.1, 0.3 and 0.5). The overload ratio ranges from 1.5 to 3.0. Within the same overload class, the higher the overload ratio, the larger the delay cycles. As seen from Figure 80 when the overload ratio is greater than 2.5, the closure model predicts the occurrence of crack arrest (or infinite delay cycles), while the generalized Wheeler model predicts delay cycles greater than two times the measured value in most cases, even though a smaller than measured a* was used in the prediction. The generalized Willenborg model gives the best prediction for $S \geq 2.5$. When the overload ratio is below 2.0, both the generalized Willenborg model and the closure model give a prediction within a factor of two of measured delay cycles. In this range, the prediction using the generalized Wheeler model is not as good as the other two models. Similar correlations of delay cycles due to tension-zero overloads are presented in Figure 81. Those results show practically no difference from those of tension-tension overload class.

Correlations of measured and predicted delay cycles due to tension-compression overloads are shown in Figure 82 for K_2=10 and in Figure 75 for K_2=7.78 and 14. As discussed earlier in this section, both the generalized Wheeler and generalized Willenborg models require the overload shut-off ratio for each overload condition while the closure model does not depend upon such ratio. Experimental determination of accurate overload shut-off ratios for tension-compression overload class is impractical. The overload shut-off ratios used to obtain the predicted delay cycles shown in Figures 82 and 83 were extrapolated values. As seen from Figures 82 and 83, for tension-compression, the correlation using the generalized Wheeler and generalized Willenborg models are not as good as the ones obtained for tension-tension and tension-zero overload classes. For an overload ratio less than or equal to 2.0, the predictions using the closure model correlate fairly good with the measured values. However, when the overload ratio is greater than or equal to 2.5, the prediction using the closure model is completely no good. Additional data were generated for the compressive underload constant at -7.5 KSI$\sqrt{in.}$, and results of measured and predicted delay cycles using the three retardation models are shown in Figure 84. With availability of the overload shut-off ratio for K_5= -7.5 KSI$\sqrt{in.}$, the predictions using the generalized Willenborg model excellently correlate with the measured values, while the closure model gives a compatible good prediction with the generalized Willenborg model for $S \leq 2.0$, but bad predictions whenever $S > 2.5$.

Correlations of measured and predicted delay cycles due to zero-tension and compression-tension overloads are shown in Figures 85 and 86, respectively. As was obtained for the other overload classes, the best prediction was obtained by using the generalized Willenborg model. Both the generalized Wheeler model and the closure model give a fairly good prediction for lower overload ratios but bad predictions for high overload ratios.

To summarize the model comparison, one may conclude that:

1) When overload ratio is greater than or equal to 2.5 the delay cycles predicted by the closure model is completely no good regardless of what type of overload; the delay cycles predicted by the generalized Wheeler model is much larger than the measured value, while the generalized Willenborg model gives the best prediction which is within a factor of two of measured delay cycles.
2) When overload ratio is less than or equal to 2.0, all three models provide a reasonable prediction except for the tension-compression overload class having high compressive load. For this overload case, the closure model gives the best prediction.

SECTION VII
GENERAL CONCLUSIONS

1) Underloads following overloads decreased the retardation effect produced by the overload and increased the overload shut-off ratio. These effects became more apparent as the constant amplitude minimum stress intensity factor was increased while holding other parameters constant. For high compressive underloads following overloads, a physically meaningful overload shut-off ratio may not exist.

2) Underloads preceeding overloads produced approximately the same number of delay cycles, overload affected zone size and overload shut-off ratio as the equivalent tension-tension case with the underload truncated.

3) In this investigation the constant amplitude maximum stress intensity factor was varied over an approximate range of 7 to 14 KSI $\sqrt{\text{In.}}$ Data obtained within that range indicate that the overload shut-off ratio is independent of the constant amplitude maximum.

4) Hold periods in tension increased delay cycles, and stabilization was not apparent after 24 hours which was the longest period evaluated. Although delay cycles increased with hold time there was no measurable effect on overload affected zone size. It was also indicated that holding in tension decreases the overload shut-off ratio.

5) Hold periods in compression resulted in a small decrease in delay cycles, and the effect was essentially stable after one hour.

6) Based upon the experimental data generated under this program, it was found that the overload affected zone, a^*, depends not only on the maxima of overload and constant amplitude load cycles, but also on the minimum of the constant amplitude cycle.

7) For overload ratios higher than two times the constant amplitude stress intensity factor maximum, the Grumman closure model, in general, gives a very unconservative prediction. In most cases, the closure model predicts that crack arrest occurs while finite delay cycles were measured.

8) The generalized Wheeler model consistently predicts higher delay cycles than the actual measured delay cycles, even though a much smaller than measured overload affected zone was used in the prediction. This implies that the effective ΔK computed by the model is much smaller than the actual value.

9) Excellent correlation of measured and predicted delay cycles can be achieved by using the generalized Willenborg model, provided that a larger than the measured overload affected zone is used in the prediction. Physically, it implies that the effective ΔK computed by the generalized Willenborg model is larger than the actual value. This is just opposite to that computed by the generalized Wheeler model.

10) The predicted delay cycles due to a single overload is highly dependent upon the size of overload affected zone chosen. If the subsequent overload is applied before the crack tip extends outside the retarded region created by the first overload, then the retarded growth rate predicted should be less sensitive to the a^*. In general, such sensitivity will decrease with the decrease of period between overloads.

11) The effect of three different crack growth rate equations discussed earlier on the predicted delay cycles was small. This was partially due to the high constant amplitude stress intensity factor ranges (ΔK=5, 7, 9 KSI$\sqrt{\text{in.}}$) used in the program. When ΔK was greater than 3 KSI$\sqrt{\text{in.}}$, the growth rate computed using the three different equations show practically no difference. If a lower ΔK is used in the analysis, substantial difference in the predicted delay cycles by using different growth rate equation may be anticipated.

12) The overload shut-off ratio is fairly sensitive to the magnitude of compressive load following the tensile overload. If the generalized Wheeler model or generalized Willenborg model is used in the life prediction of fatigue crack growth under varying amplitude spectrum load, a choice of proper overload shut-off ratios may be a problem, especially for a new material where the shut-off ratio data are not available.

SECTION VIII
RECOMMENDATIONS

Based on results of this program, areas have been identified as recommended future efforts directed toward improving crack growth prediction methodology. These are briefly discussed below for consideration in future programs sponsored by the Air Force or industry.

1) The overload affected zone size formulation plays a very important role in crack growth predictions. Generally, current formulations consider only the maxima of the overload and constant amplitude cycles as controlling parameters. The majority of data reported herein indicate that, with all other parameters constant, the measured overload affected zone size decreases with an increase in stress intensity factor ratio, R. This suggests that a* may depend not only on the maxima of the overload and constant amplitude stress intensity factors, but also the minimum of the constant amplitude cycle. In order to improve current prediction methodology or to develop a better load-interaction model, development of a mathematical model to characterize the overload affected zone more accurately is necessary. Some additional data are considered necessary to identify the influence of key parameters and guide the formulation of such a model.

2) Current retardation models do not account for hold time effects on subsequent crack growth, but current data indicate that they should be modified to do so. According to current data, hold time in tension increases the delay cycles but does not practically change the overload affected zone size. Incorporation of the overload shut-off ratio as a function of hold time in the generalized Wheeler and generalized Willenborg models or the closure stress intensity factor as a function of hold time in the closure model appears to be the proper direction for hold time accountability in tension. Holding in compression resulted in a small decrease in delay cycles, and additional data are required to determine the need or an approach for accountability. Also, an extension of the data reported herein on holding in tension will be required to guide model modifications.

3) Since both the generalized Wheeler and generalized Willenborg models require overload shut-off ratios, it is recommended that procedures for determining S_{so} and mathematically representing S_{so} in the models be established. Data reported herein

indicate that underload preceeding overload can be adequately represented by the equivalent overload case with the underload truncated, and that S_{so} is independent of the constant amplitude maximum. Consequently, the important parameters for consideration are limited to the magnitude of underload following overload and the constant amplitude load ratio. Mathematically representing S_{so} may be more straight forward for the generalized Willenborg model since it is less sensitive to S_{so} variance than the generalized Wheeler model. Consequently, it may be possible to adequatel y represent S_{so} as a function only of underload in the generalized Willenborg model.

4) All data generated under this program were for single overload/underload cases. Data for periodic loading or simple blocked spectrum should be developed as the next step in model evaluations.

5) In crack growth analysis, a good load-interaction model alone does not necessarily guarantee a good prediction. The prediction is also highly dependent upon the baseline crack growth rate data and stress intensity factor solution. Efforts in developing a better model or improving the existing models should couple with the development of more reliable baseline data as well as method for presenting these data.

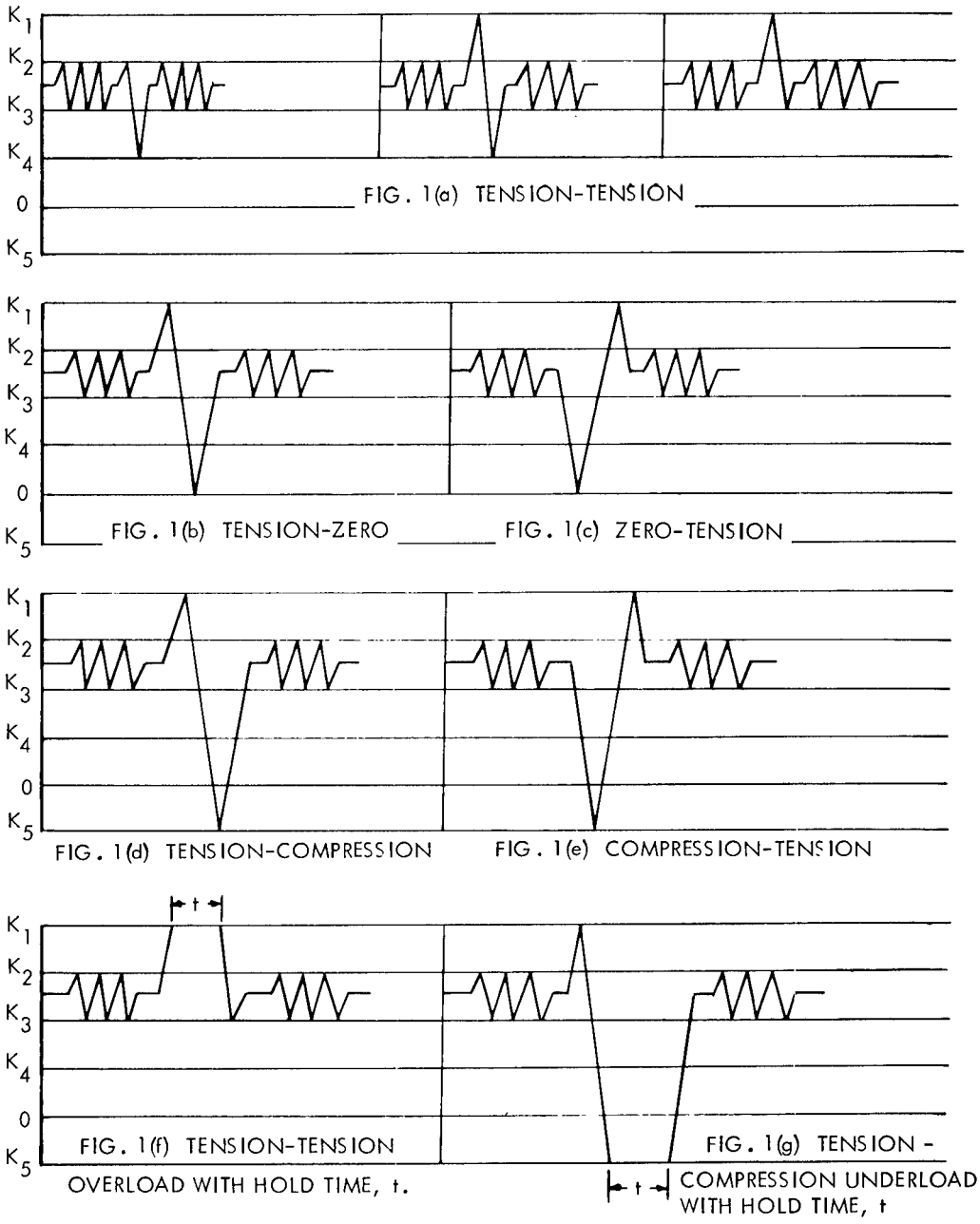

Figure 1. Load Profile Classifications

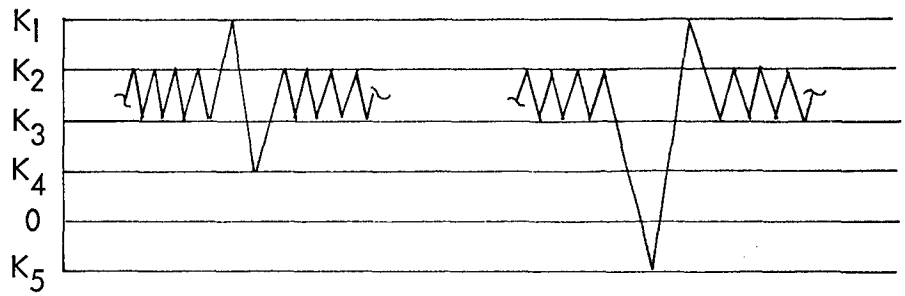

$S=K_1/K_2$, Overload Ratio

$R = K_3/K_2$, Constant Amplitude Stress Intensity Ratio

$U=K_1/K_4$, Underload Stress Intensity Ratio

$U_c=K_1/K_5$, Compressive Stress Intensity Ratio

$\Delta K=K_2-K_3$, Constant Amplitude Stress Intensity Range

Figure 2. Stress Intensity Factor Parameter Definitions

1, 2, 3, 4, 5, 6 - L-1 (Plate Numbers)	L-8	L-15
L-2	L-9	L-16
L-3	L-10	L-17
L-4	L-11	L-18
L-5	L-12	L-19
L-6	L-13	L-20
L-7	L-14	L-21

Figure 3. Test Specimen Locations

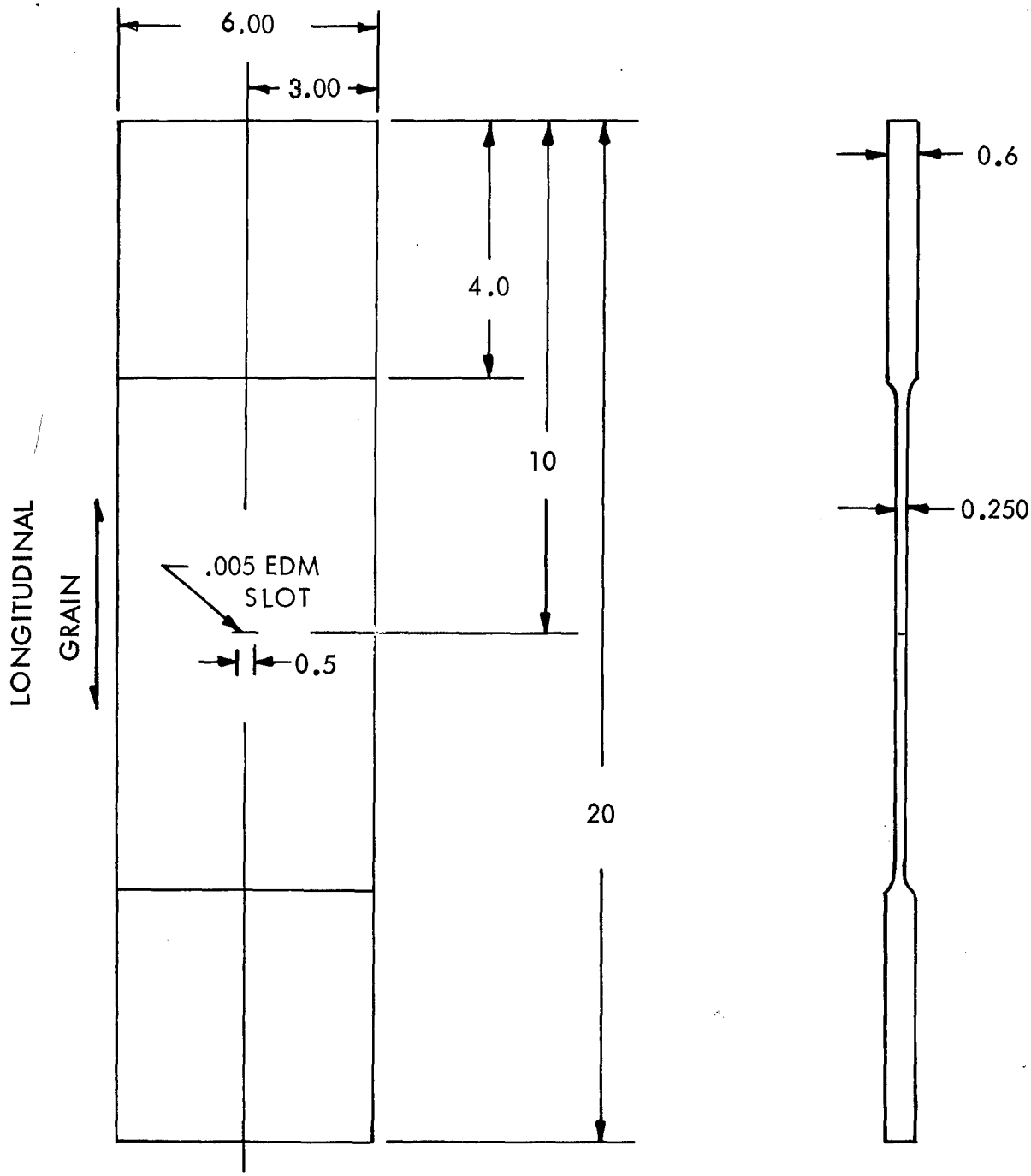

Figure 4. Test Specimen Configuration

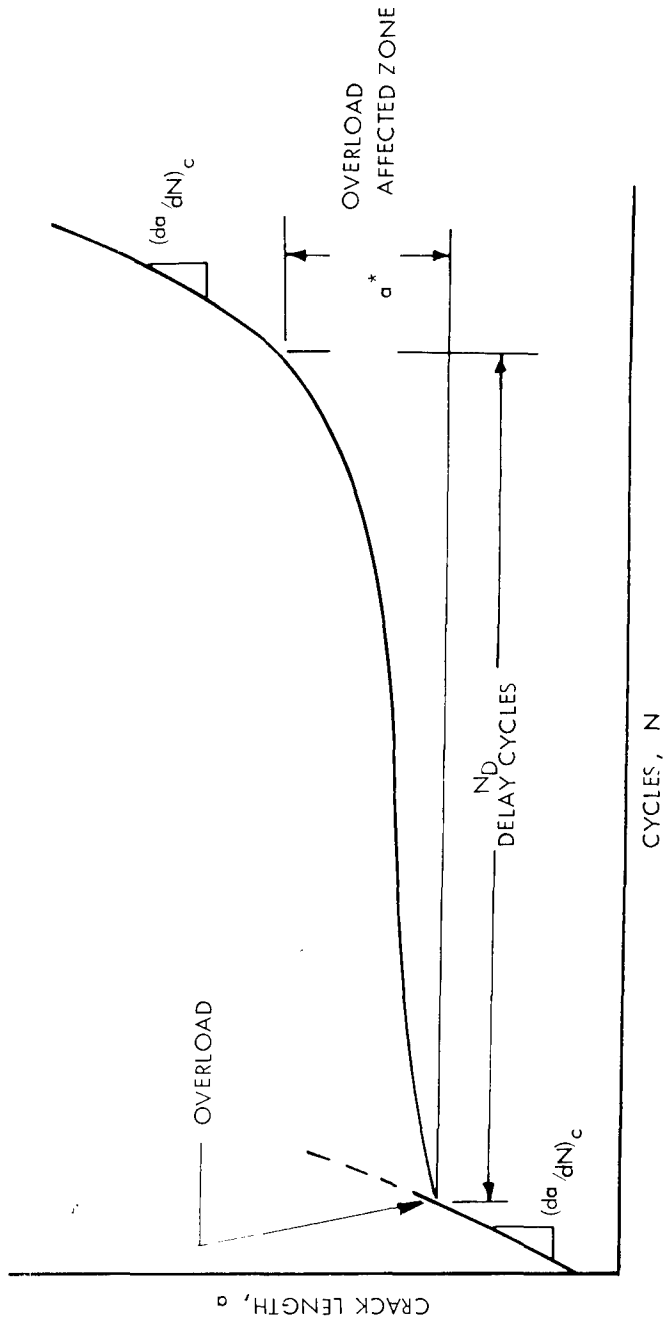

Figure 5. Stress Intensity Factor Parameters

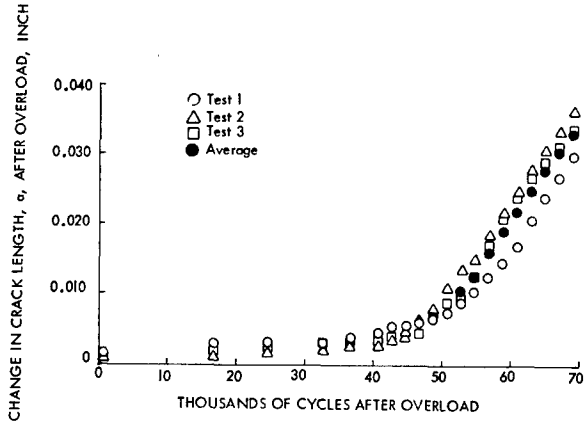

Figure 6. Crack Length Versus Cycles After Overload for Specimens 5-L-17 - K_2=10, R=0.5, U_c = -1, S=2

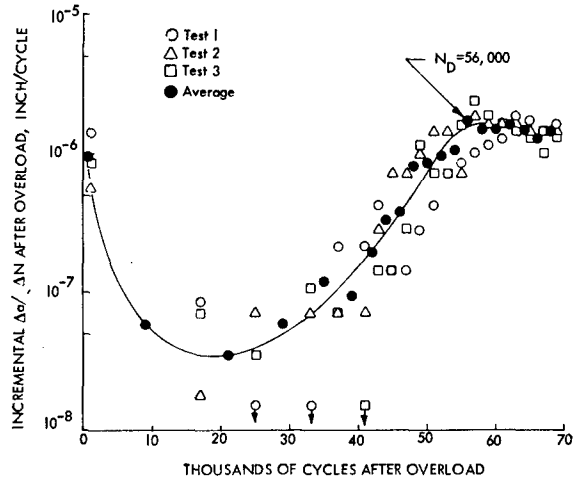

Figure 7. Δa/ ΔN Versus Cycles After Overload for Specimens 5-L-17 - K_2=10, R=0.5, U_c = -1, S=2

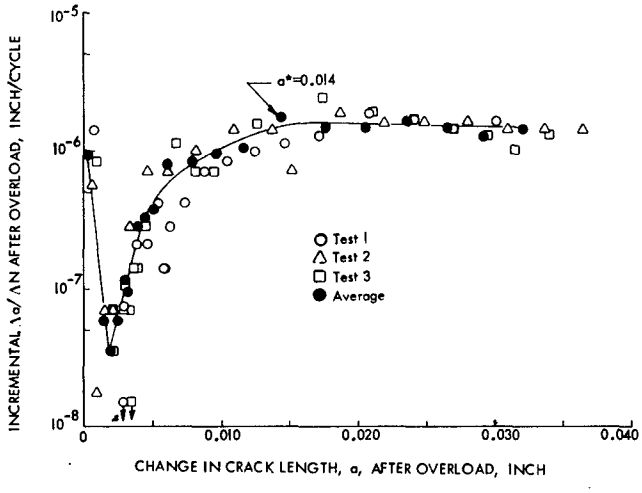

Figure 8. Δa/ ΔN Versus Change in Crack Length After Overload for Specimen 5-L-17 - K_2=10, R=0.5, U_c = -1, S=2

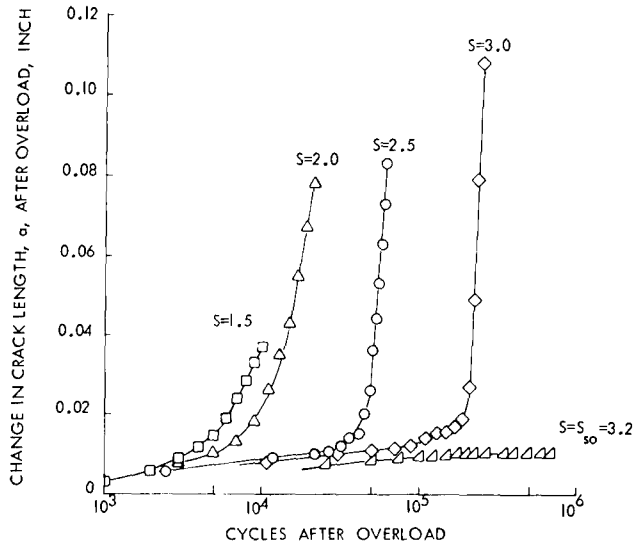

Figure 9. Effect of Overload Ratio on Crack Growth for Tension-Tension Load Class Without Underload, K_2=10, R=0.1, K_3=K_4

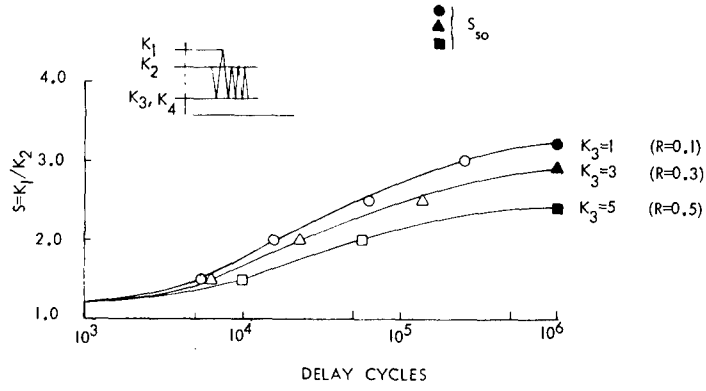

Figure 10. Effect of Overload Ratio, S, and Constant Amplitude Stress Intensity Ratio, R=K_3/K_2, on Delay Cycles for Tension-Tension Load Class Without Underload, K_2=10, K_3=K_4

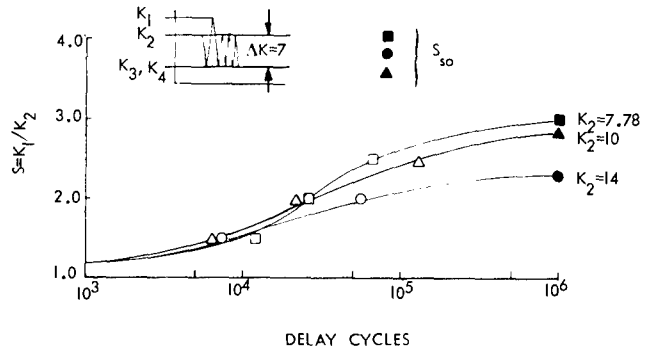

Figure 11. Effect of Overload Ratio, S, and K_2 on Delay Cycles for Constant Amplitude Stress Intensity Range, ΔK=K_2 - K_3, of 7 Without Underloads

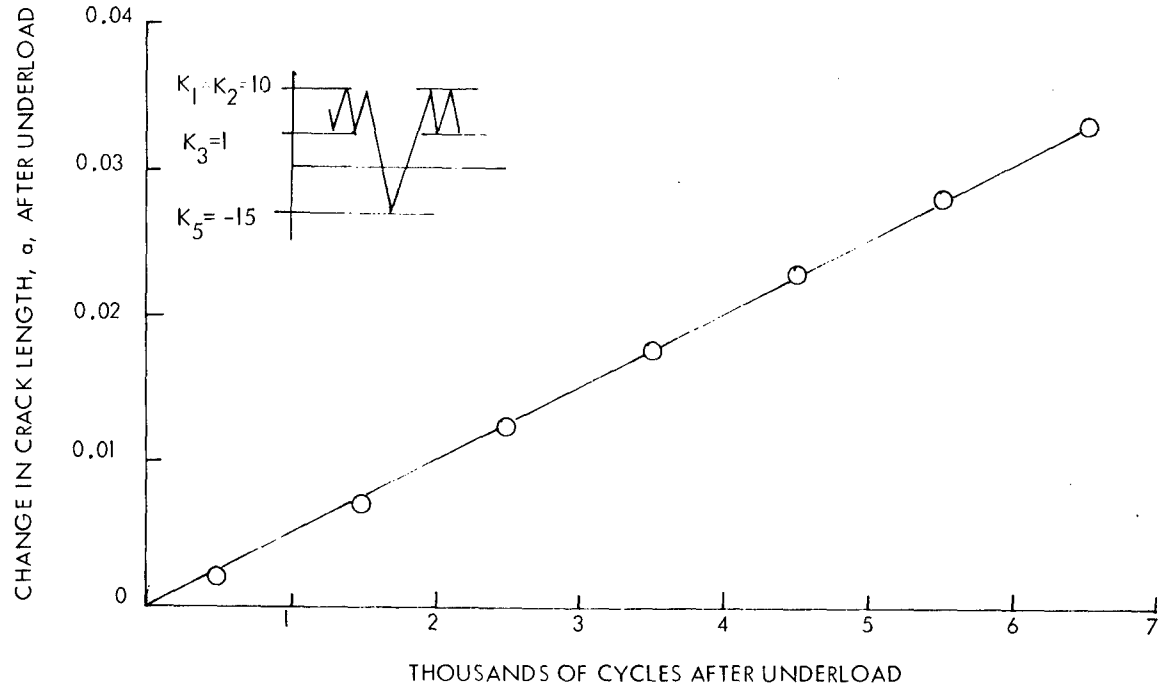

Figure 12. Crack Growth History For Underload Without Overload

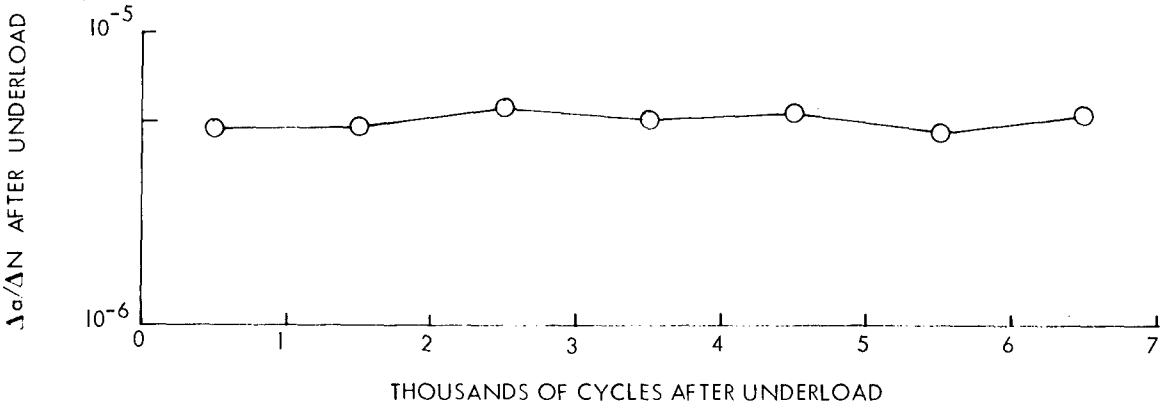

Figure 13. Crack Growth Rate History For Underload Without Overload - From Figure 12 Data

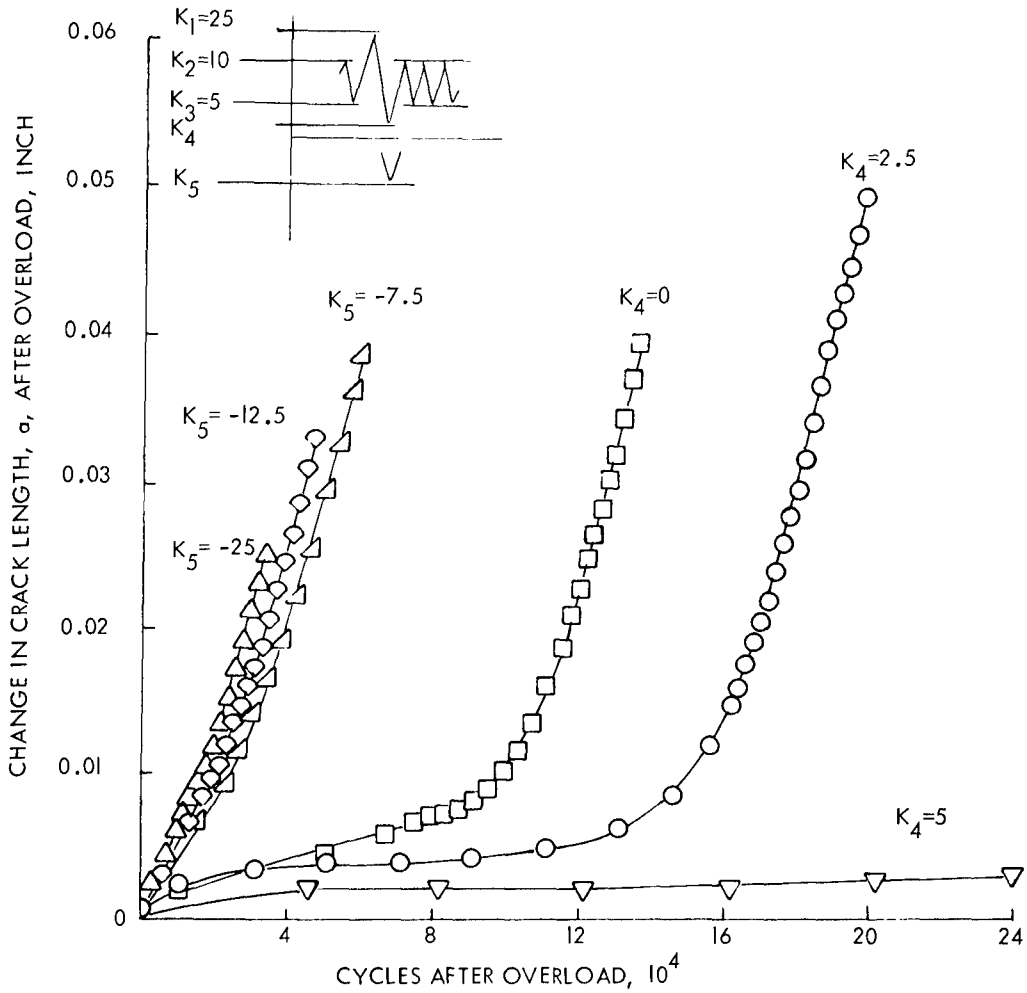

Figure 14. Effects of Underload on Decay of Retardation Due to Overload

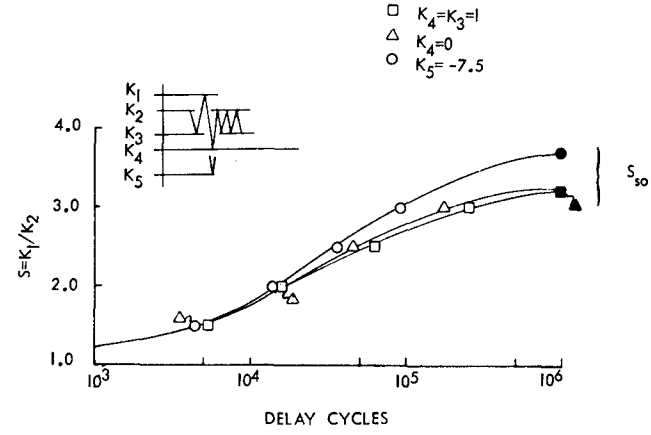

Figure 15. Effect of Overload Ratio and Underload on Delay Cycles for R=0.10 and K_2=10

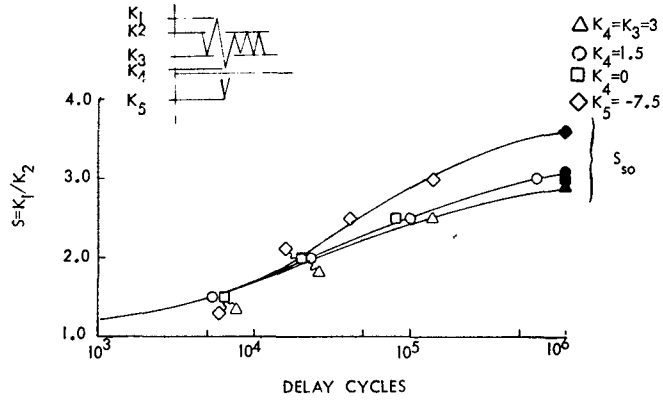

Figure 16. Effect of Overload Ratio and Underload on Delay Cycles for R=0.3 and K_2=10

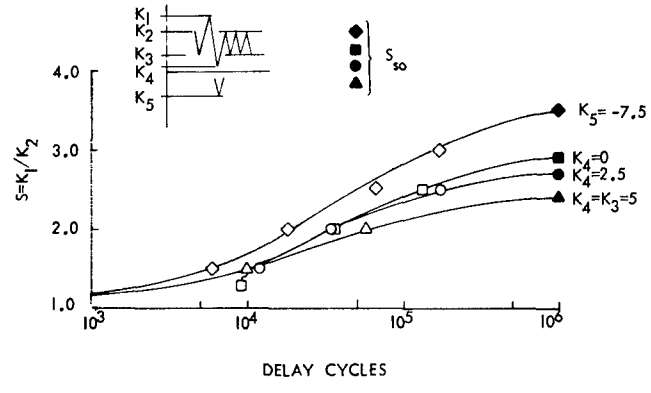

Figure 17. Effect of Overload Ratio and Underload on Delay Cycles for R=0.5 and K_2=10

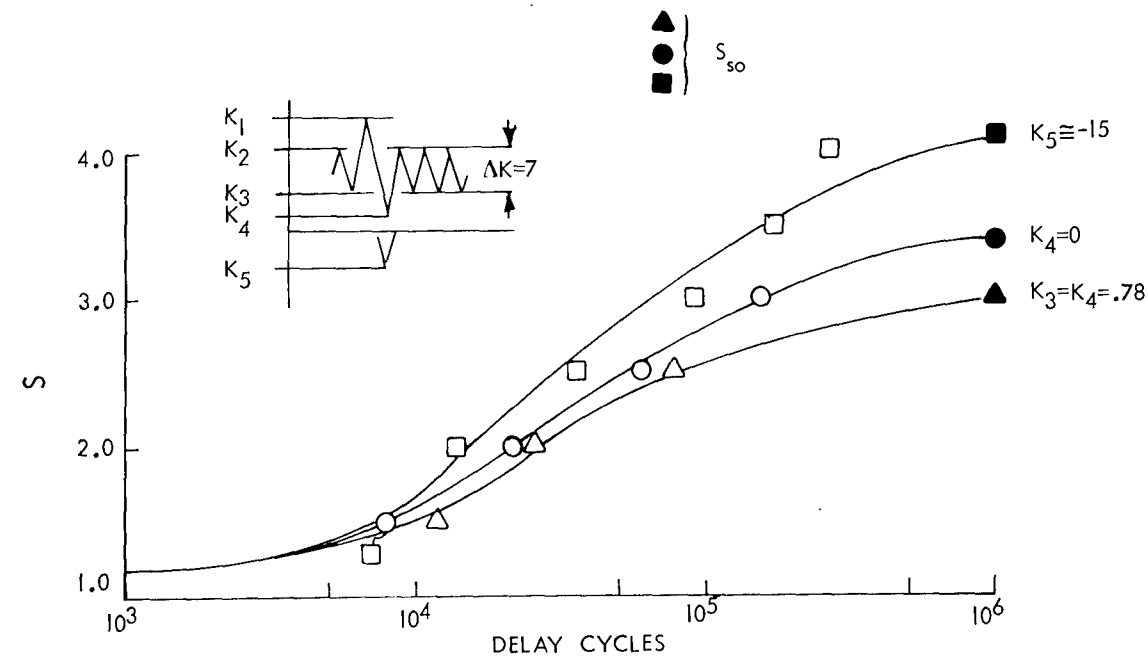

Figure 18. Effect of Overload Ratio and Underload on Delay Cycles for R=0.1 and K_2=7.78

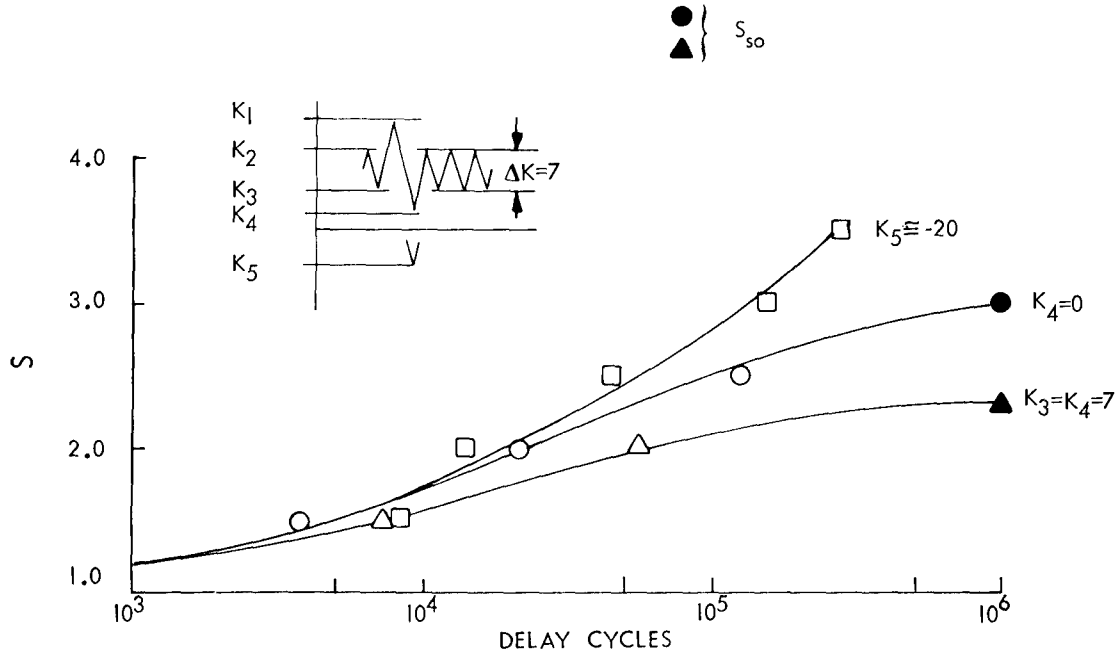

Figure 19. Effect of Overload Ratio and Underload on Delay Cycles for R=0.5 and K_2=14

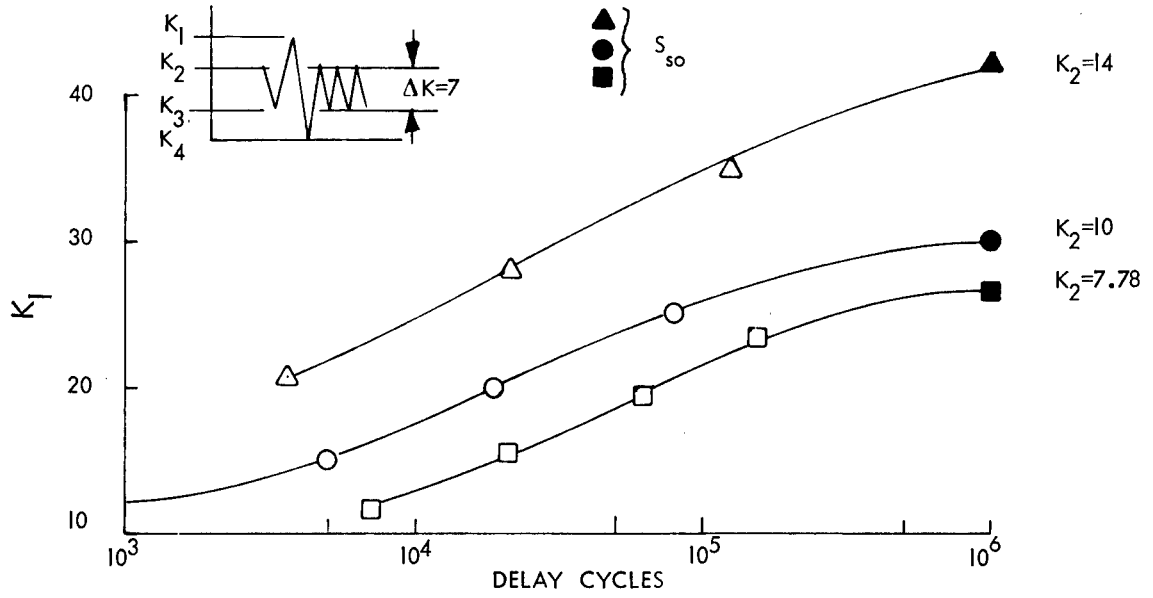

Figure 20. Effect of K_1 and K_2 on Delay Cycles for $\Delta K=7$ and $K_4=0$

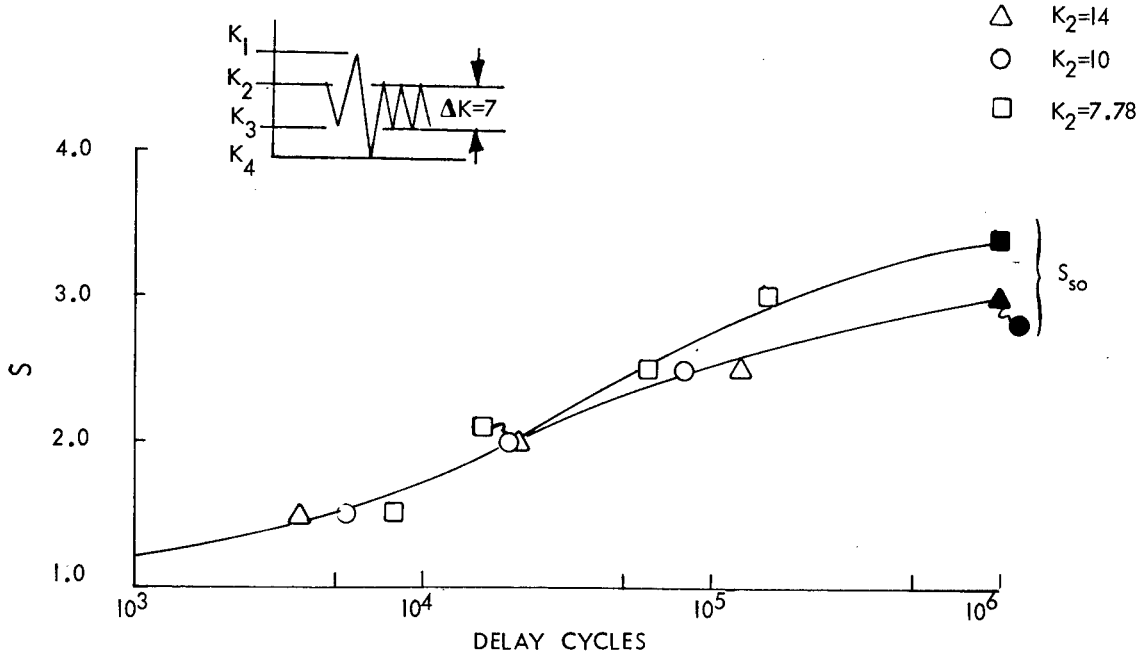

Figure 21. Effect of K_2 and Overload Ratio on Delay Cycles for $\Delta K=7$ and $K_4=0$

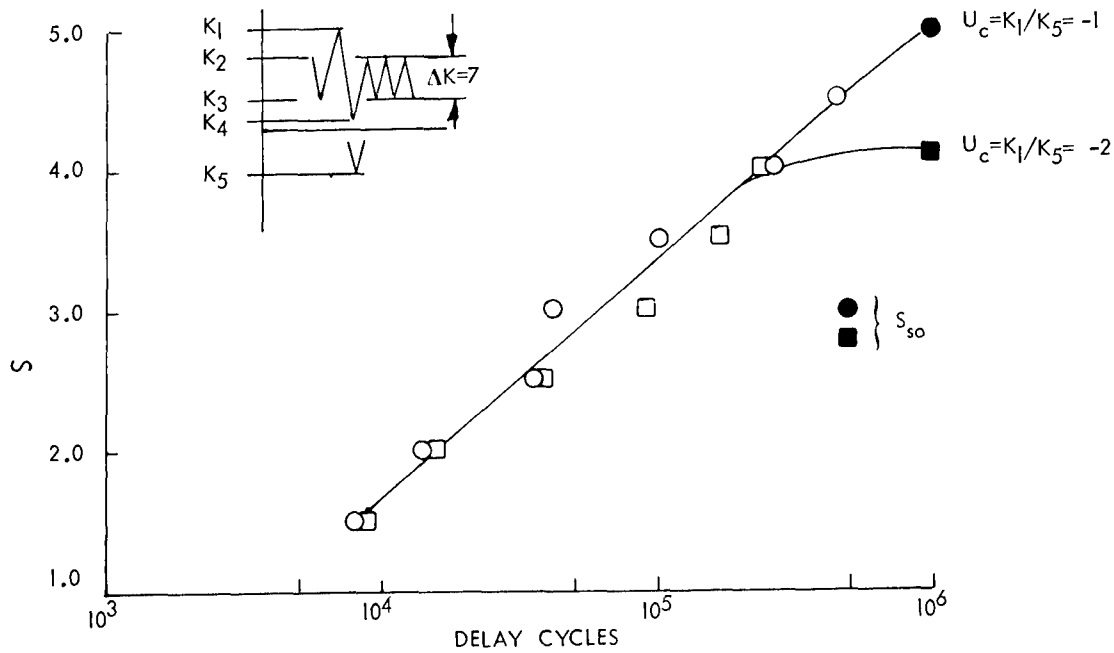

Figure 22. Effect of Overload Ratio and Underload Ratio on Delay Cycles for R=0.1 and K_2=7.78

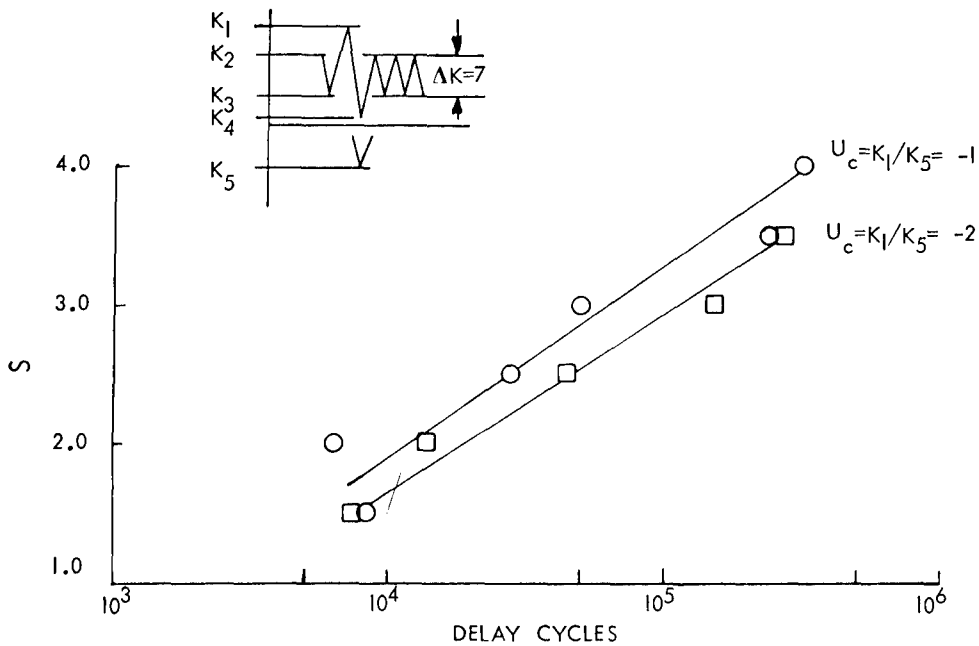

Figure 23. Effect of Overload Ratio and Underload Ratio on Delay Cycles for R=0.5 and K_2=14

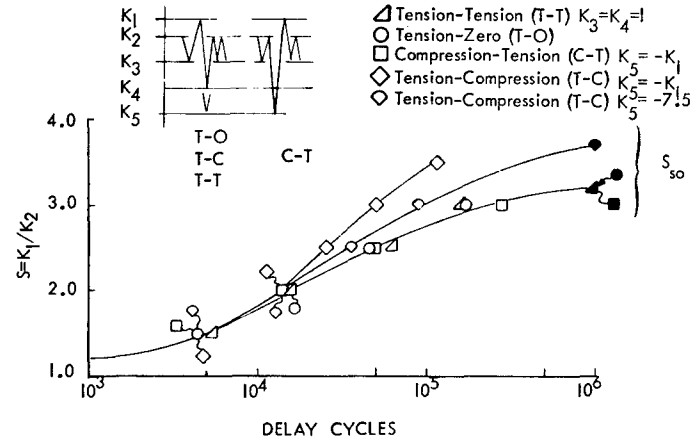

Figure 24. Effect of Load Class on Delay Cycles for Constant Amplitude Stress Intensity Ratio, $R=K_3/K_2$. of 0.1 and $K_2=10$

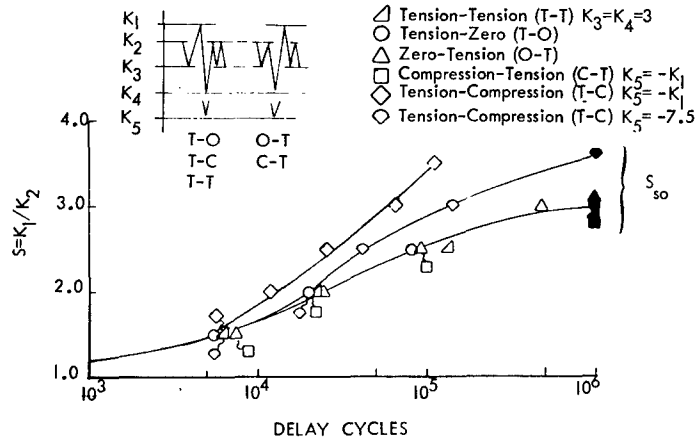

Figure 25. Effect of Load Class on Delay Cycles for Constant Amplitude Stress Intensity Ratio, $R=K_3/K_2$ of 0.3 and $K_2=10$

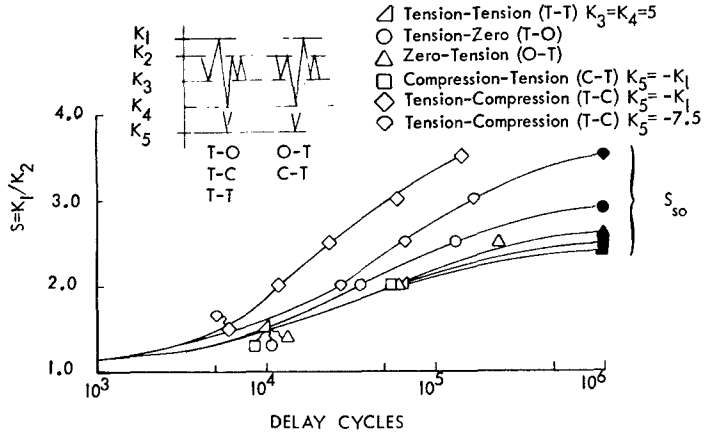

Figure 26. Effect of Load Class on Delay Cycles for Constant Amplitude Stress Intensity Ratio, $R=K_3/K_2$, of 0.5 and $K_2=10$

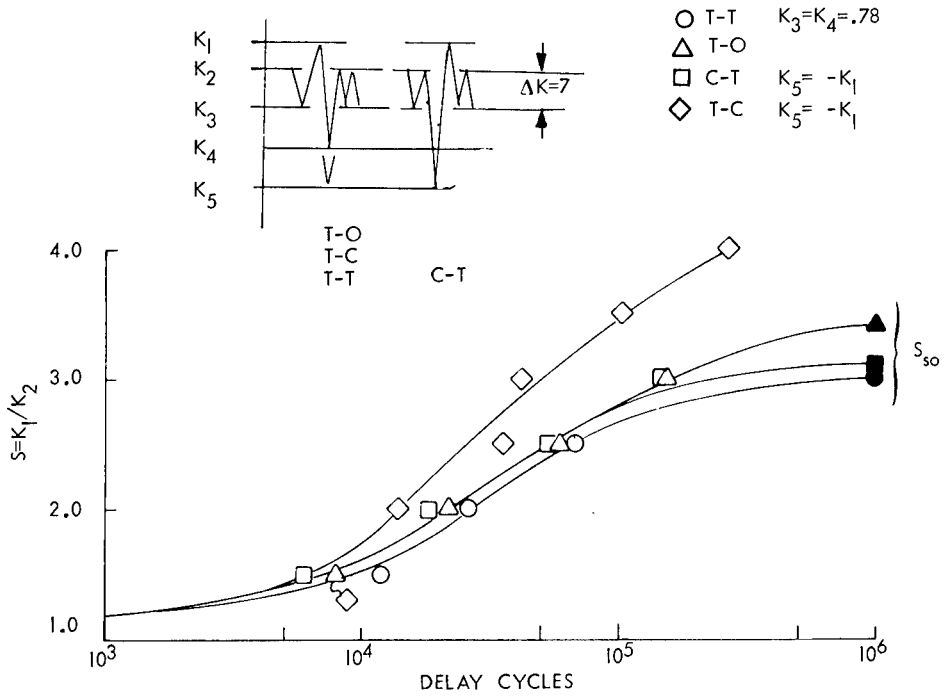

Figure 27. Effect of Load Class on Delay Cycles for R=0.1 and K_2=7.78

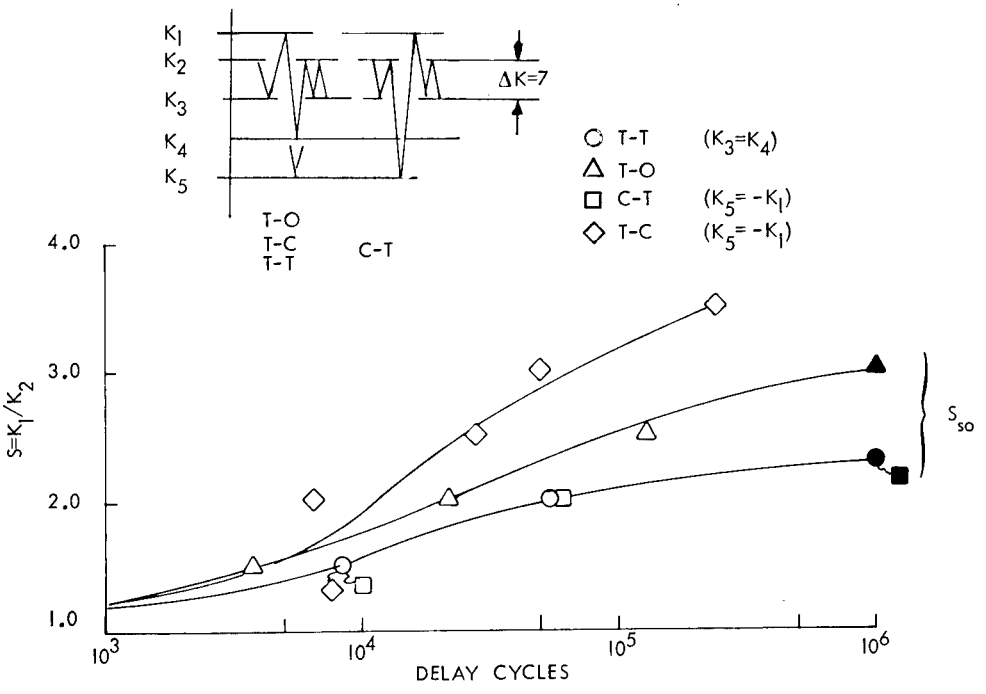

Figure 28. Effect of Load Class on Delay Cycles for R=0.5 and K_2=14

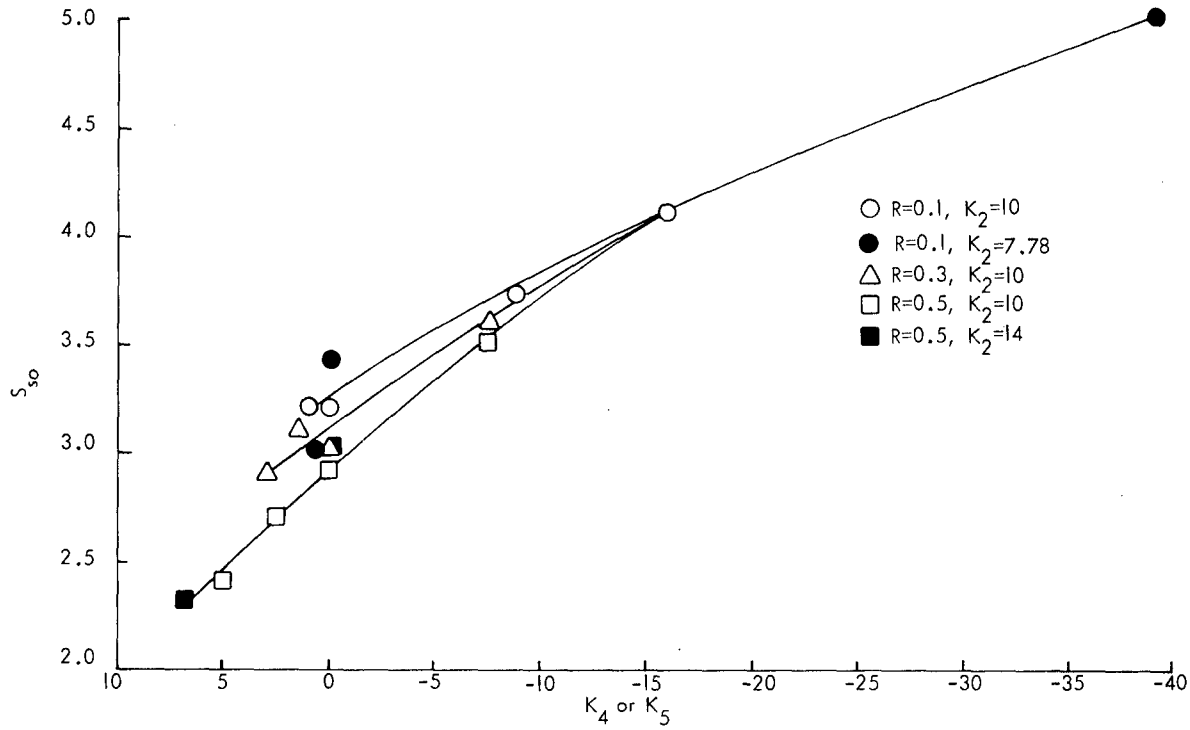

Figure 29. Effect of K_4 or K_5 on Shut-Off Ratio for Tension-Tension, Tension-Zero and Tension-Compression

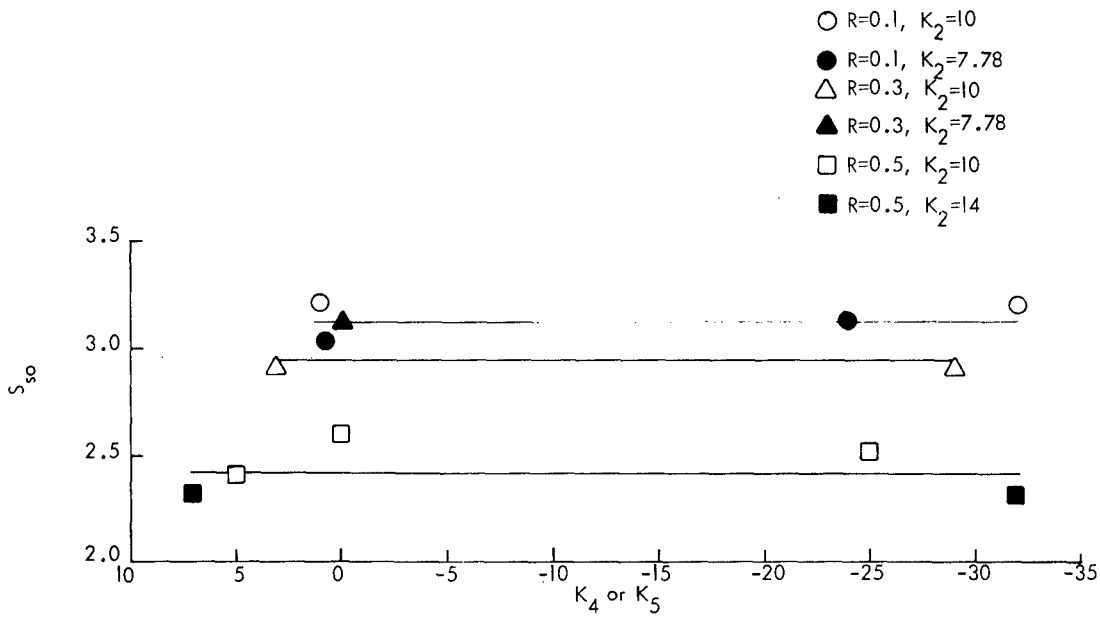

Figure 30. Effect of K_4 or K_5 on Shut-Off Ratio For Zero-Tension, Compression-Tension and Tension-Tension Without Underload

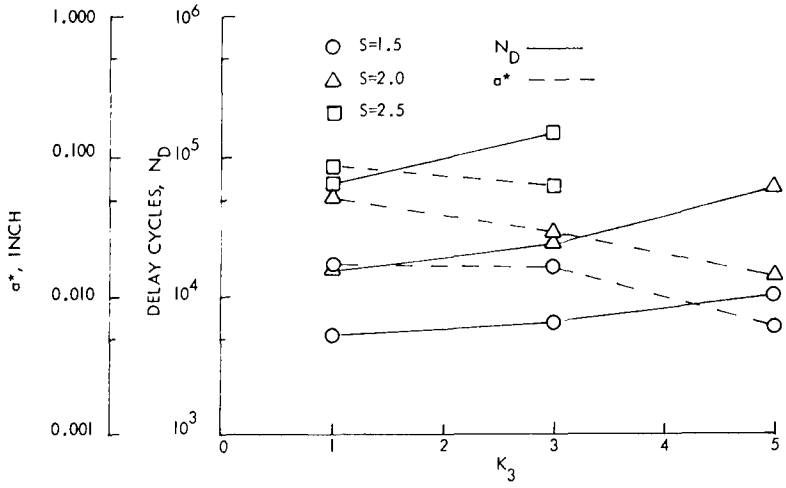

Figure 31. Effect of K_3 and Overload Ratio on Delay Cycles and Affected Zone Size for K_2=10 and K_3=K_4

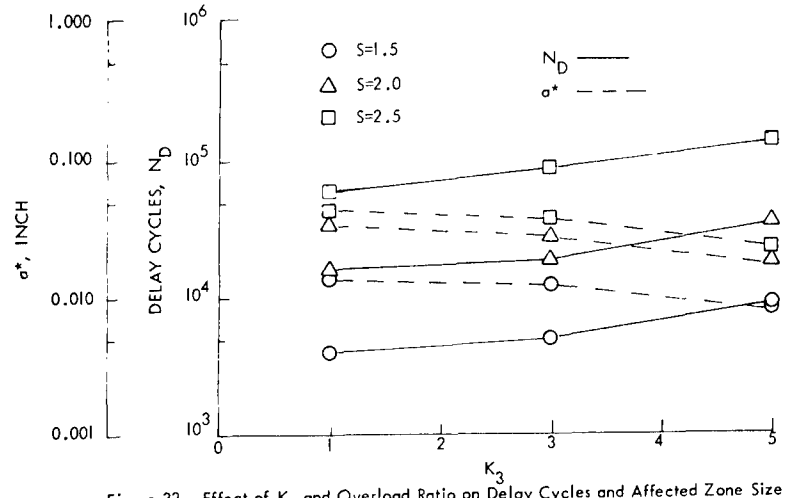

Figure 32. Effect of K_3 and Overload Ratio on Delay Cycles and Affected Zone Size for K_2=10 and K_4=0

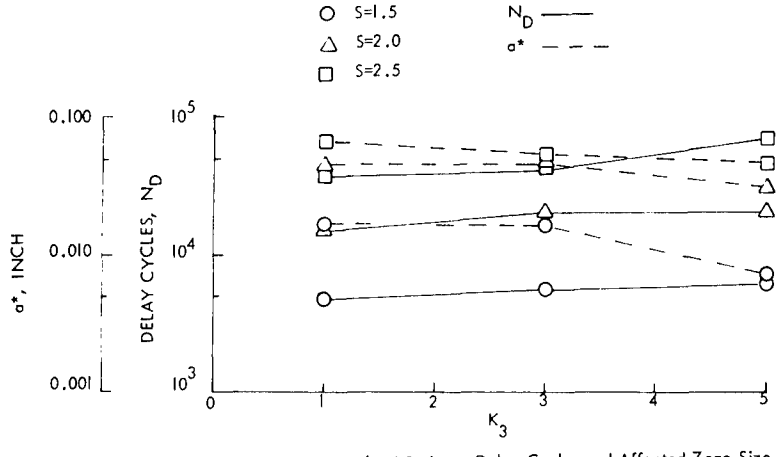

Figure 33. Effect of K_3 and Overload Ratio on Delay Cycles and Affected Zone Size for K_2=10 and K_5= -7.5

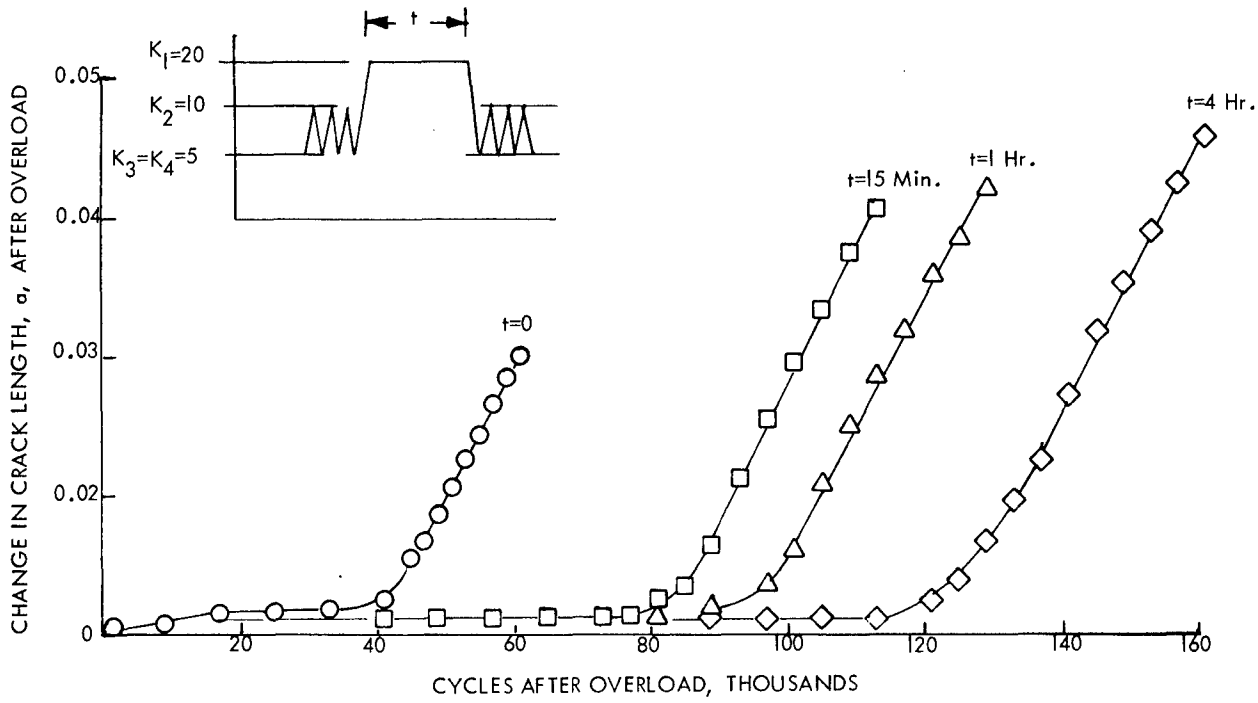

Figure 34. Effect of Hold Time in Tension on Crack Growth History

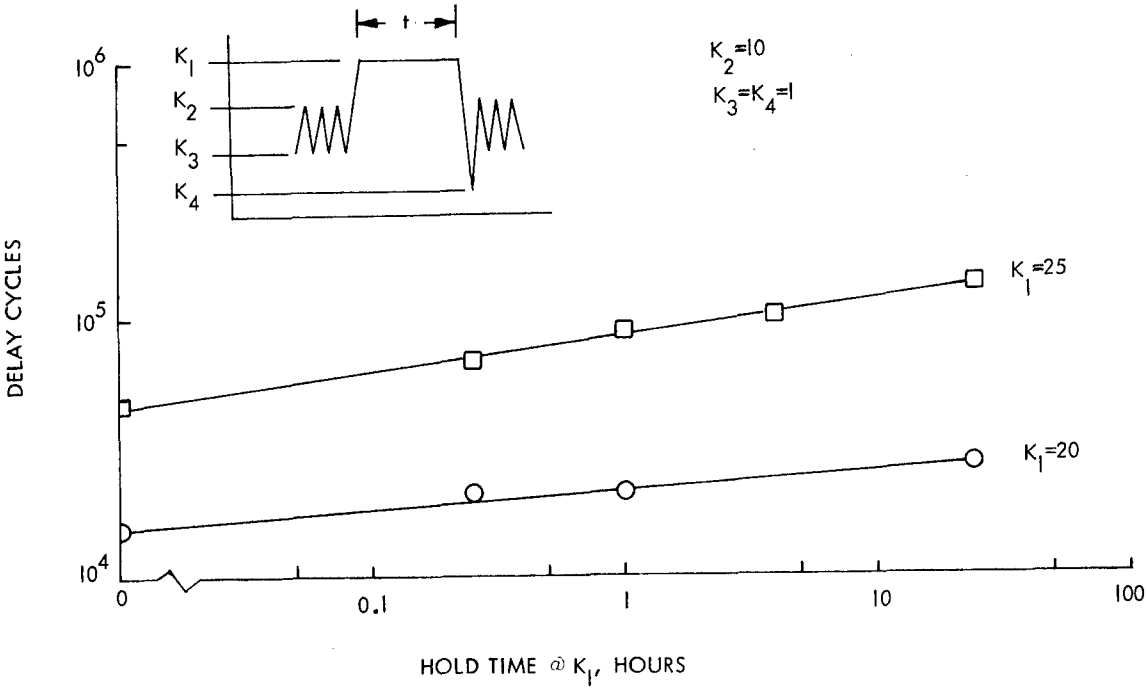

Figure 35. Effect of K_1 and Hold Time at K_1 on Delay Cycles

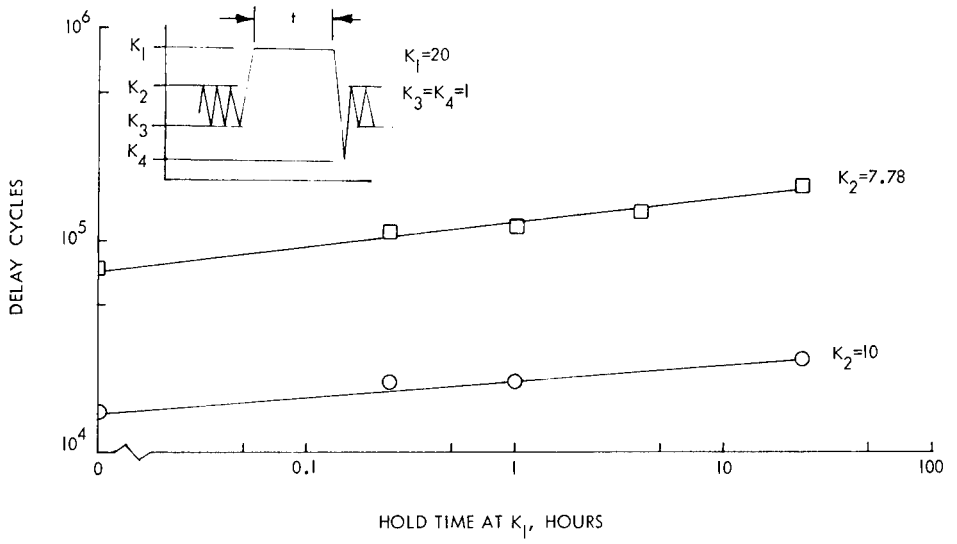

Figure 36. Effect of K_2 and Hold Time at K_1 on Delay Cycles

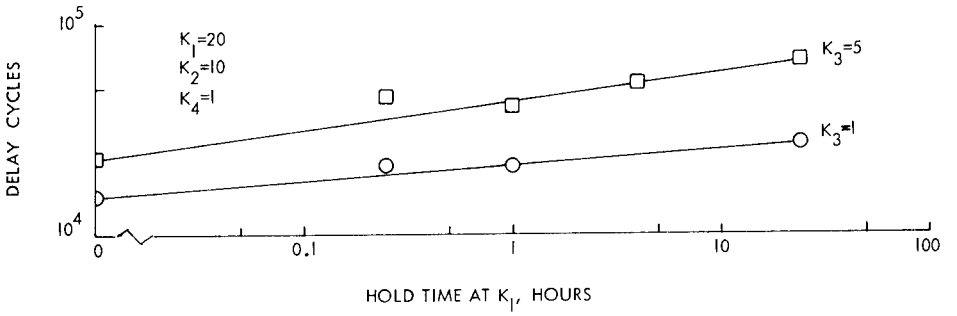

Figure 37. Effect of K_3 and Hold Time at K_1 on Delay Cycles

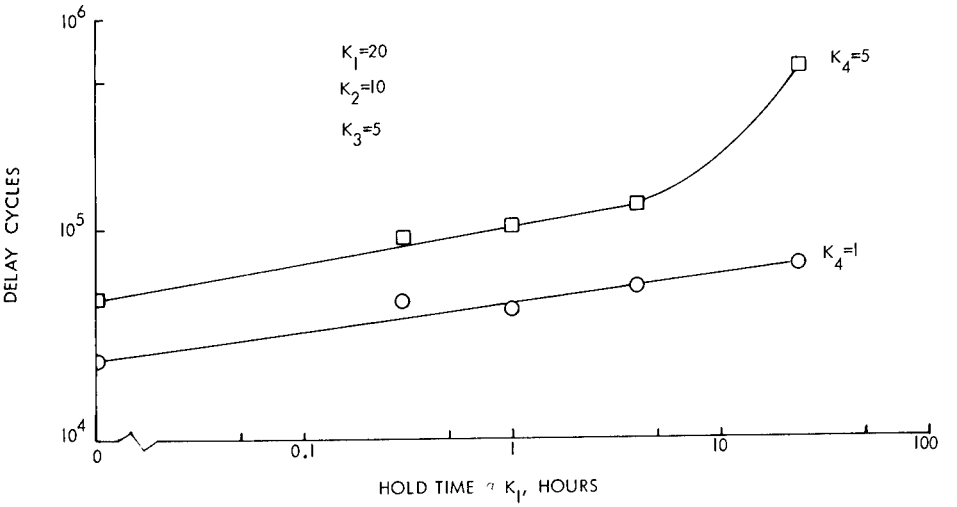

Figure 38. Effect of K_4 and Hold Time at K_1 on Delay Cycles

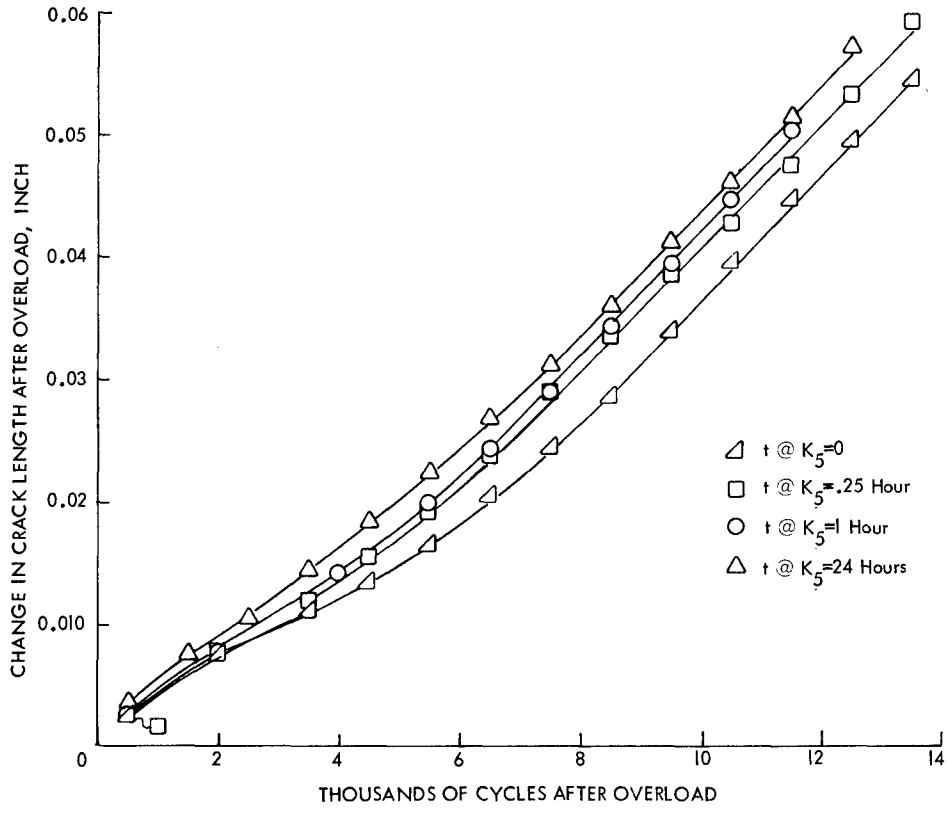

Figure 39. Effect of Hold Time at K_5 for K_1=20, K_2=10, K_3=1 and K_5= -25

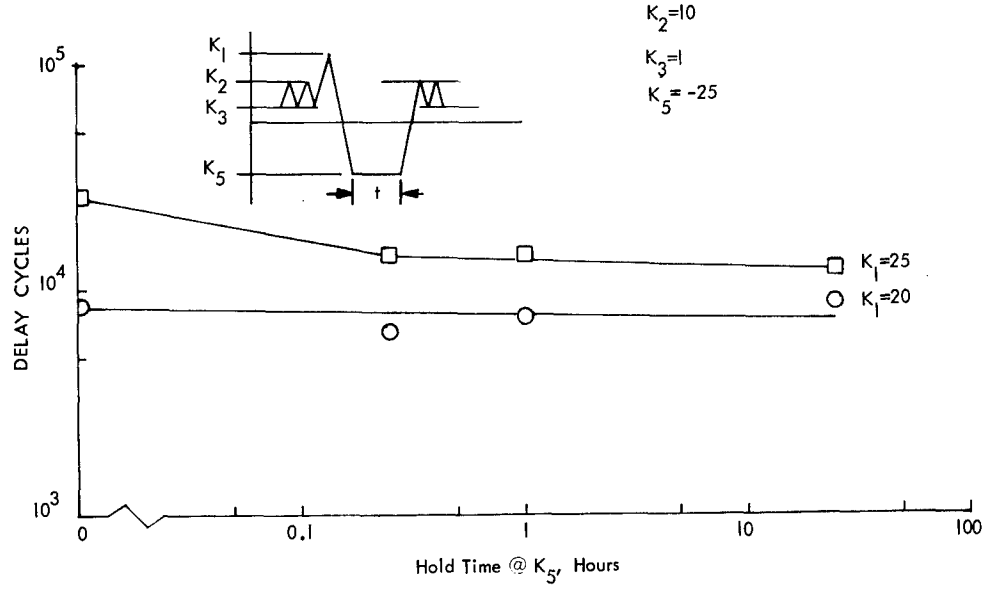

Figure 40. Effect of K_1 and Hold Time at K_5 on Delay Cycles

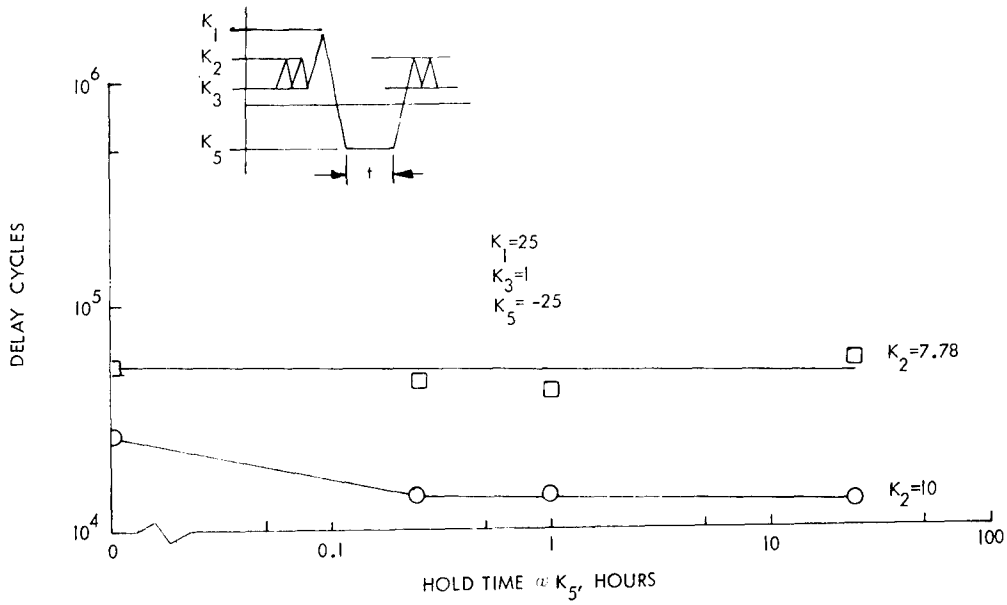

Figure 41. Effects of K_2 and Hold Time at K_5 on Delay Cycles

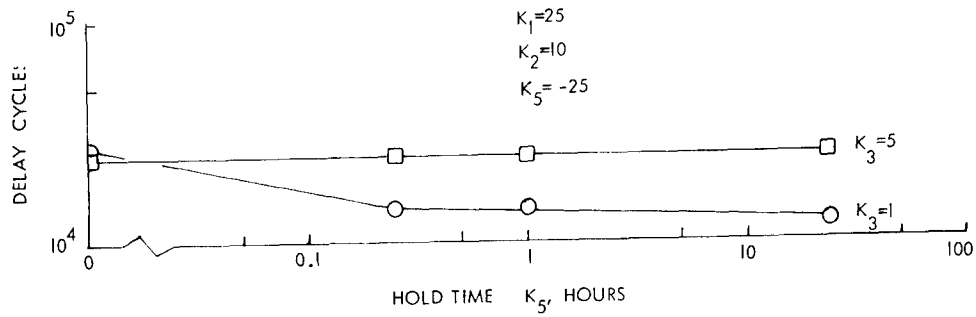

Figure 42. Effects of K_3 and Hold Time at K_5 on Delay Cycles

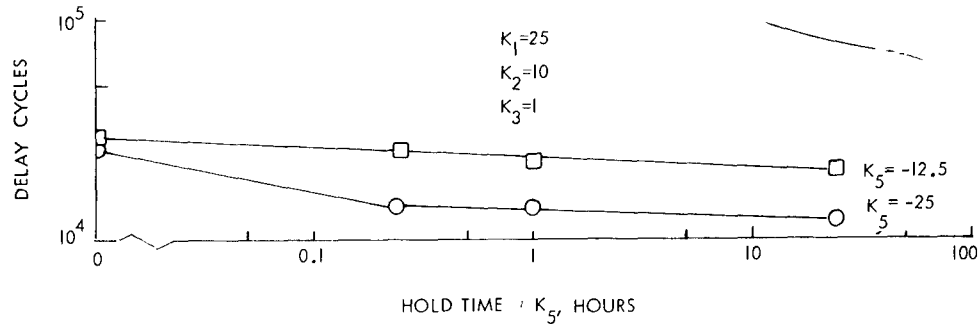

Figure 43. Effects of K_5 and Hold Time at K_5 on Delay Cycles

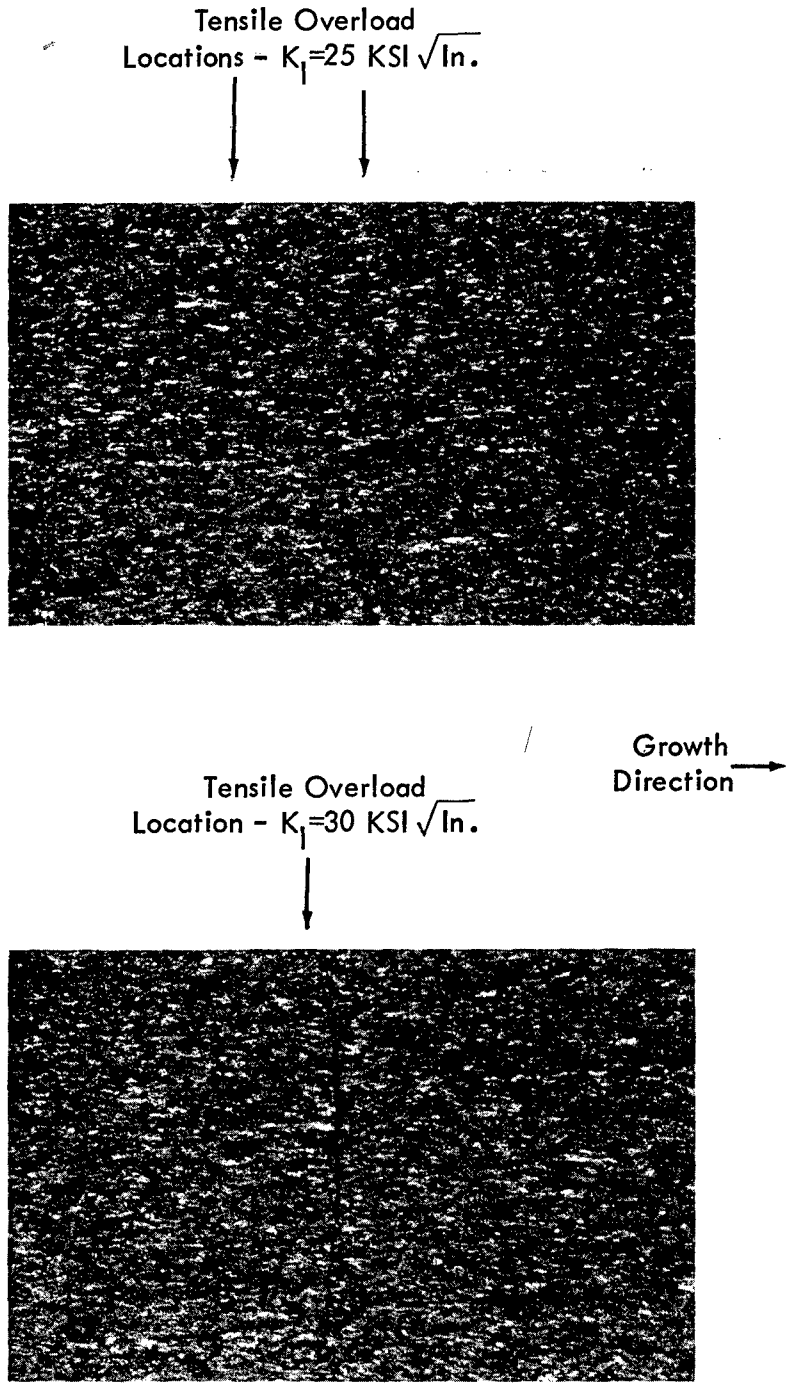

Figure 44. Fracture Surface Features Produced by Tensile Overloads of 25 and 30 KSI$\sqrt{In.}$, Magnification = 10

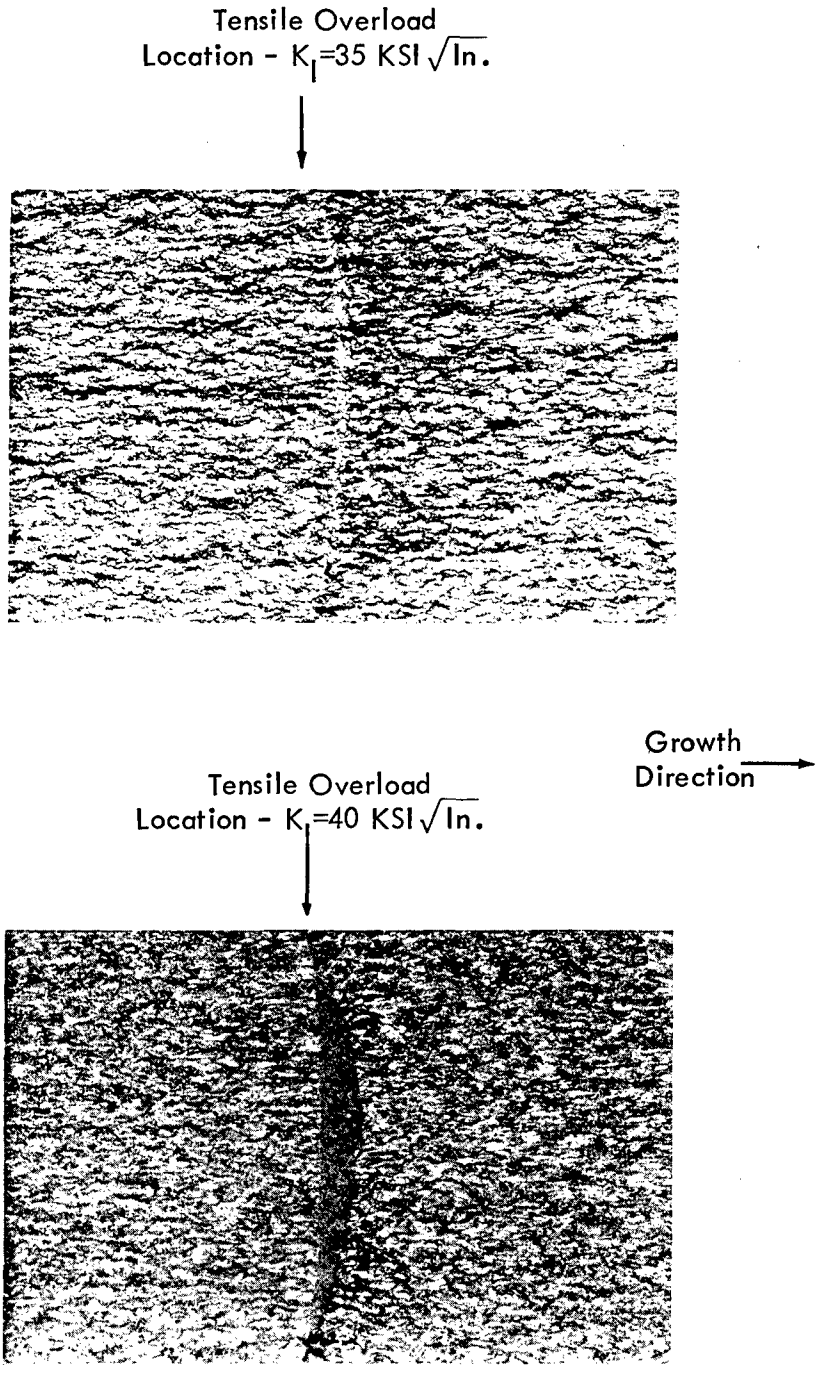

Figure 45. Fracture Surface Features Produced by Tensile Overloads of 35 and 40 KSI $\sqrt{In.}$, Magnification - 10

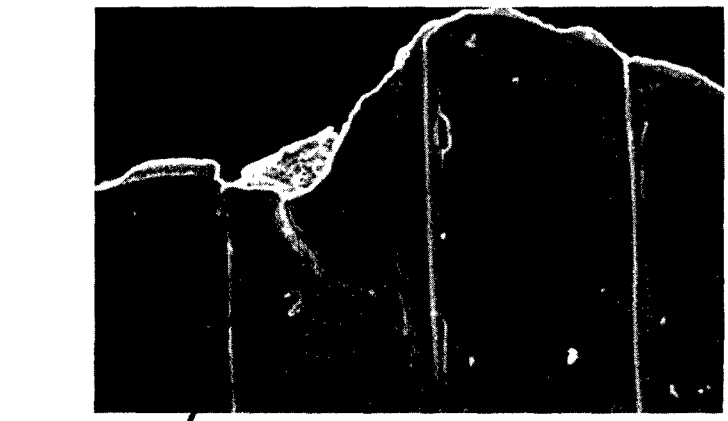

Specimen Surface

100X

Tensile Overload Location - K_I=49 KSI$\sqrt{\text{In.}}$

Growth Direction →

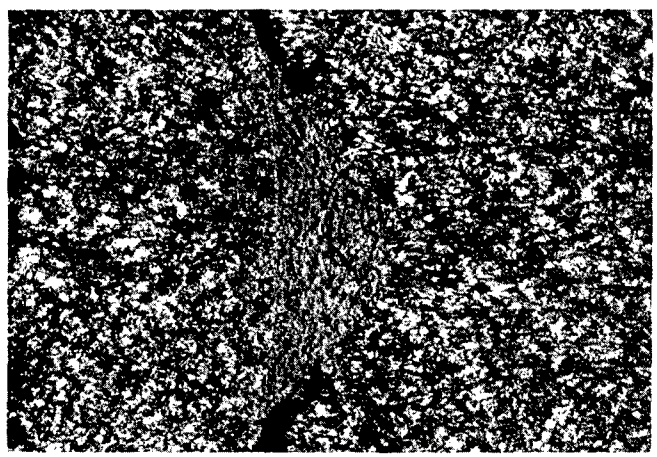

Fracture Surface

10X

Figure 46. Fracture Surface and Specimen Surface Showing Features Produced by a Tensile Overload of 49 KSI$\sqrt{\text{In.}}$

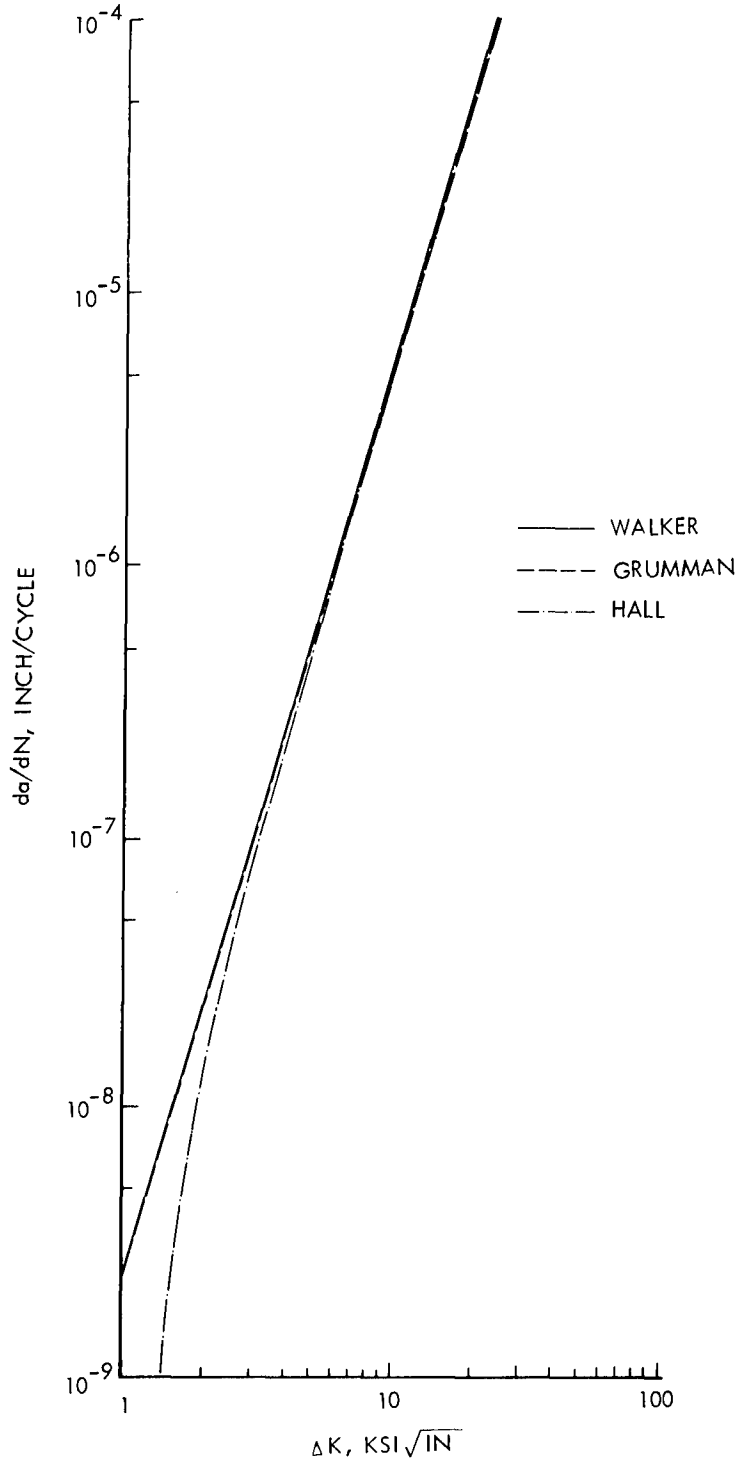

Figure 47. da/dN vs. ΔK Calculated for R=0.1 Using Three Different Growth Rate Equations for 2219-T851 Aluminum Alloy

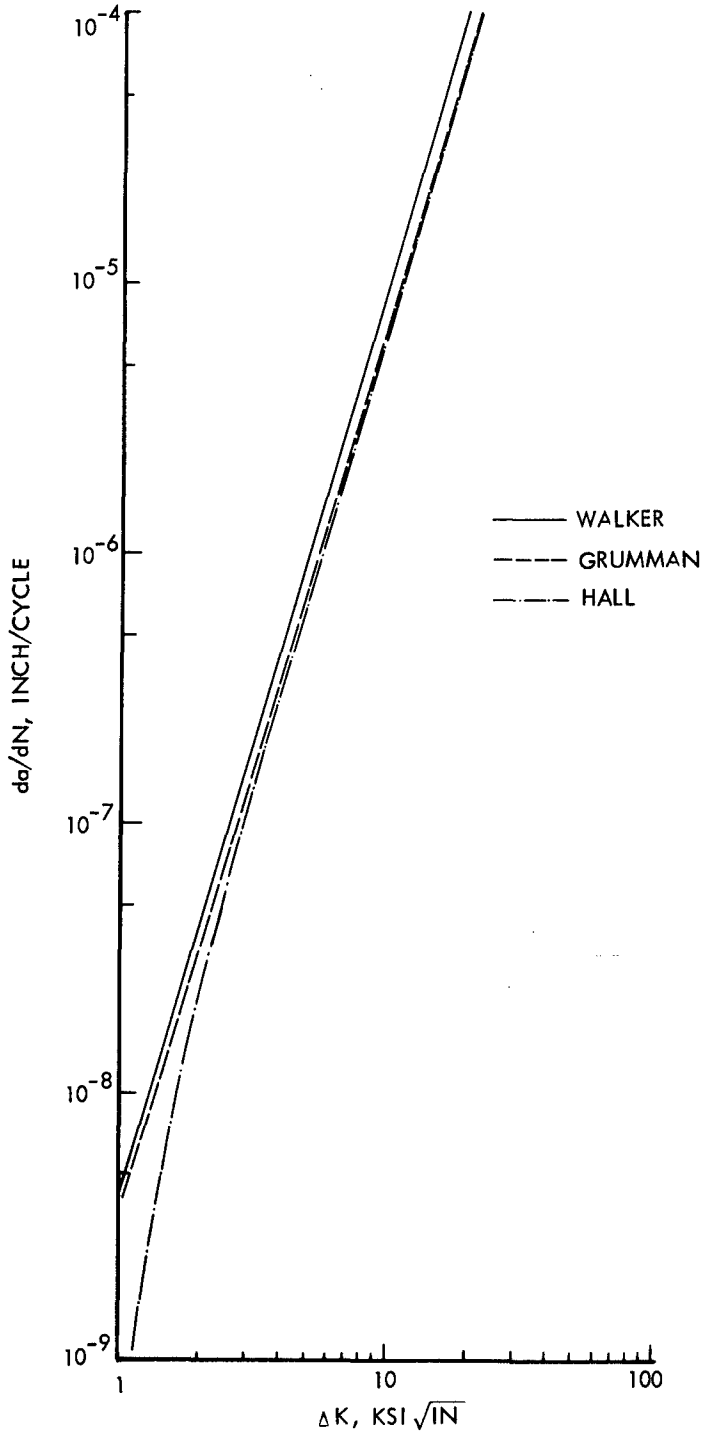

Figure 48. da/dN vs. ΔK Calculated for R=0.3 Using Three Different Growth Rate Equations for 2219-T851 Aluminum Alloy

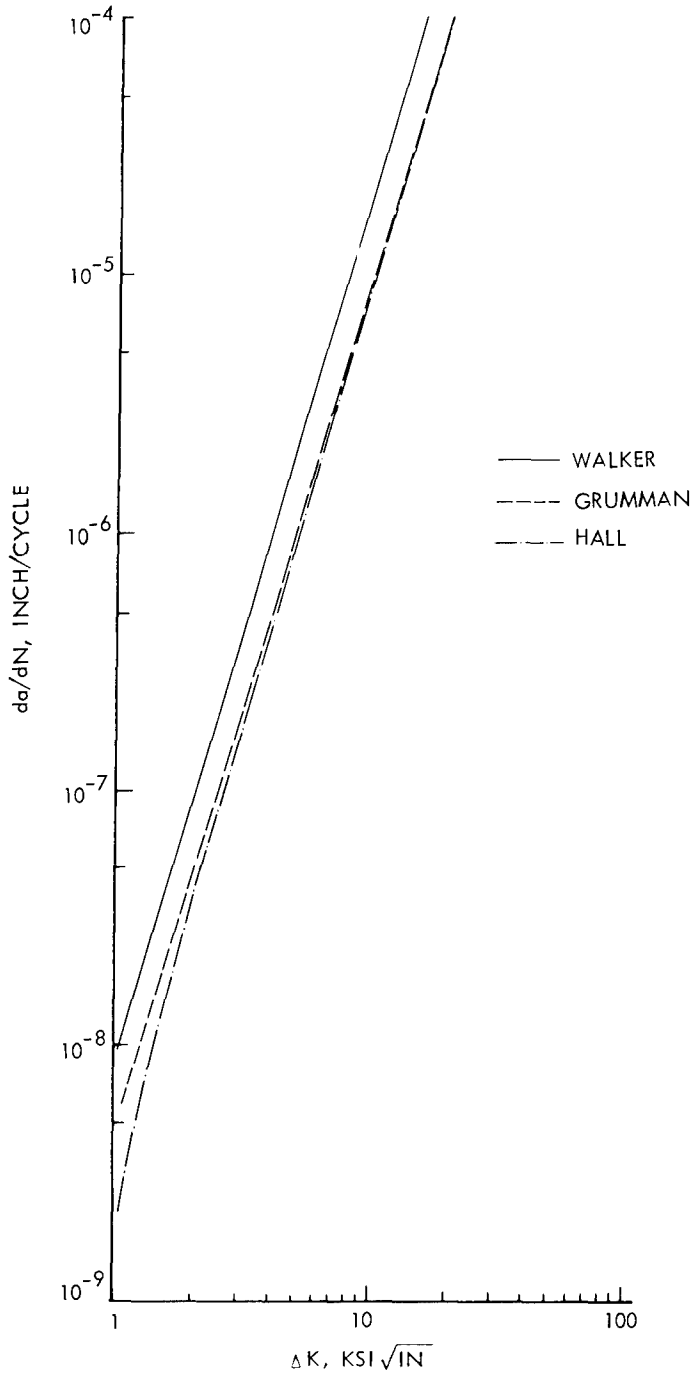

Figure 49. da/dN vs. ΔK Calculated for R=0.5 Using Three Different Growth Rate Equations for 2219-T851 Aluminum Alloy

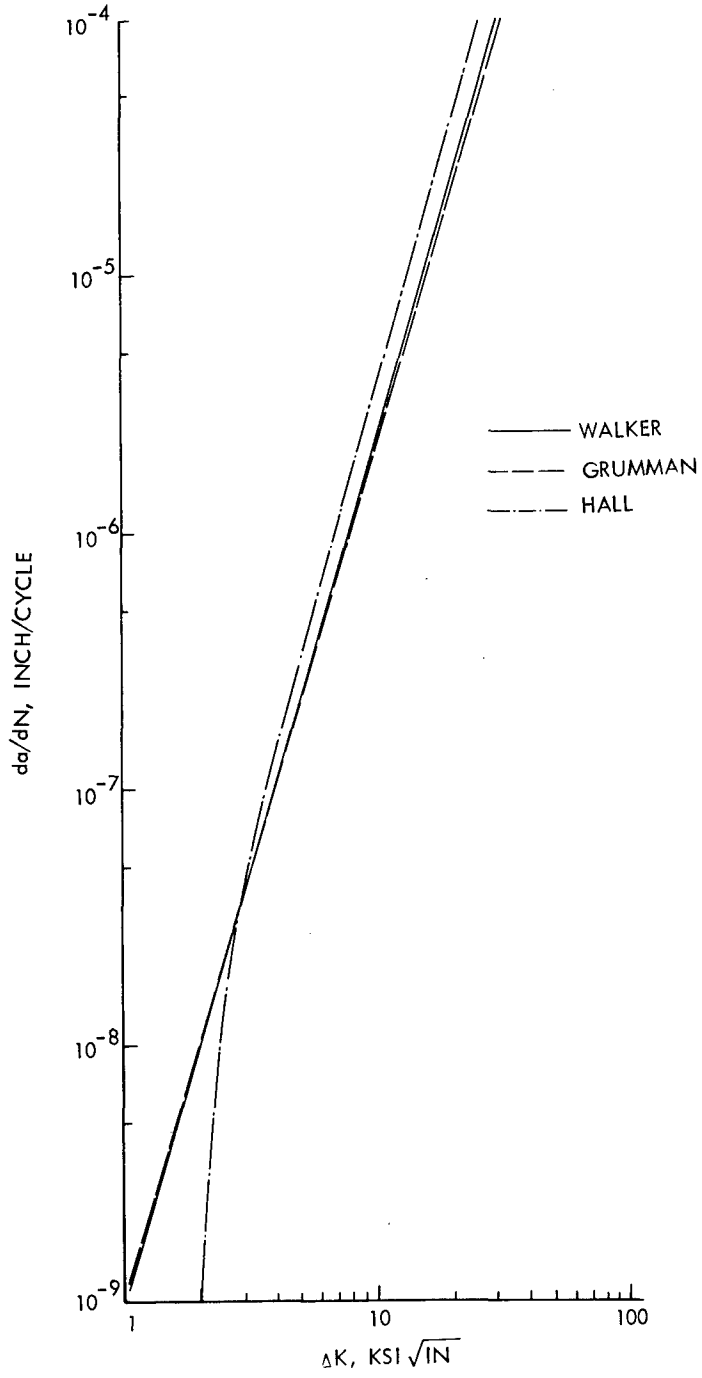

Figure 50. da/dN vs. ΔK Calculated for R= -0.3 Using Three Different Growth Rate Equations for 2219-T851 Aluminum Alloy

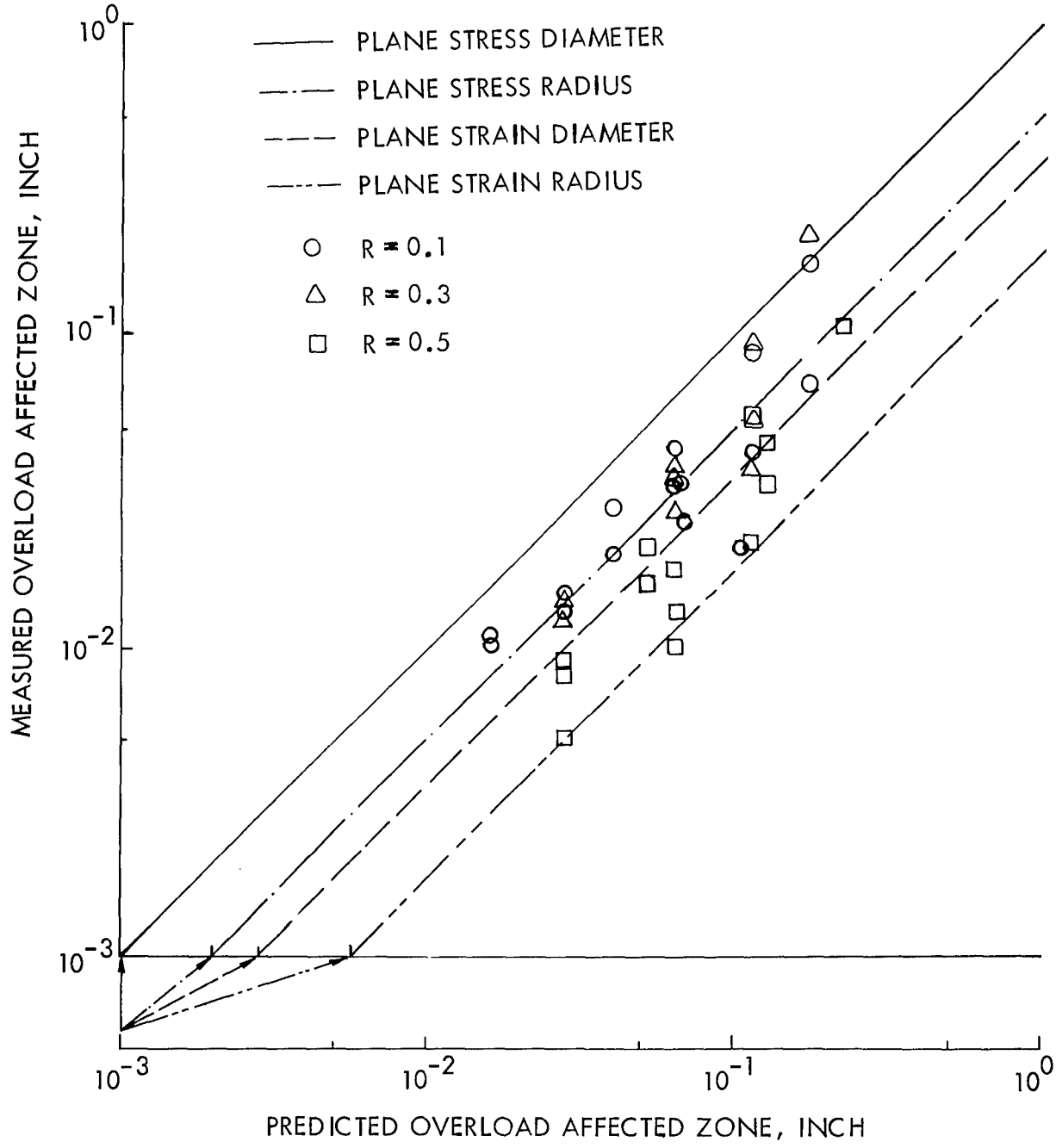

Figure 51 . Correlations of Predicted and Measured Overload Affected Zones for 2219-T851 Aluminum Alloy Plates Subjected to Tension-Tension and Tension-Zero Overloads

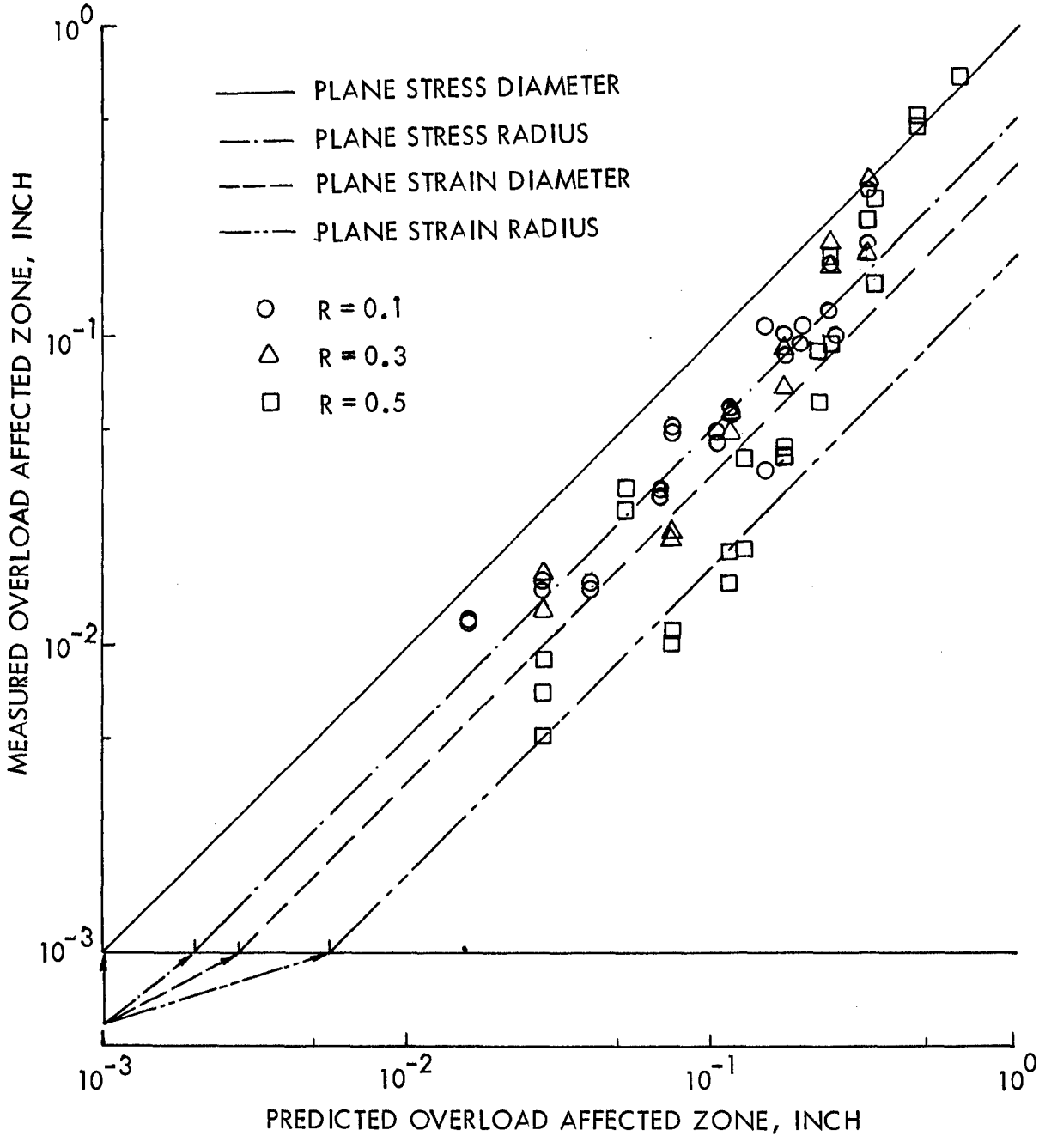

Figure 52 . Correlations of Predicted and Measured Overload Affected Zones for 2219-T851 Aluminum Alloy Plates Subjected to Tension-Compression Overloads

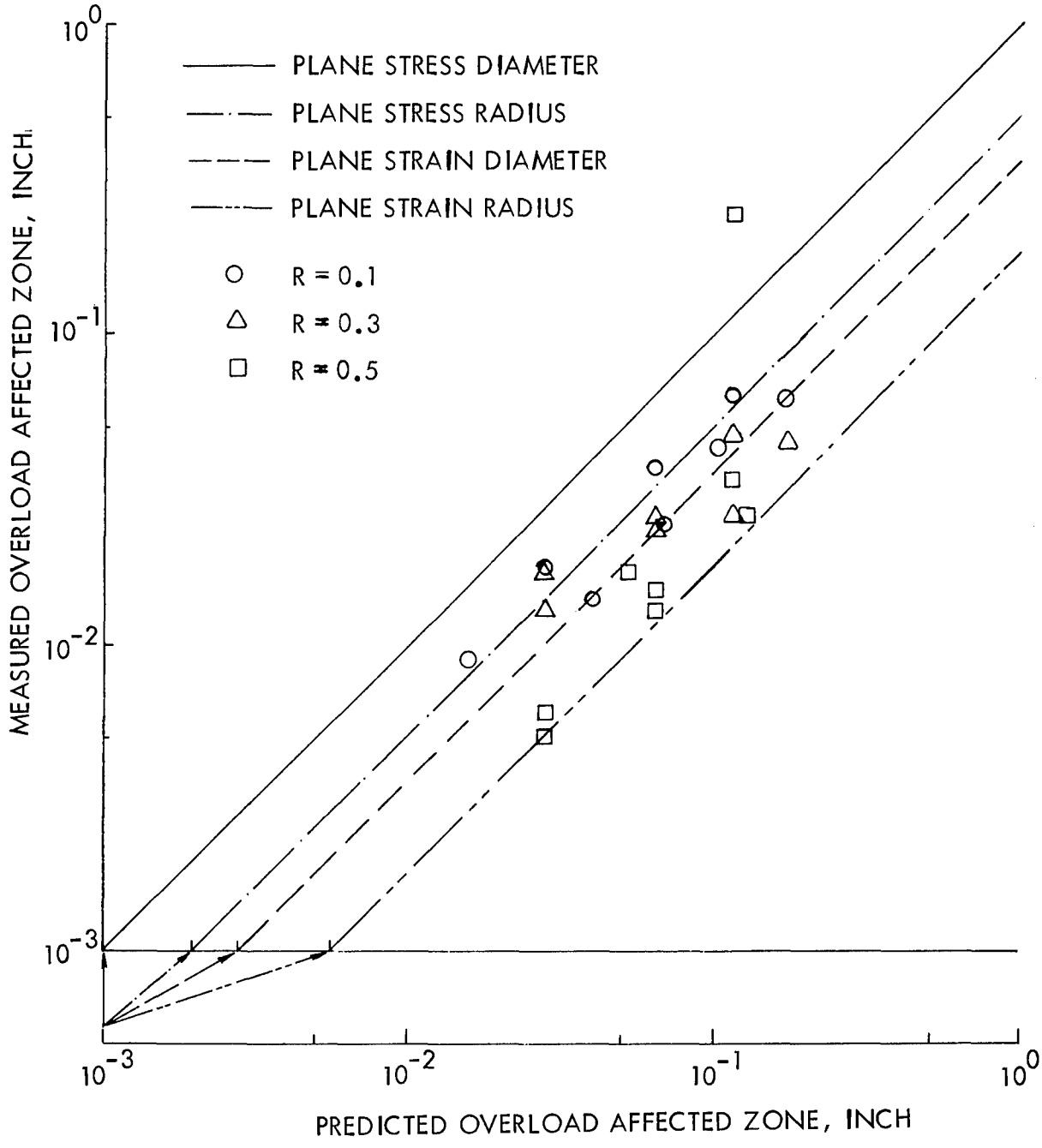

Figure 53 . Correlations of Predicted and Measured Overload Affected Zones for 2219-T851 Aluminum Alloy Plates Subjected to Zero-Tension and Compression-Tension Overloads

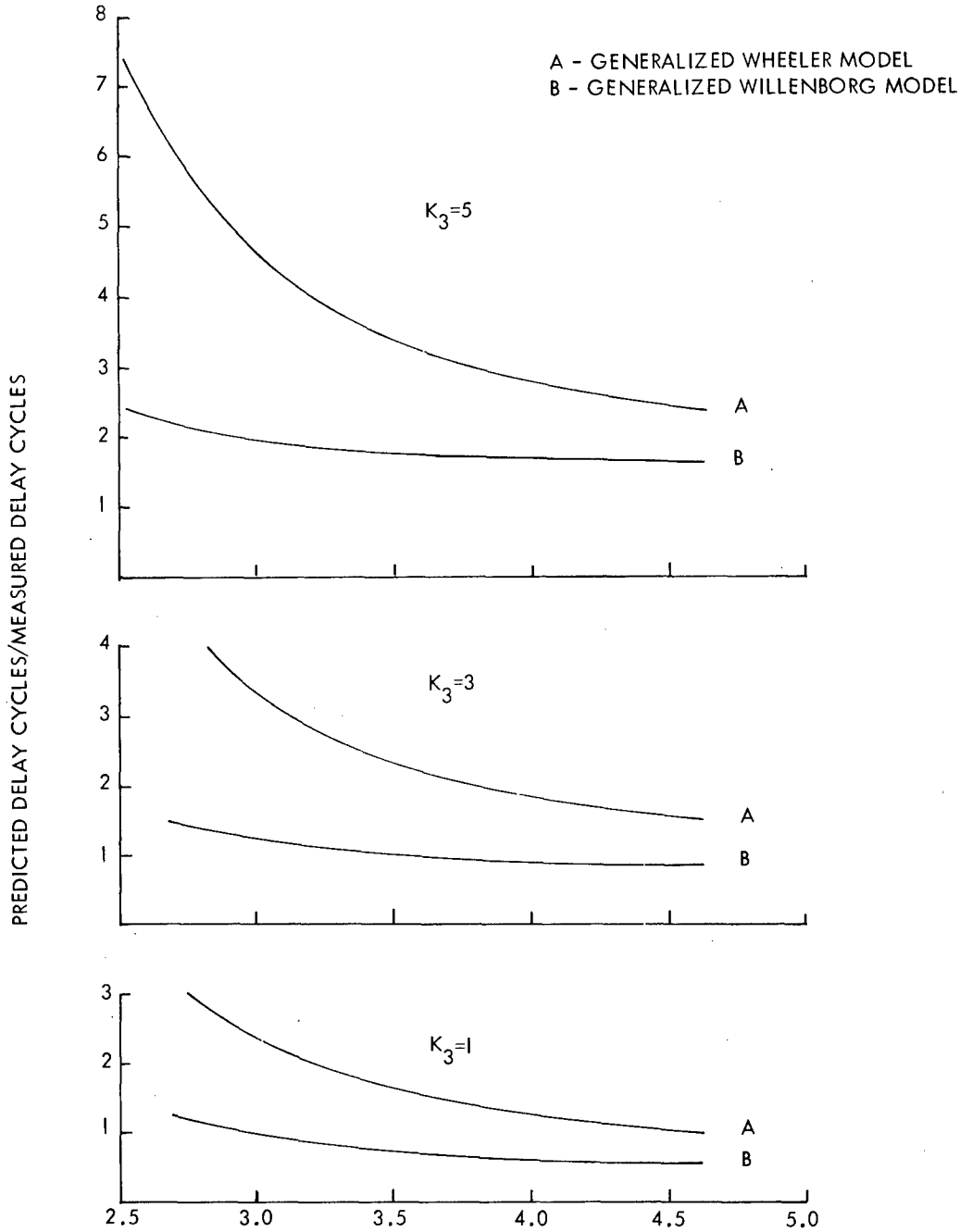

Figure 54. Effect of Overload Shut-Off Ratio on Predicted Delay Cycles for K_1=20, K_2=10, K_4=20 and Various K_3

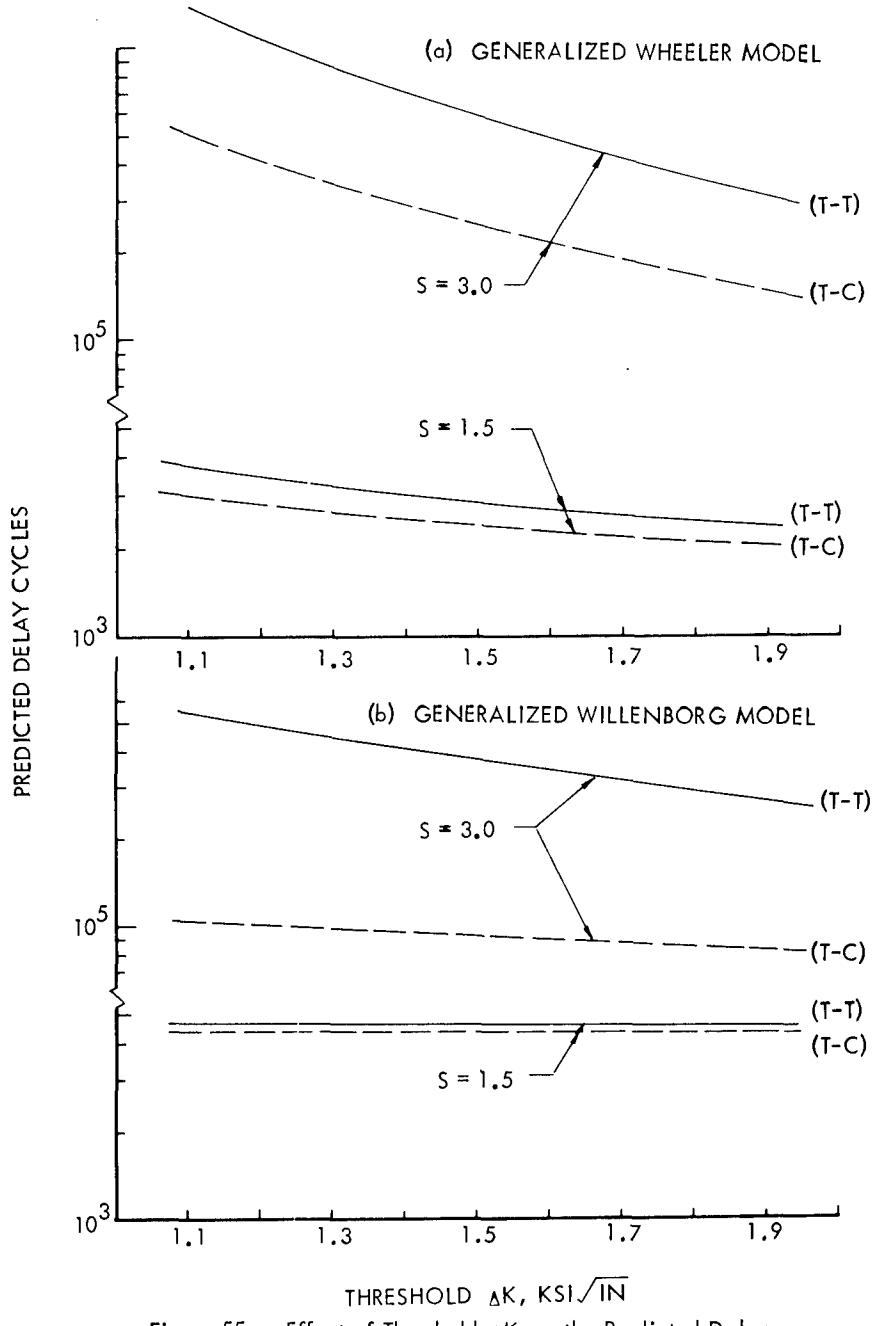

Figure 55 . Effect of Threshold ΔK on the Predicted Delay Cycles Using the Generalized Wheeler and Generalized Willenborg Models for K_2=10, K_3=1 and Various Overloads and Compressive Loads (K_5= - 1/2 K_1)

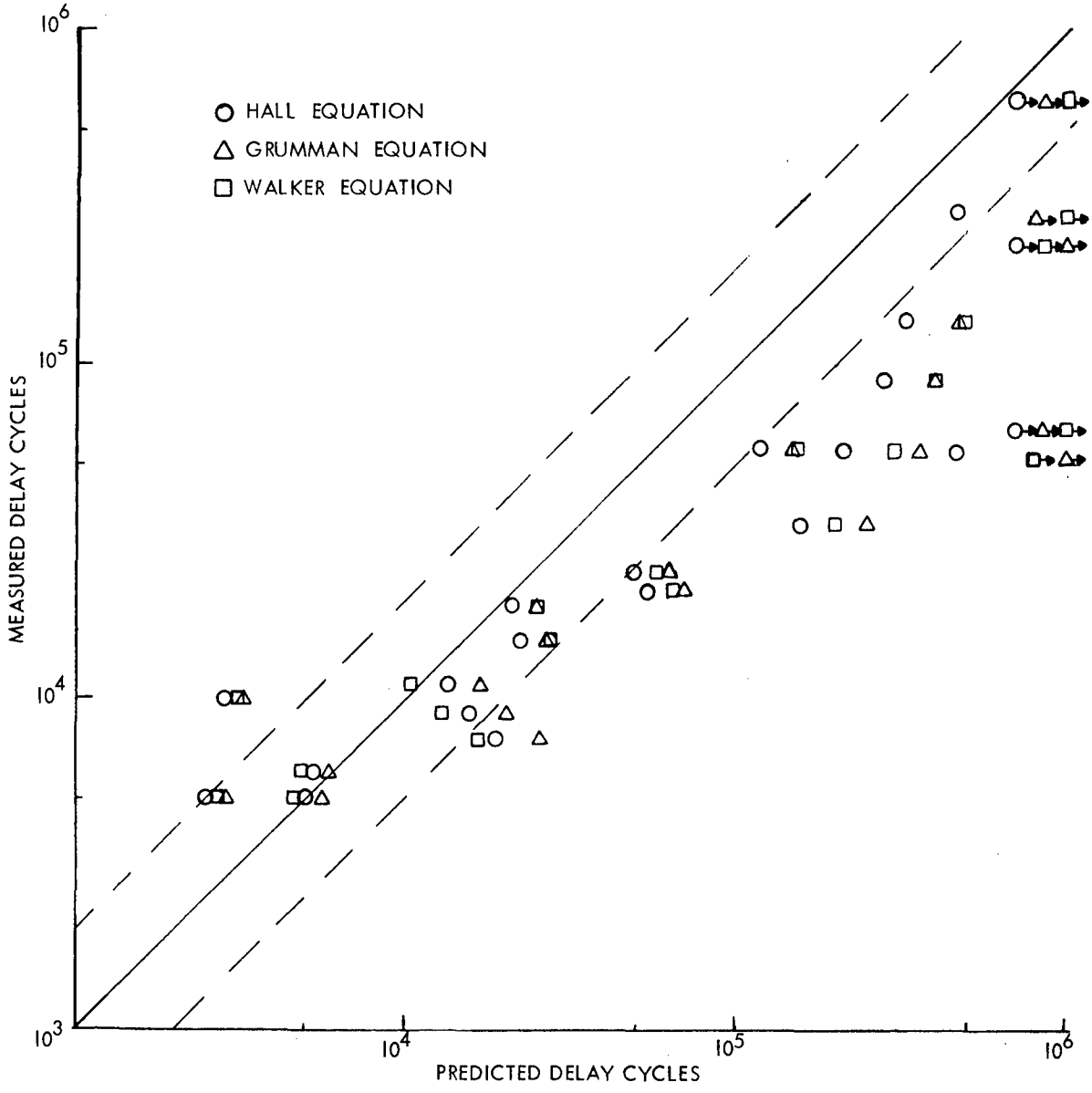

Figure 56. Correlations of Predicted and Measured Delay Cycles Using the Generalized Wheeler Model and Various Crack Growth Rate Equations for 2219-T851 Aluminum Alloy Plate Subjected to Tension-Tension Overloads

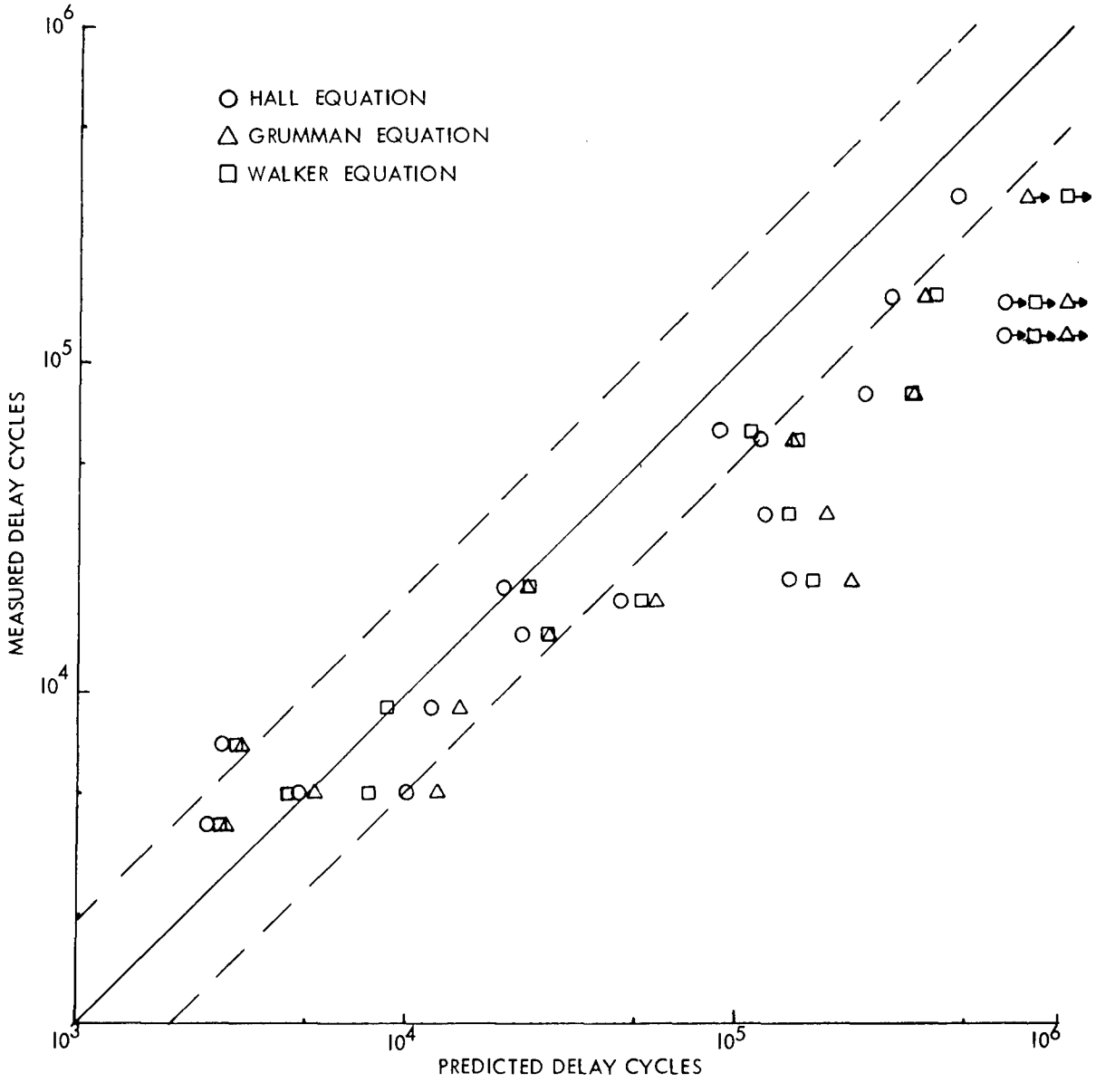

Figure 57. Correlations of Predicted and Measured Delay Cycles Using the Generalized Wheeler Model and Various Crack Growth Rate Equations for 2219-T851 Aluminum Alloy Plate Subjected to Tension-Zero Overloads

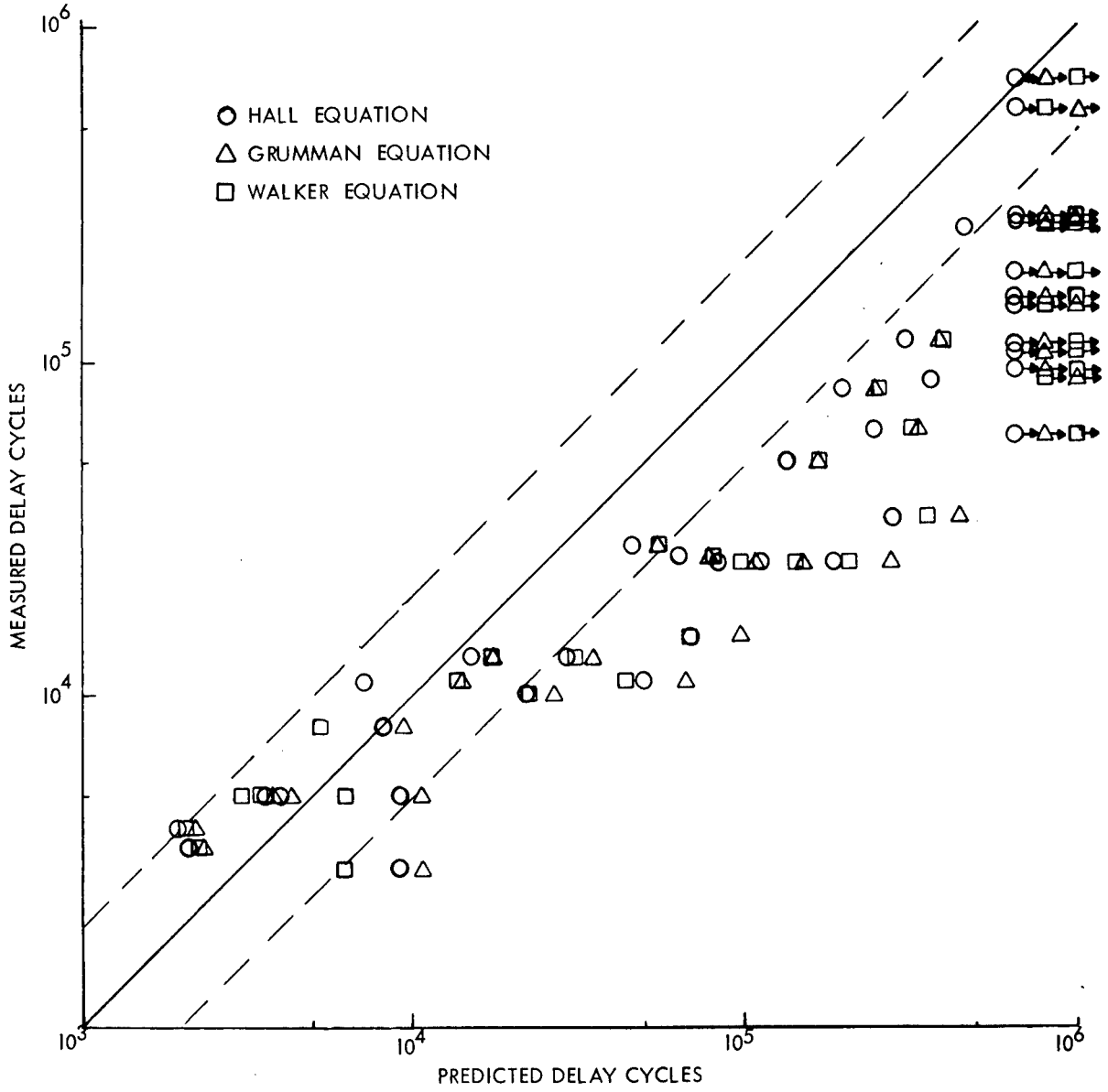

Figure 58. Correlations of Predicted and Measured Delay Cycles Using the Generalized Wheeler Model and Various Crack Growth Rate Equations for 2219-T851 Aluminum Alloy Plate Subjected to Tension-Compression Overloads and K_2=10 KSI$\sqrt{in.}$

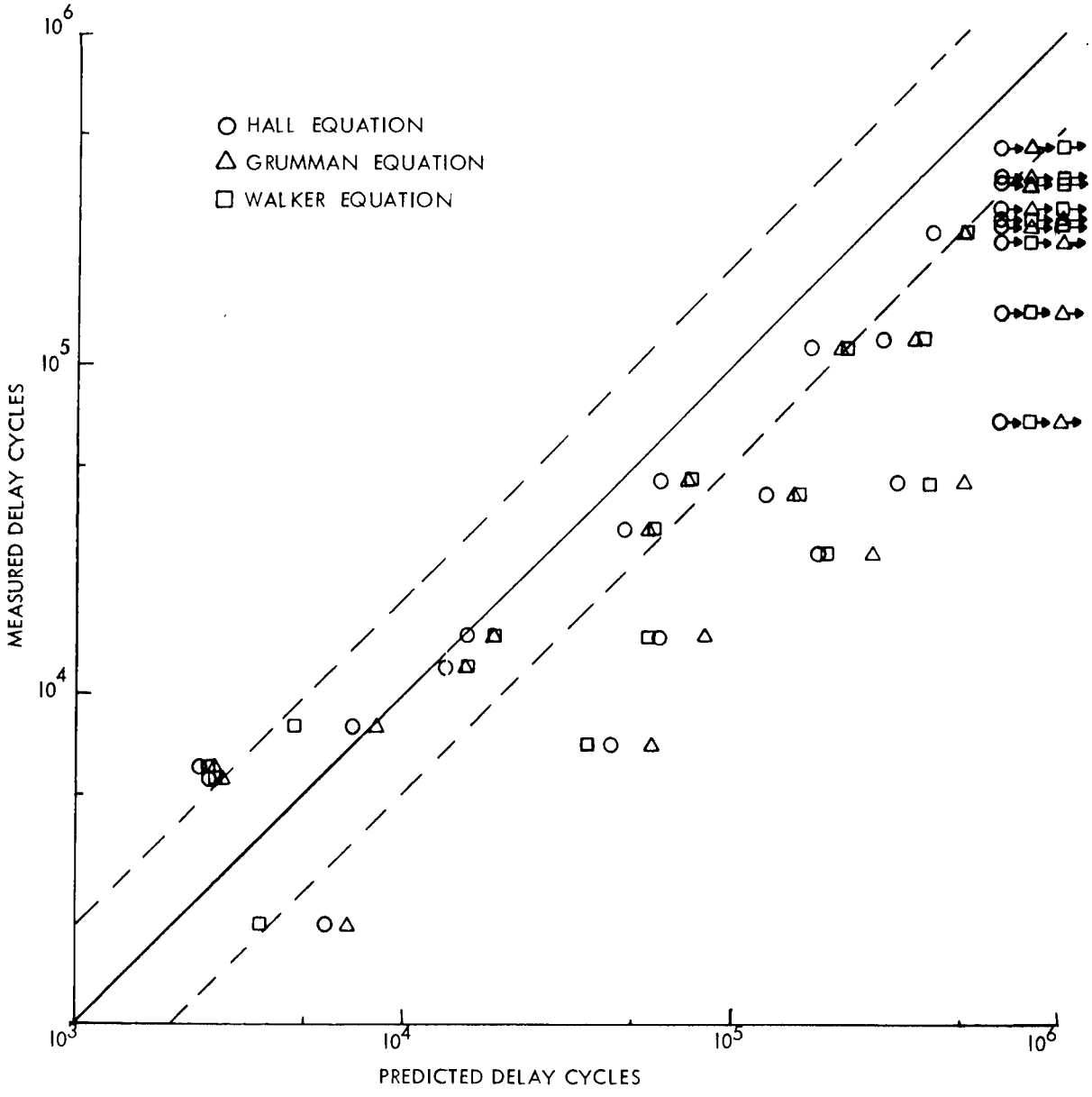

Figure 59. Correlations of Predicted and Measured Delay Cycles Using the Generalized Wheeler Model and Various Crack Growth Rate Equations for 2219-T851 Aluminum Alloy Plate Subjected to Tension-Compression Overloads and K_2=7.78 and 14 KSI $\sqrt{in.}$

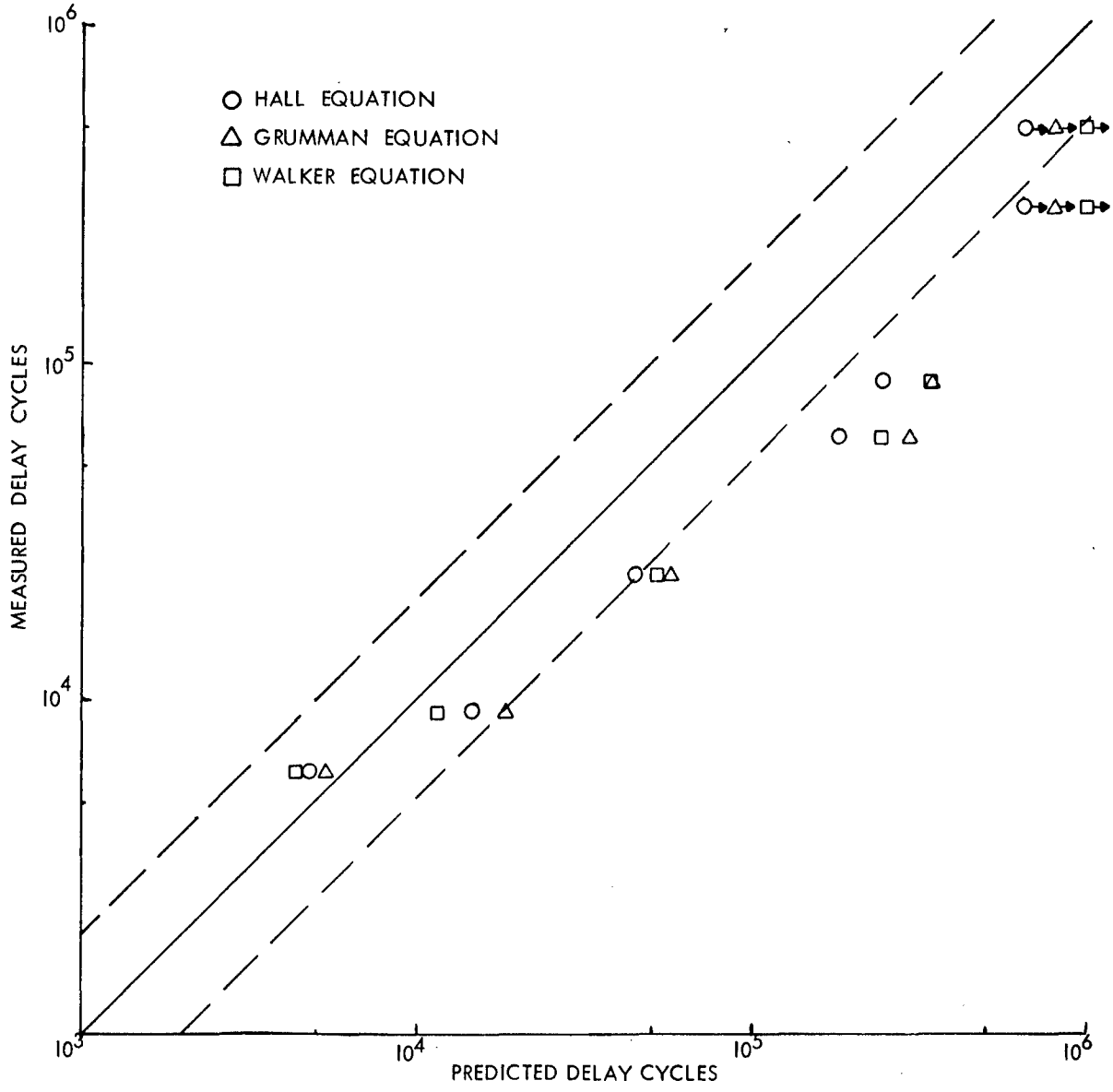

Figure 60. Correlations of Predicted and Measured Delay Cycles Using the Generalized Wheeler Model and Various Crack Growth Rate Equations for 2219-T851 Aluminum Alloy Plate Subject to Zero-Tension Overloads

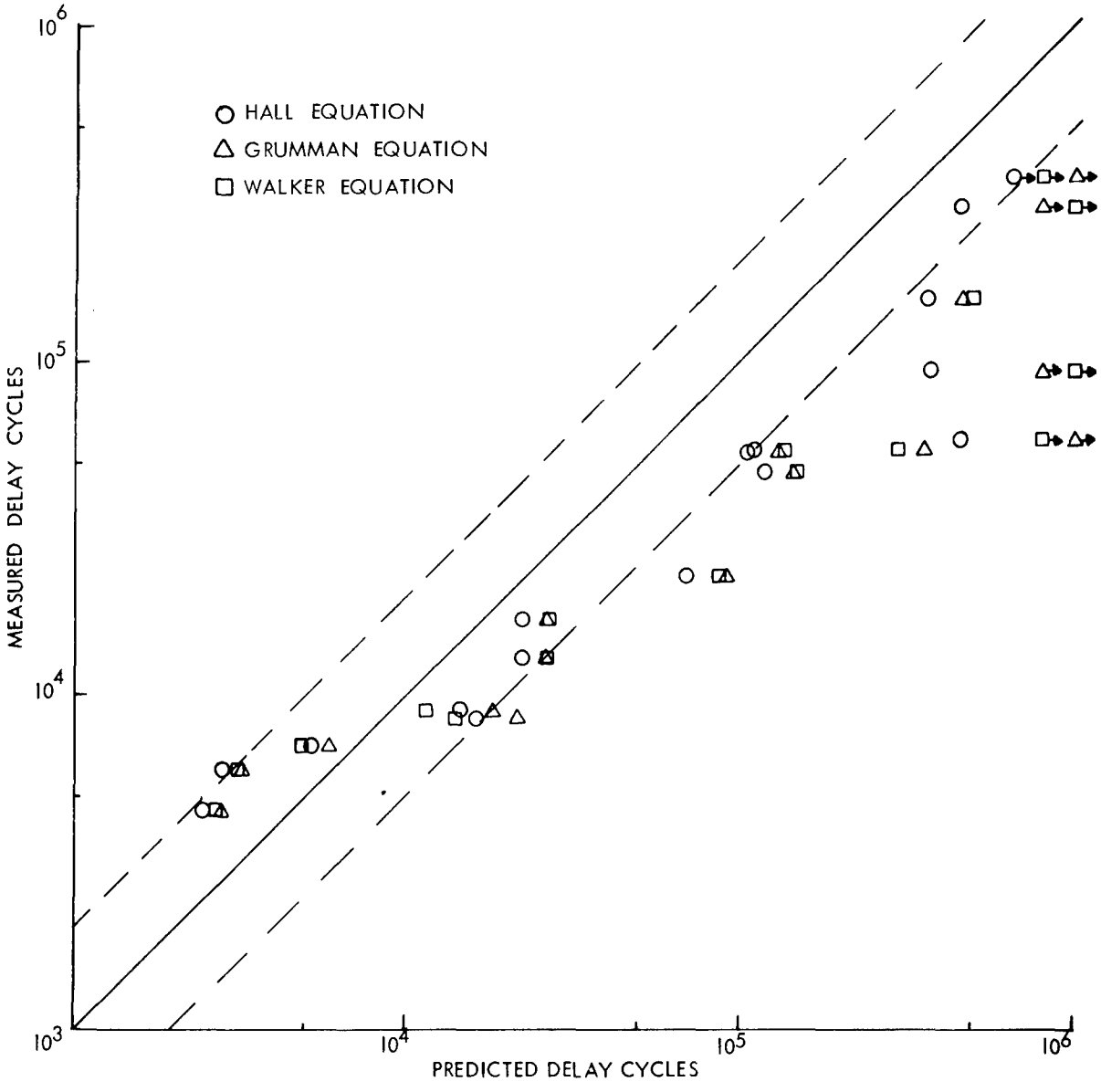

Figure 61. Correlations of Predicted and Measured Delay Cycles Using the Generalized Wheeler Model and Various Crack Growth Rate Equations for 2219-T851 Aluminum Alloy Plate Subjected to Compression-Tension Overloads

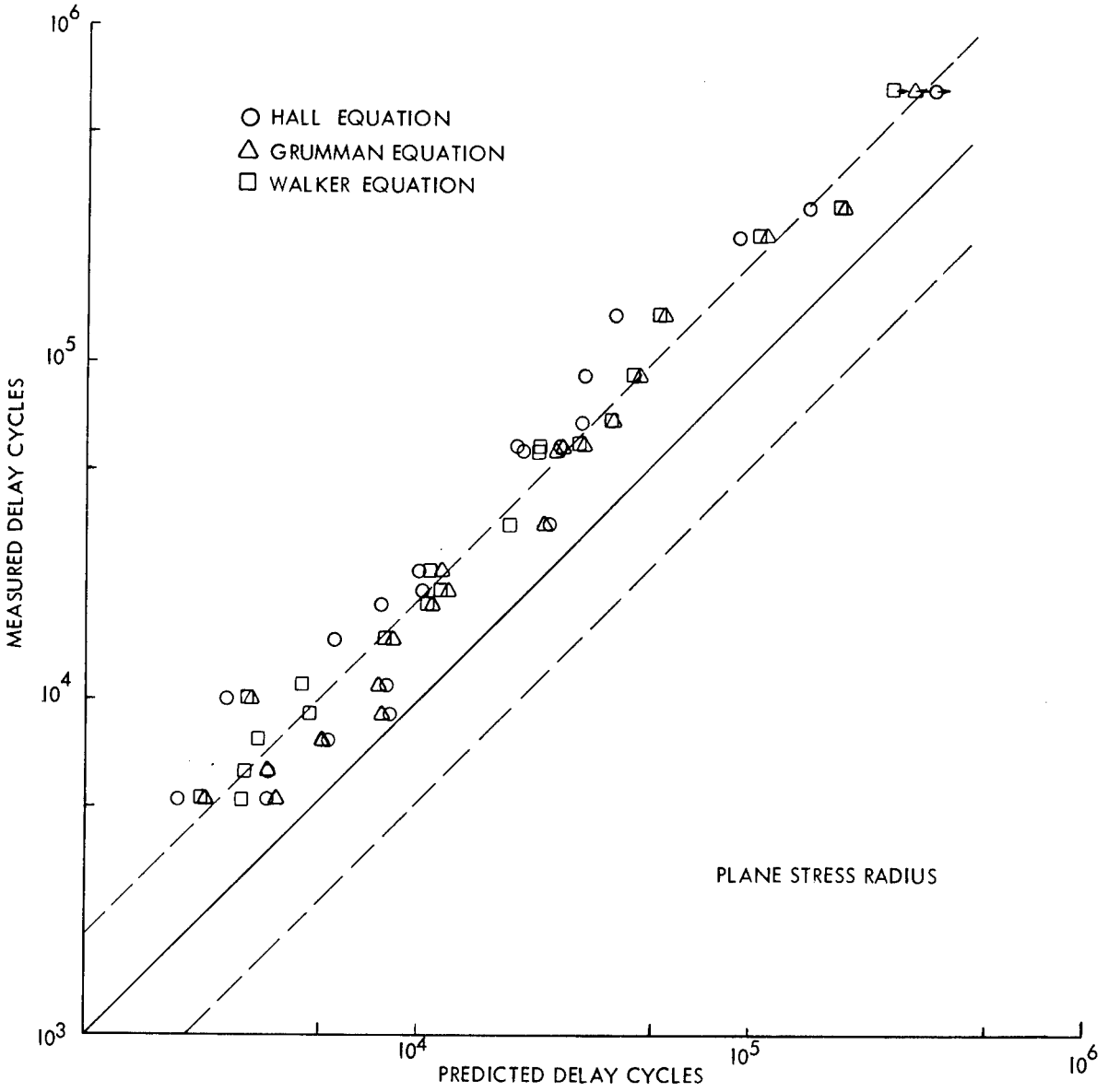

Figure 62. Correlations of Predicted and Measured Delay Cycles Using the Generalized Willenborg Model and Various Crack Growth Rate Equations for 2219-T851 Aluminum Alloy Plate Subjected to Tension-Tension Overloads

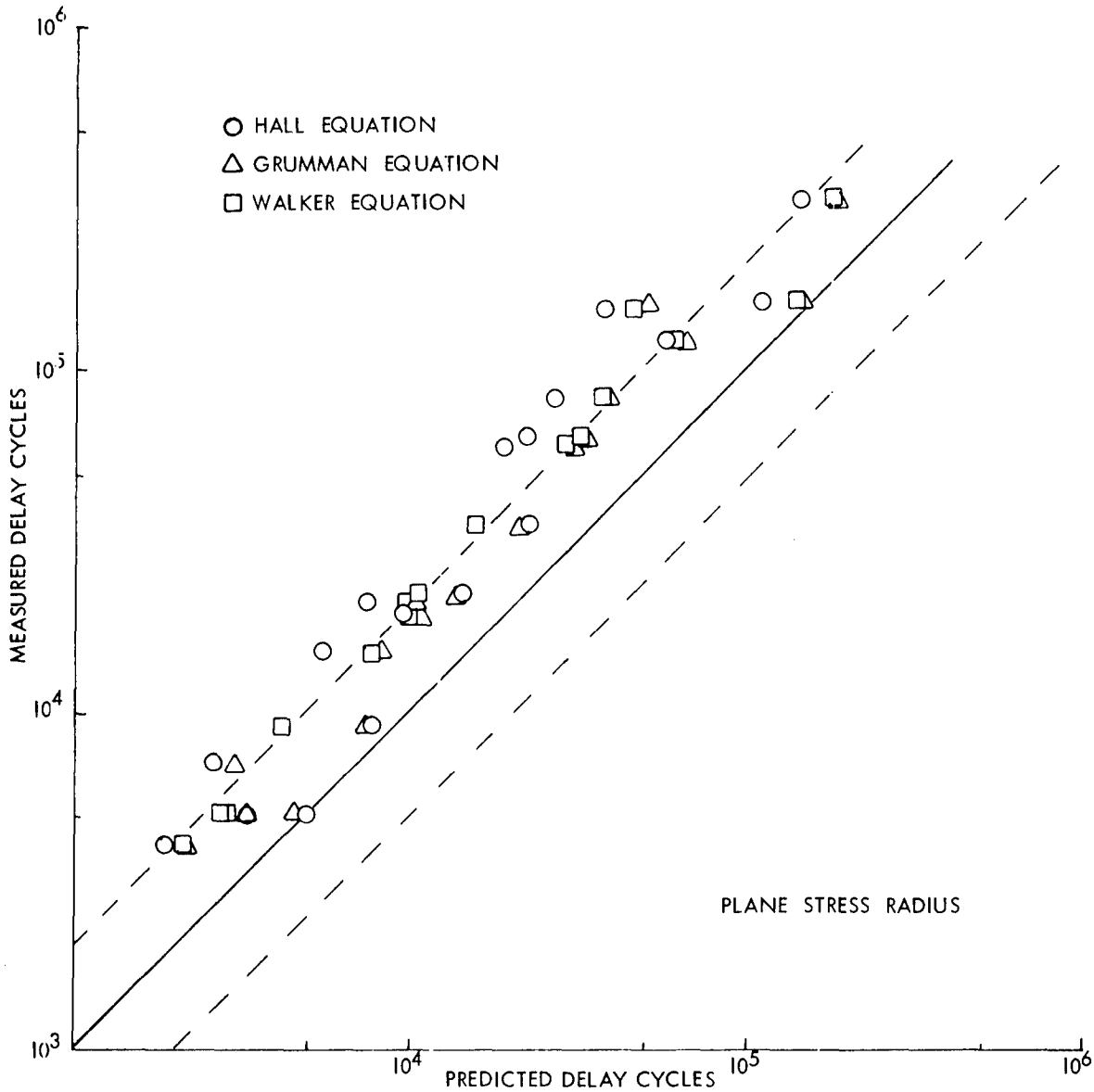

Figure 63. Correlations of Predicted and Measured Delay Cycles Using the Generalized Willenborg Model and Various Crack Growth Rate Equations for 2219-T851 Aluminum Alloy Plate Subjected to Tension-Zero Overloads

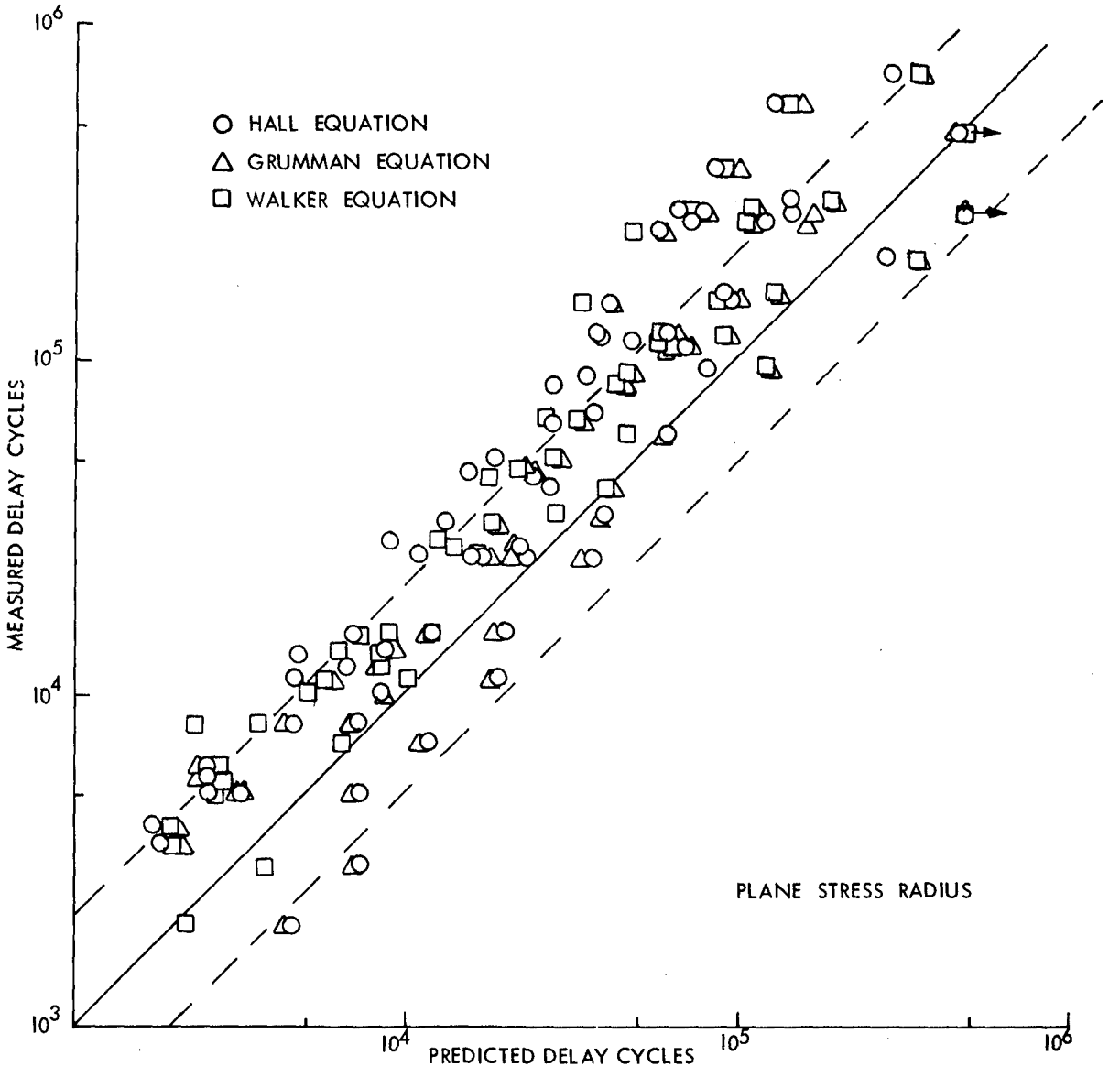

Figure 64. Correlations of Predicted and Measured Delay Cycles Using the Generalized Willenborg Model and Various Crack Growth Rate Equations for 2219-T851 Aluminum Alloy Plate Subjected to Tension-Compression Overloads

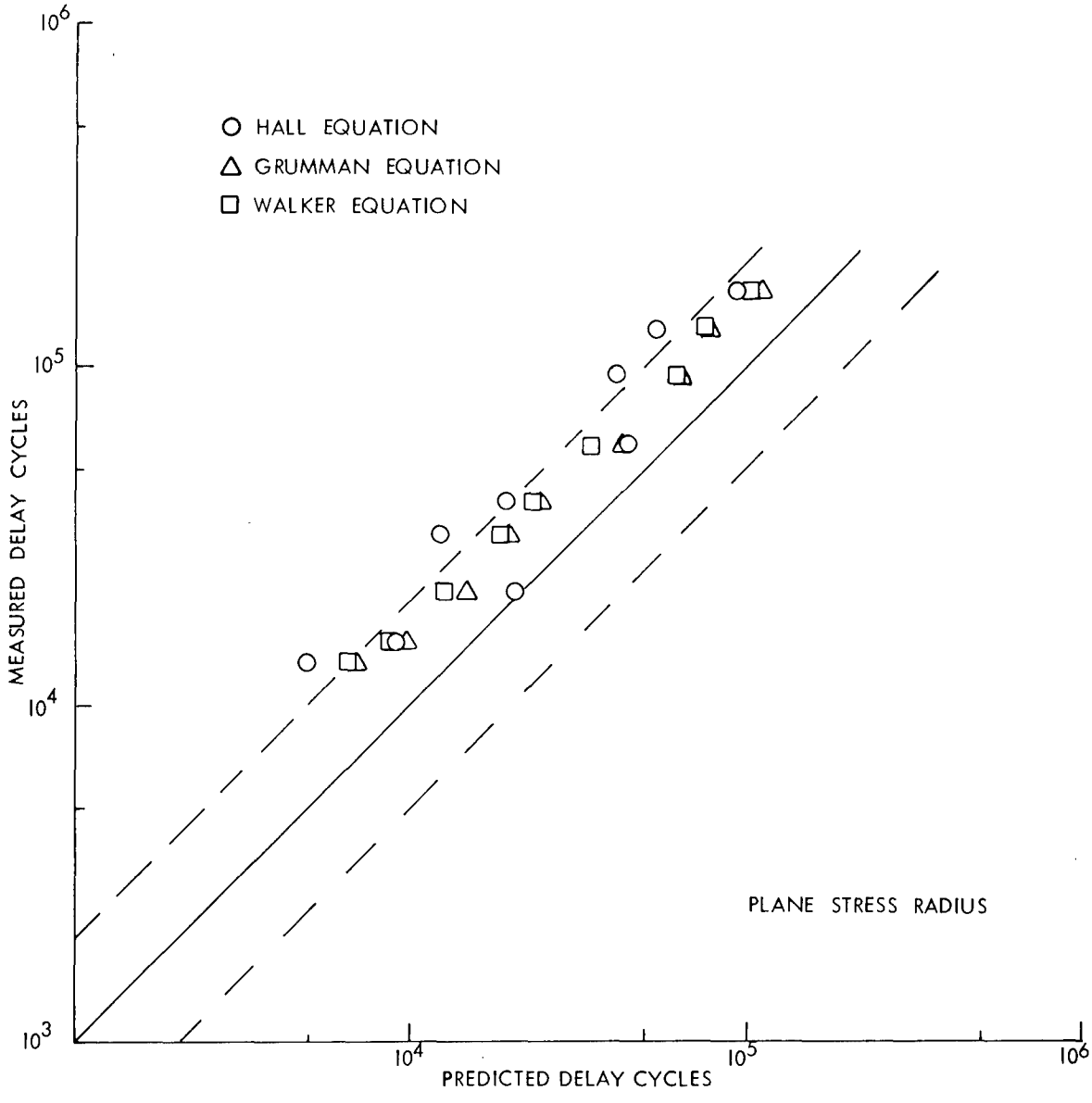

Figure 65. Correlations of Predicted and Measured Delay Cycles Using the Generalized Willenborg Model and Various Crack Growth Rate Equations for 2219-T851 Aluminum Alloy Plate Subjected to Tension-Compression Overloads and K_2=10 and K_5= -7.5 KSI$\sqrt{in.}$

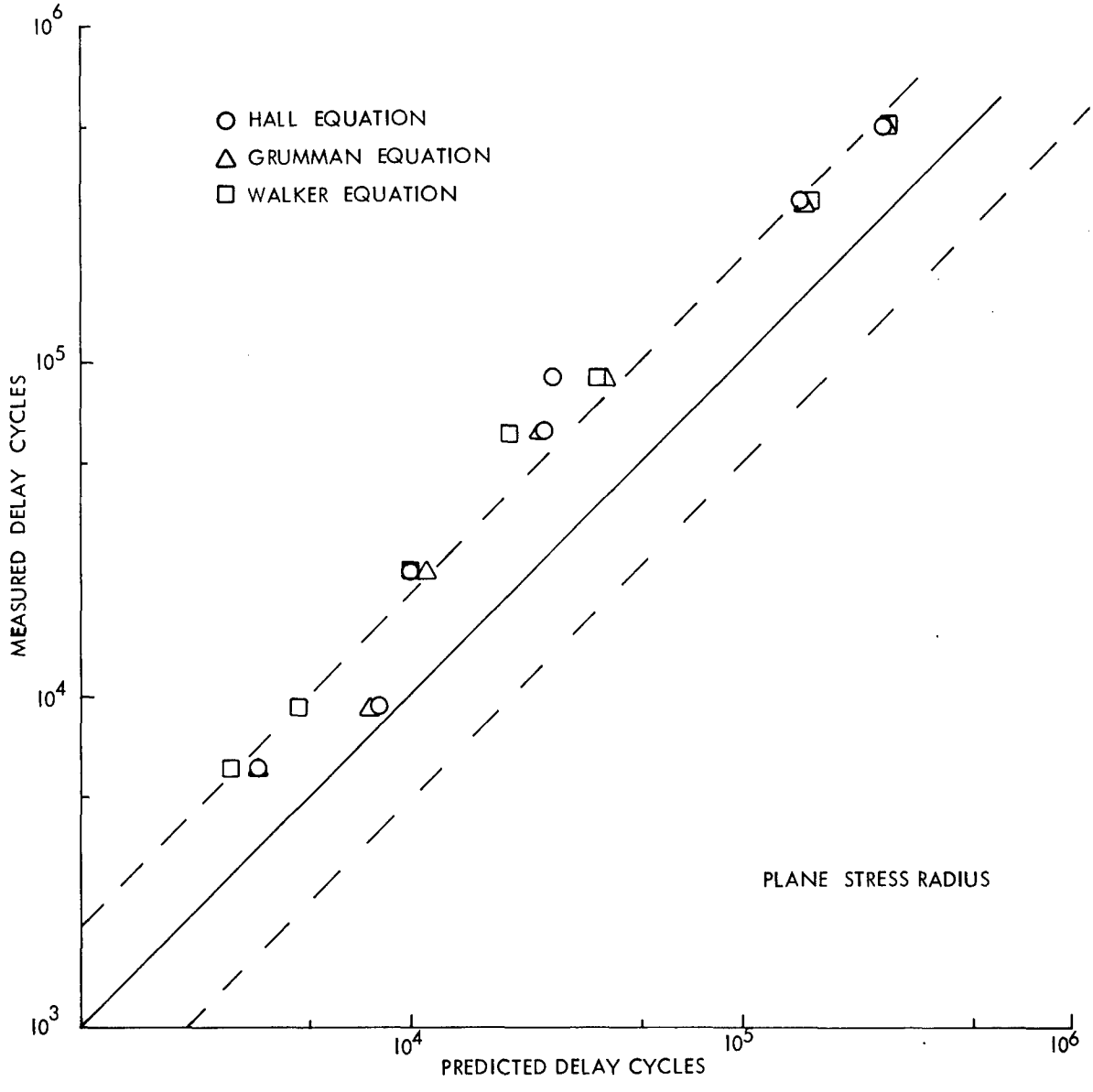

Figure 66. Correlations of Predicted and Measured Delay Cycles Using the Generalized Willenborg Model and Various Crack Growth Rate Equations for 2219-T851 Aluminum Alloy Plate Subjected to Zero-Tension Overloads

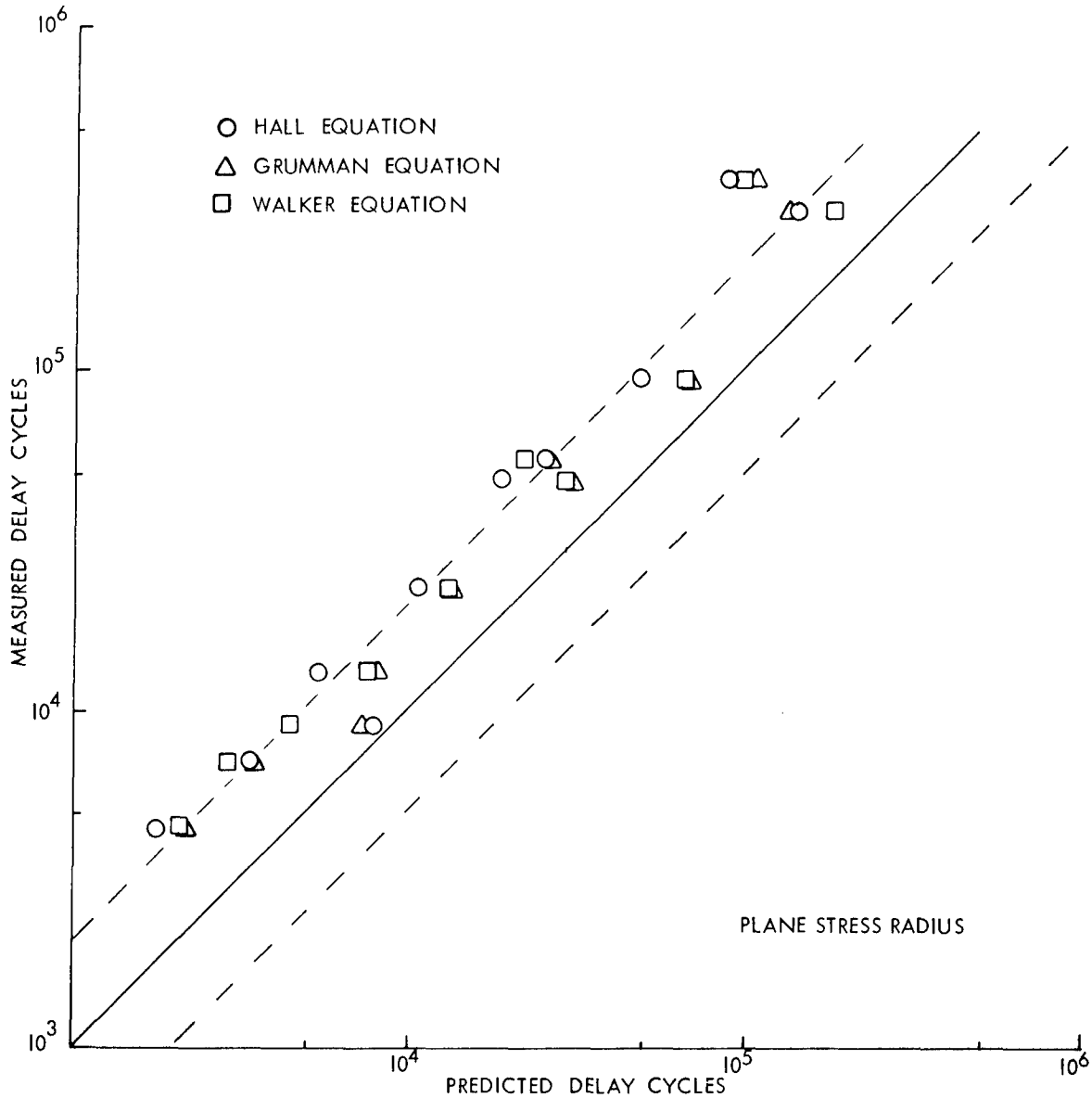

Figure 67. Correlations of Predicted and Measured Delay Cycles Using the Generalized Willenborg Model and Various Crack Growth Rate Equations for 2219-T851 Aluminum Alloy Plate Subjected to Compression-Tension Overloads

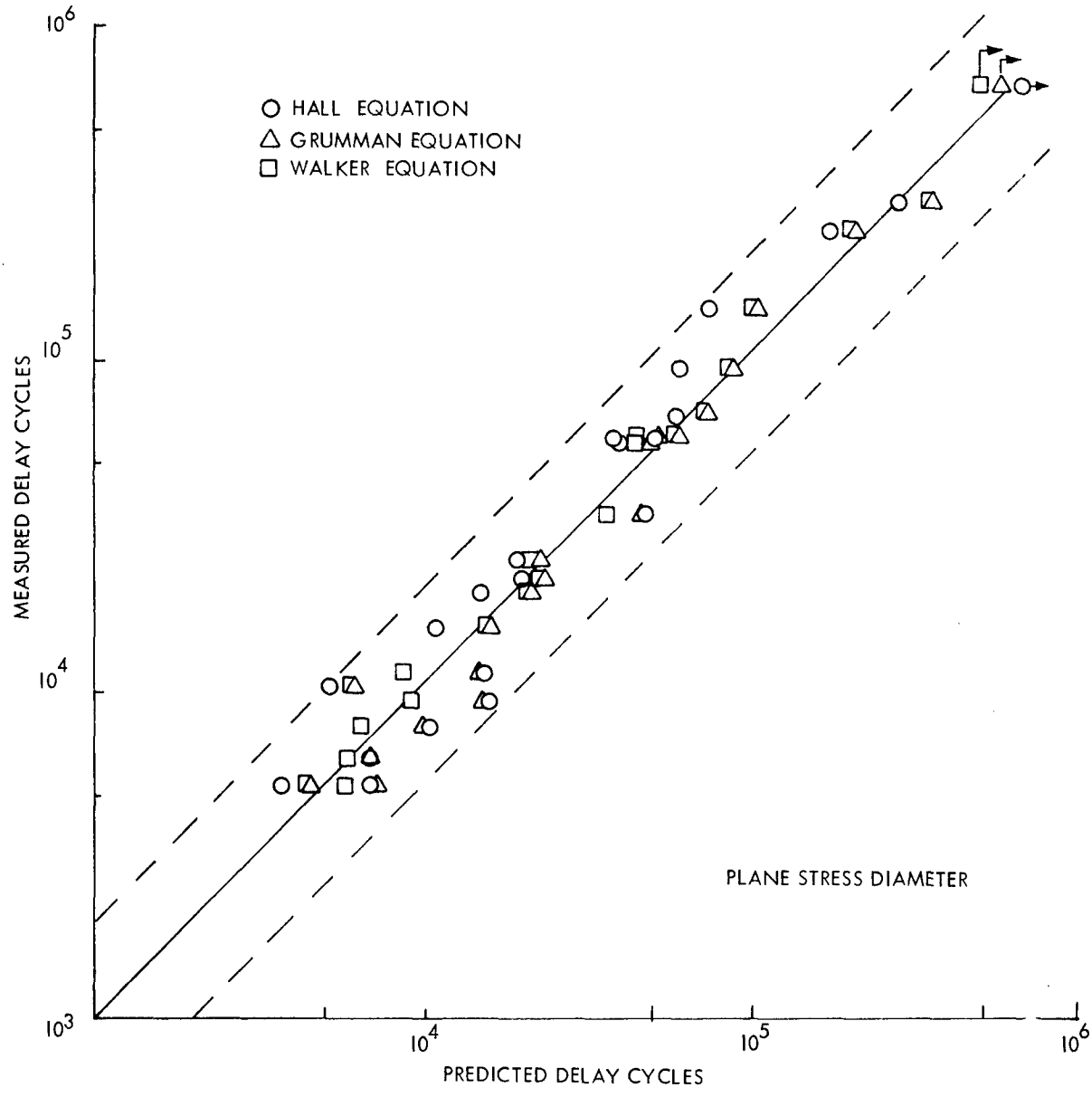

Figure 68. Correlations of Predicted and Measured Delay Cycles Using the Generalized Willenborg Model and Various Crack Growth Rate Equations for 2219-T851 Aluminum Alloy Plate Subjected to Tension-Tension Overloads

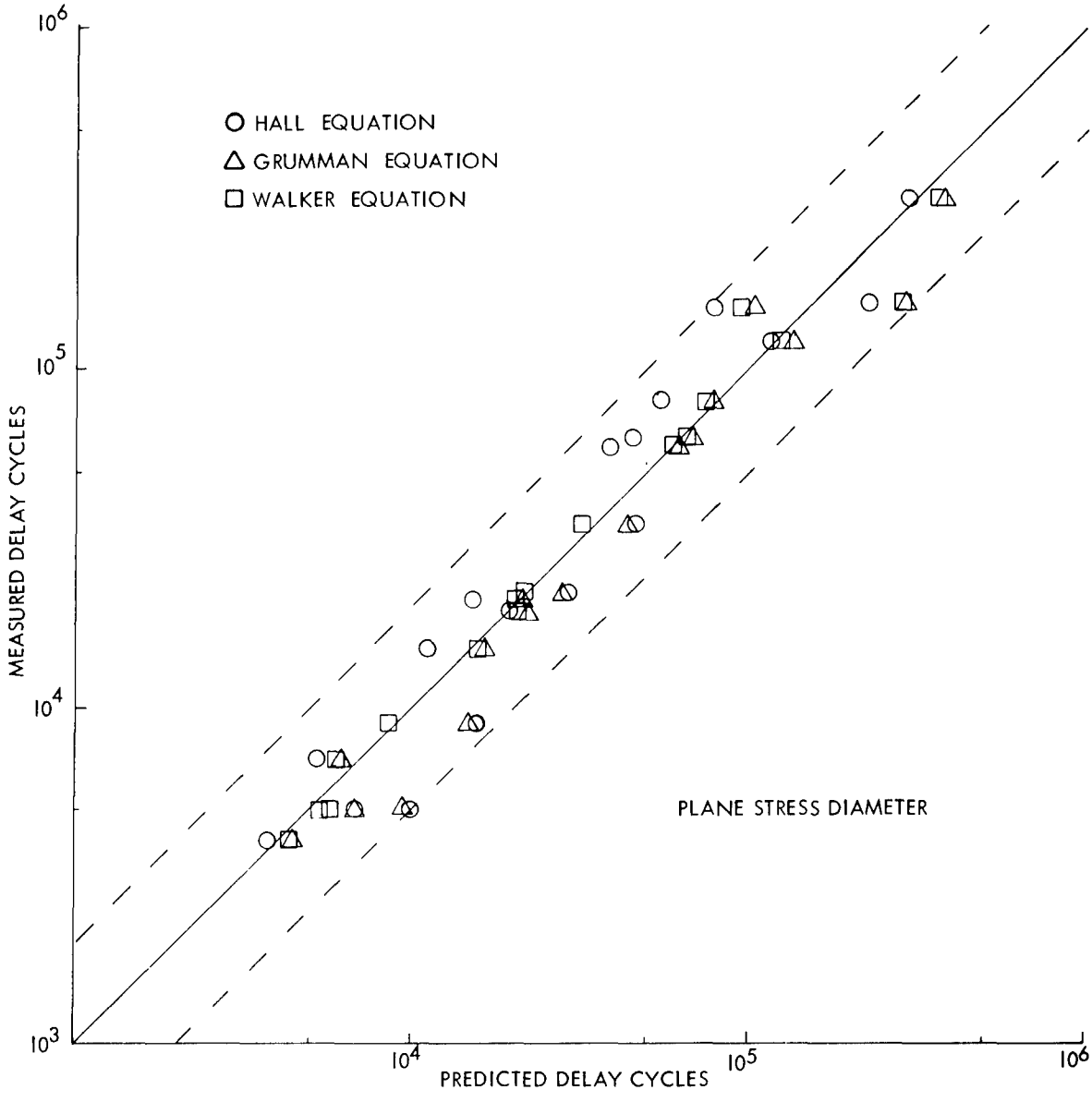

Figure 69. Correlations of Predicted and Measured Delay Cycles Using the Generalized Willenborg Model and Various Crack Growth Rate Equations for 2219-T851 Aluminum Alloy Plate Subjected to Tension-Zero Overloads

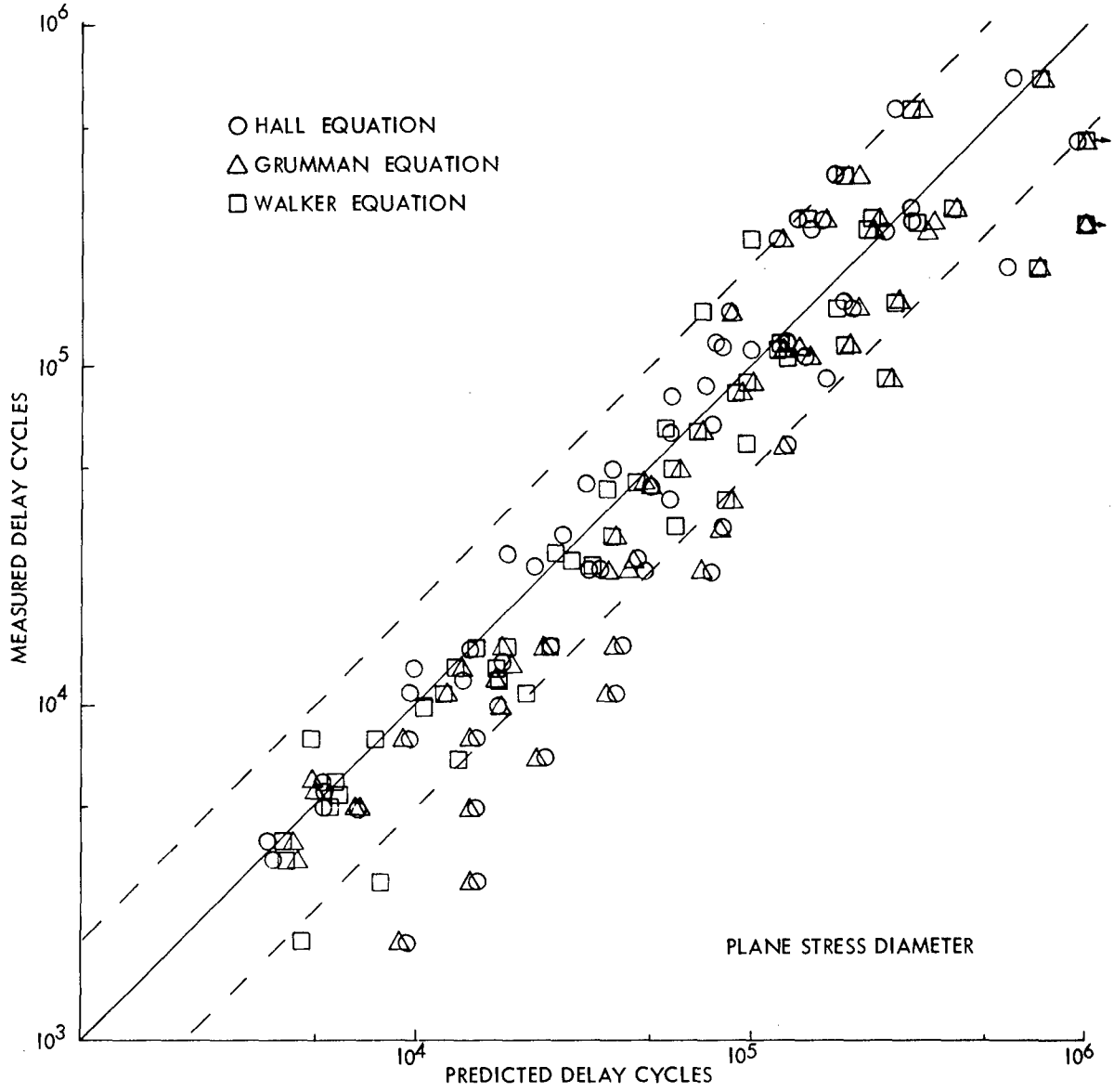

Figure 70. Correlations of Predicted and Measured Delay Cycles Using the Generalized Willenborg Model and Various Crack Growth Rate Equations for 2219-T851 Aluminum Alloy Plate Subjected to Tension-Compression Overloads

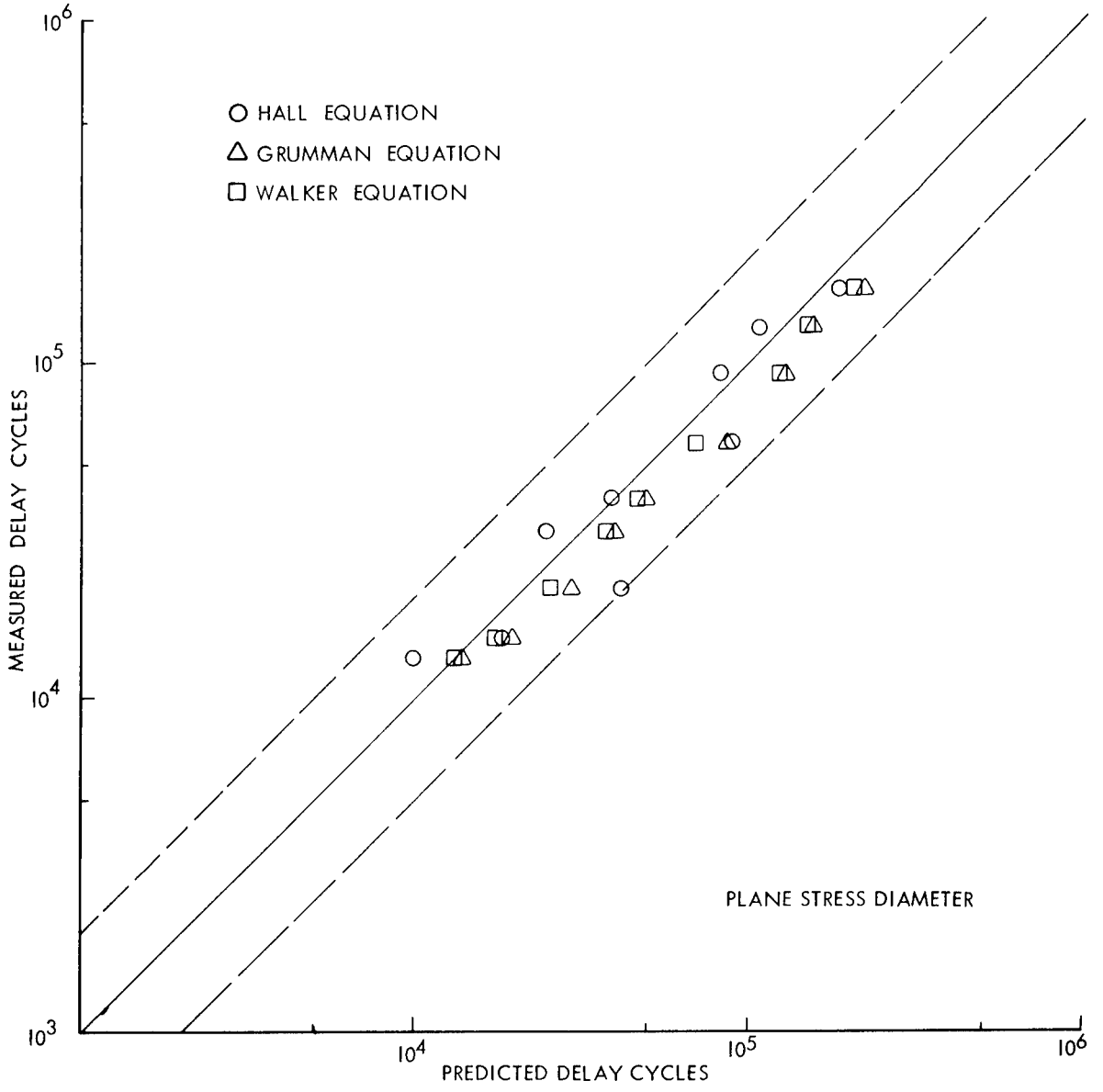

Figure 71. Correlations of Predicted and Measured Delay Cycles Using the Generalized Willenborg Model and Various Crack Growth Rate Equations for 2219-T851 Aluminum Alloy Plate Subjected to Tension-Compression Overloads and K_2=10 and K_5= -7.5 KSI$\sqrt{in.}$

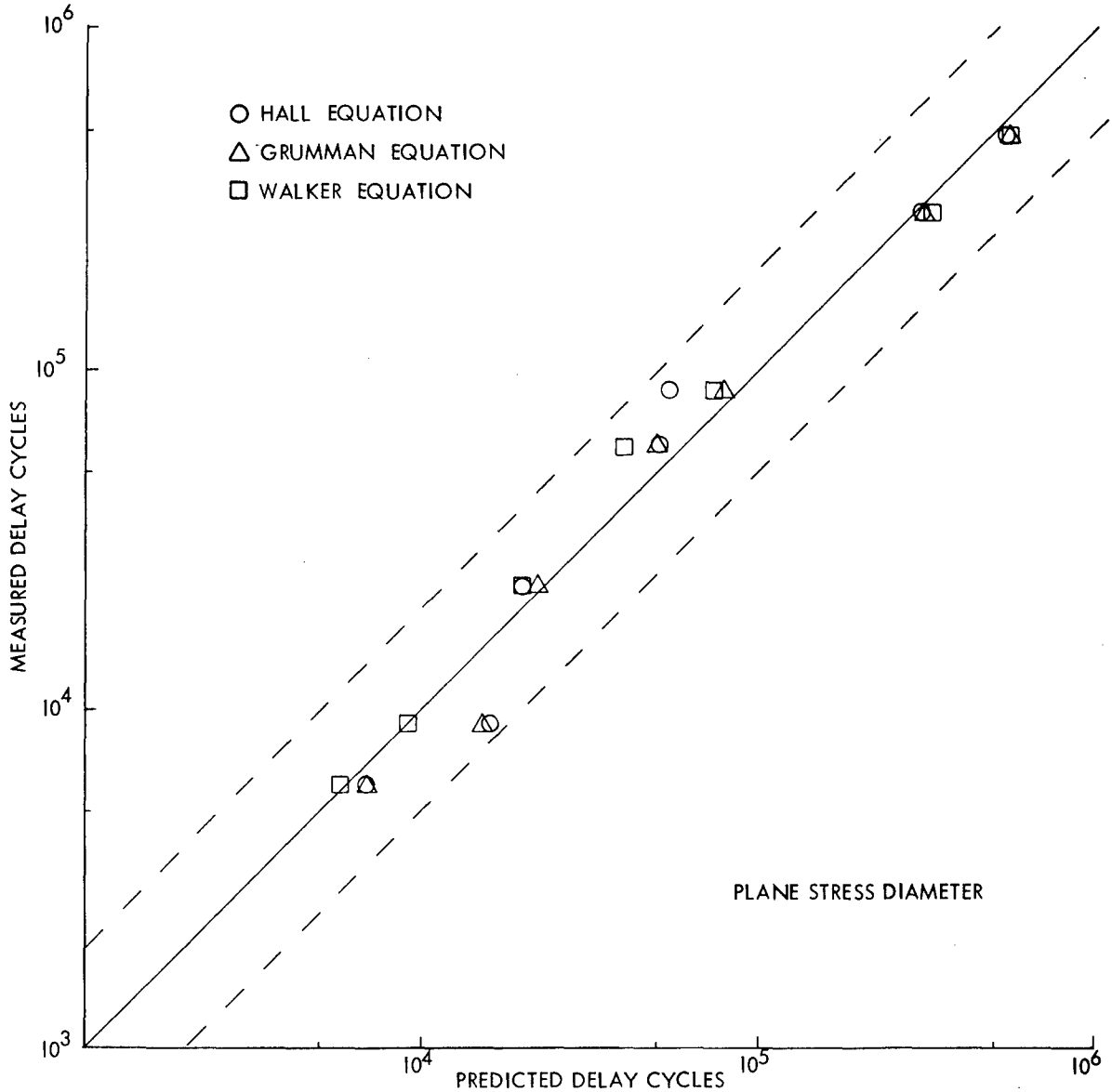

Figure 72. Correlations of Predicted and Measured Delay Cycles Using the Generalized Willenborg Model and Various Crack Growth Rate Equations for 2219-T851 Aluminum Alloy Plate Subjected to Zero-Tension Overloads

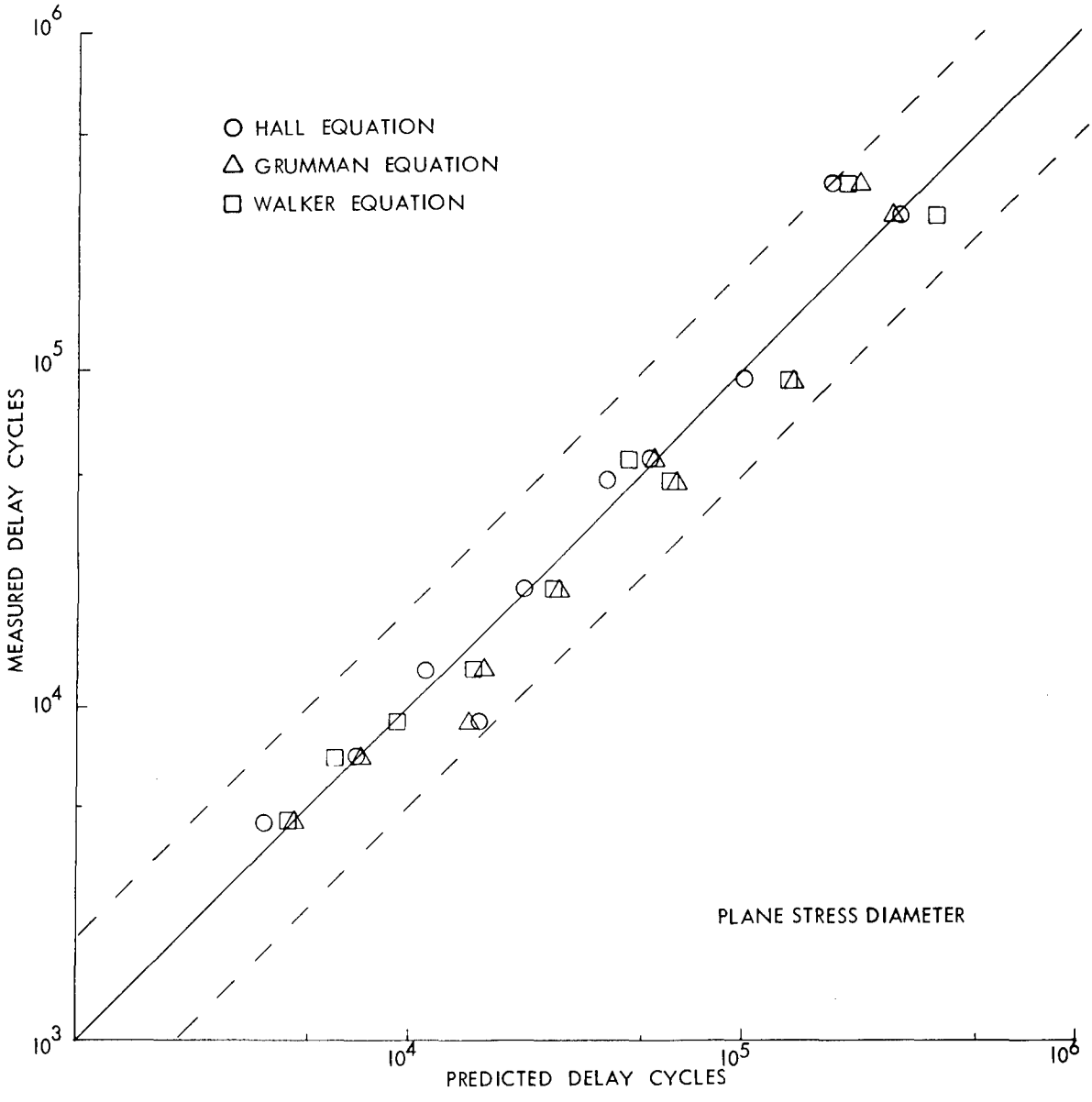

Figure 73. Correlations of Predicted and Measured Delay Cycles Using the Generalized Willenborg Model and Various Crack Growth Rate Equations for 2219-T851 Aluminum Alloy Plate Subjected to Compression-Tension Overloads

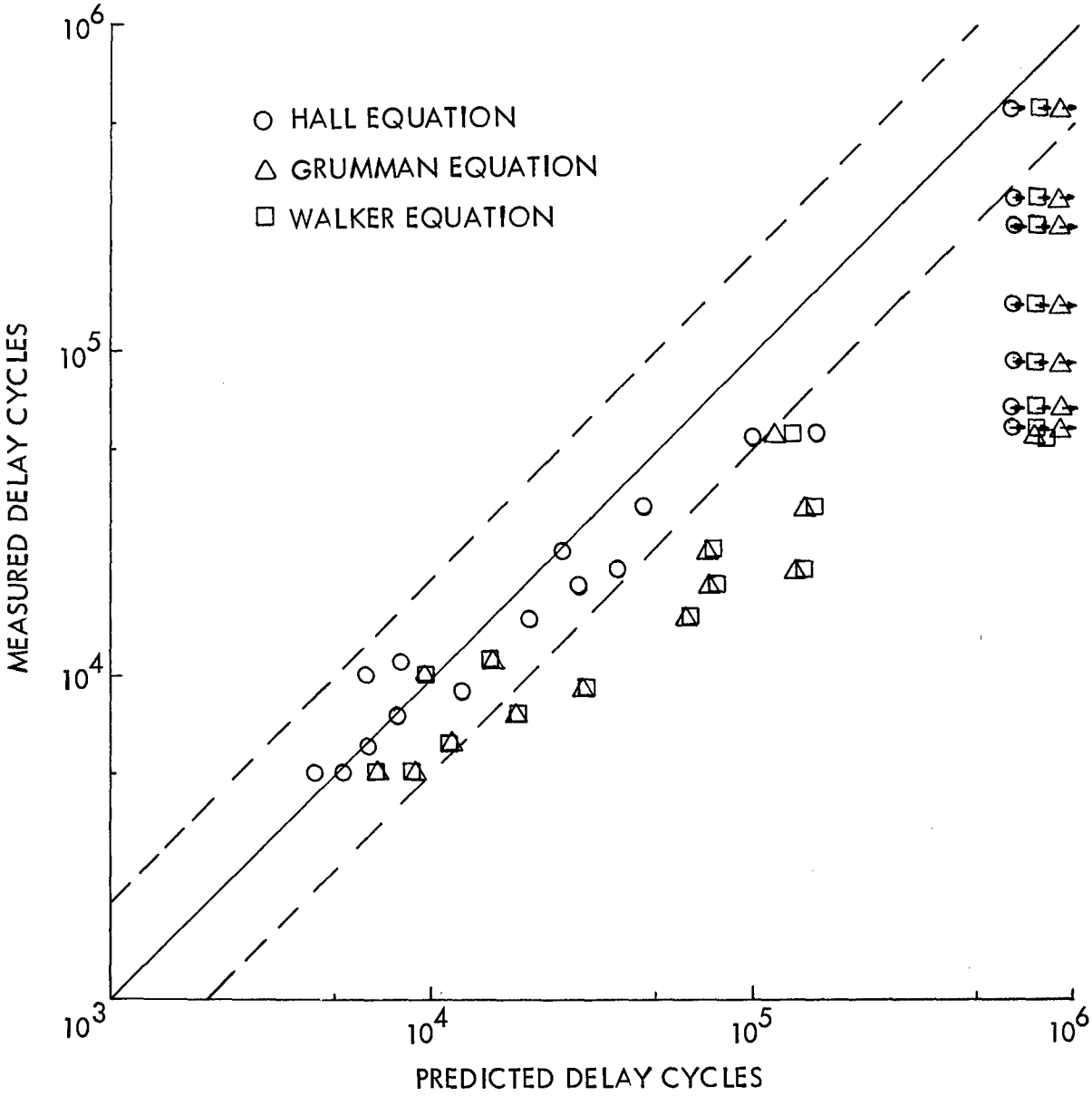

Figure 74 . Correlations of Measured and Predicted Delay Cycles Using the Closure model and Various Crack Growth Rate Equations for 2219-T851 Aluminum Alloy Plates Subjected to Tension-Tension Overloads

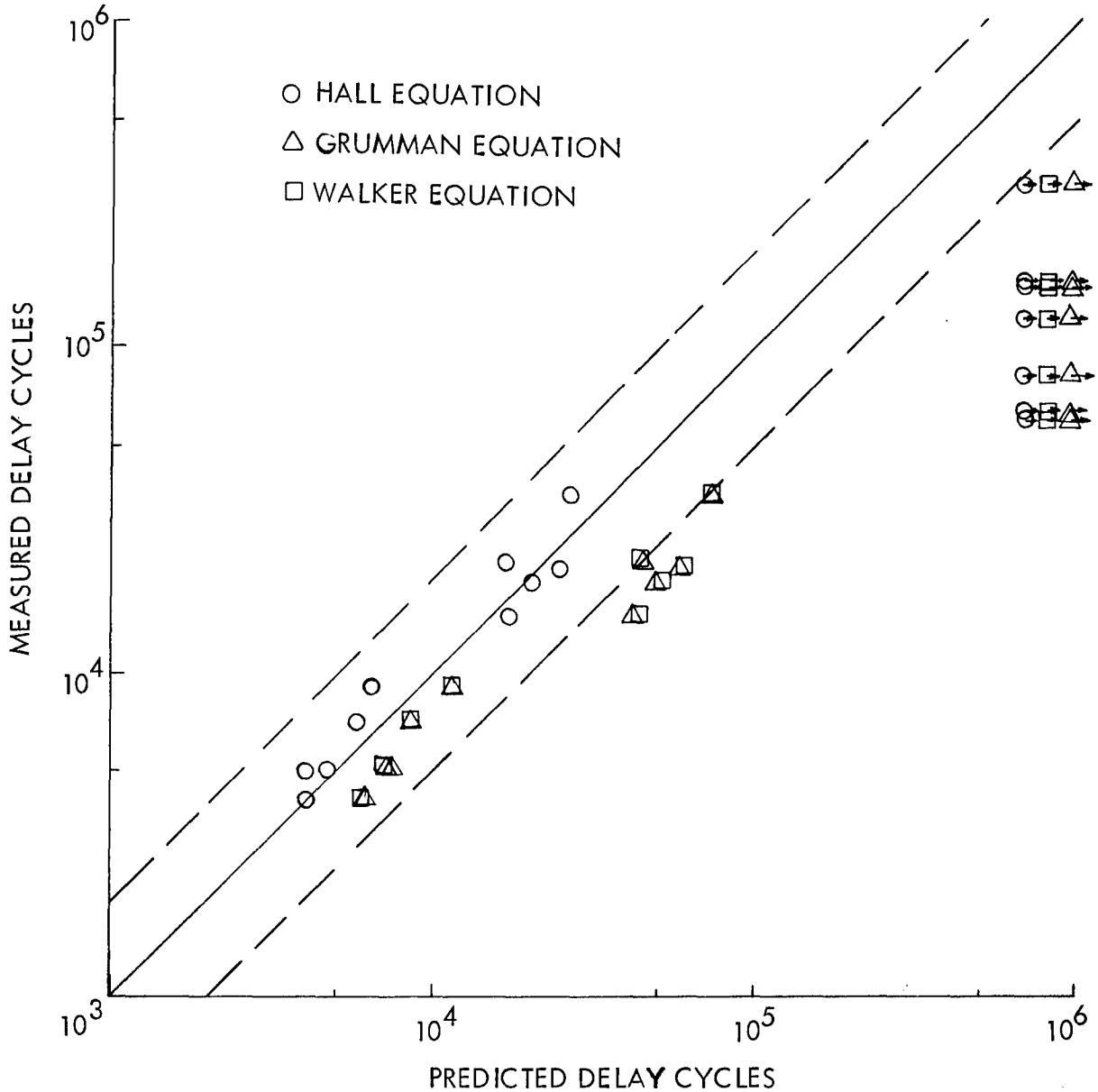

Figure 75 . Correlations of Measured and Predicted Delay Cycles Using the Closure Model and Various Crack Growth Rate Equations for 2219-T851 Aluminum Alloy Plates Subjected to Tension-Zero Overloads

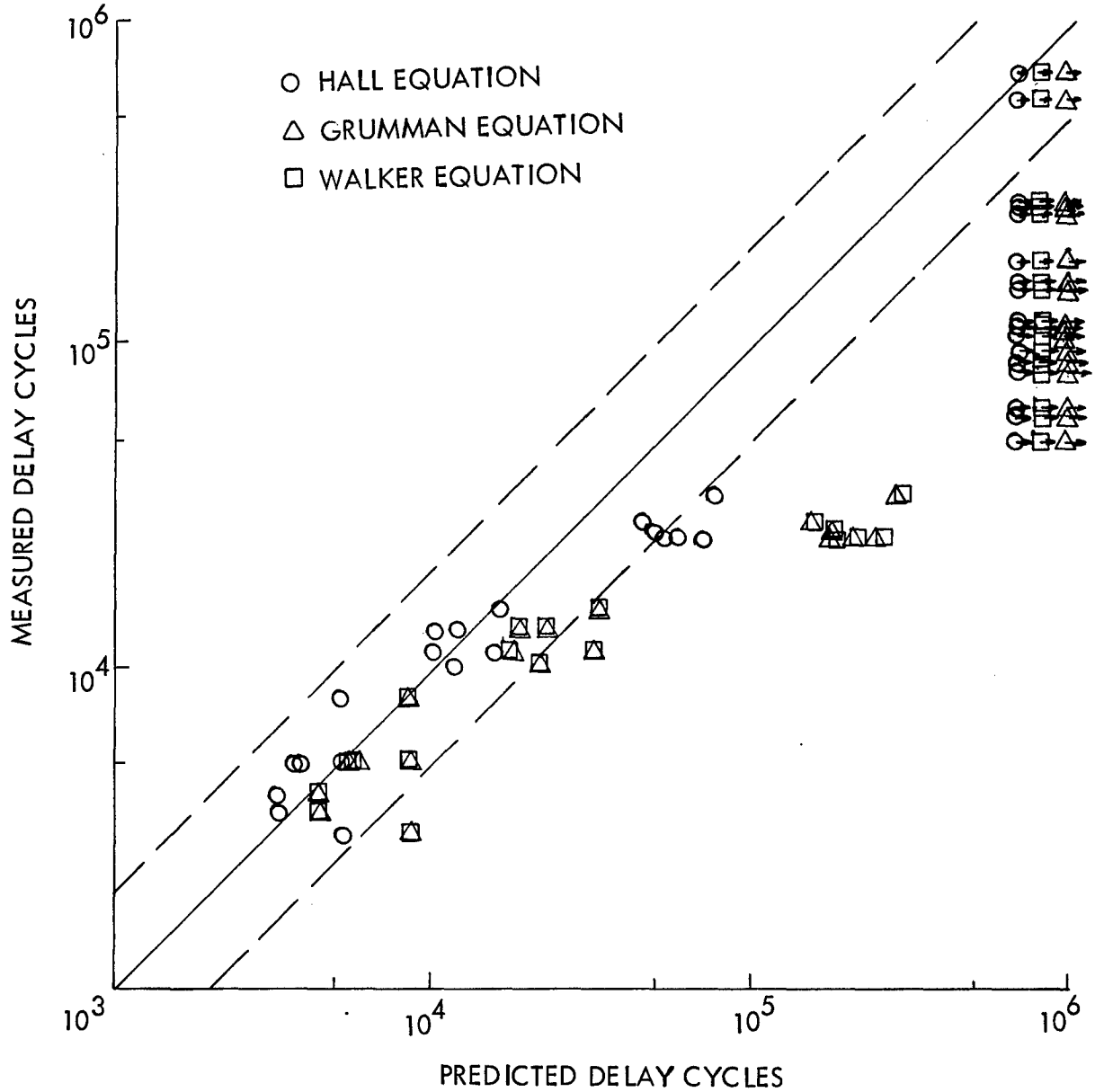

Figure 76 . Correlations of Measured and Predicted Delay Cycles Using the Closure Model and Various Crack Growth Rate Equations for 2219-T851 Aluminum Alloy Plates Subjected to Tension-Compression Overloads and $K_2 = 10 \text{ Ksi}\sqrt{\text{in}}$

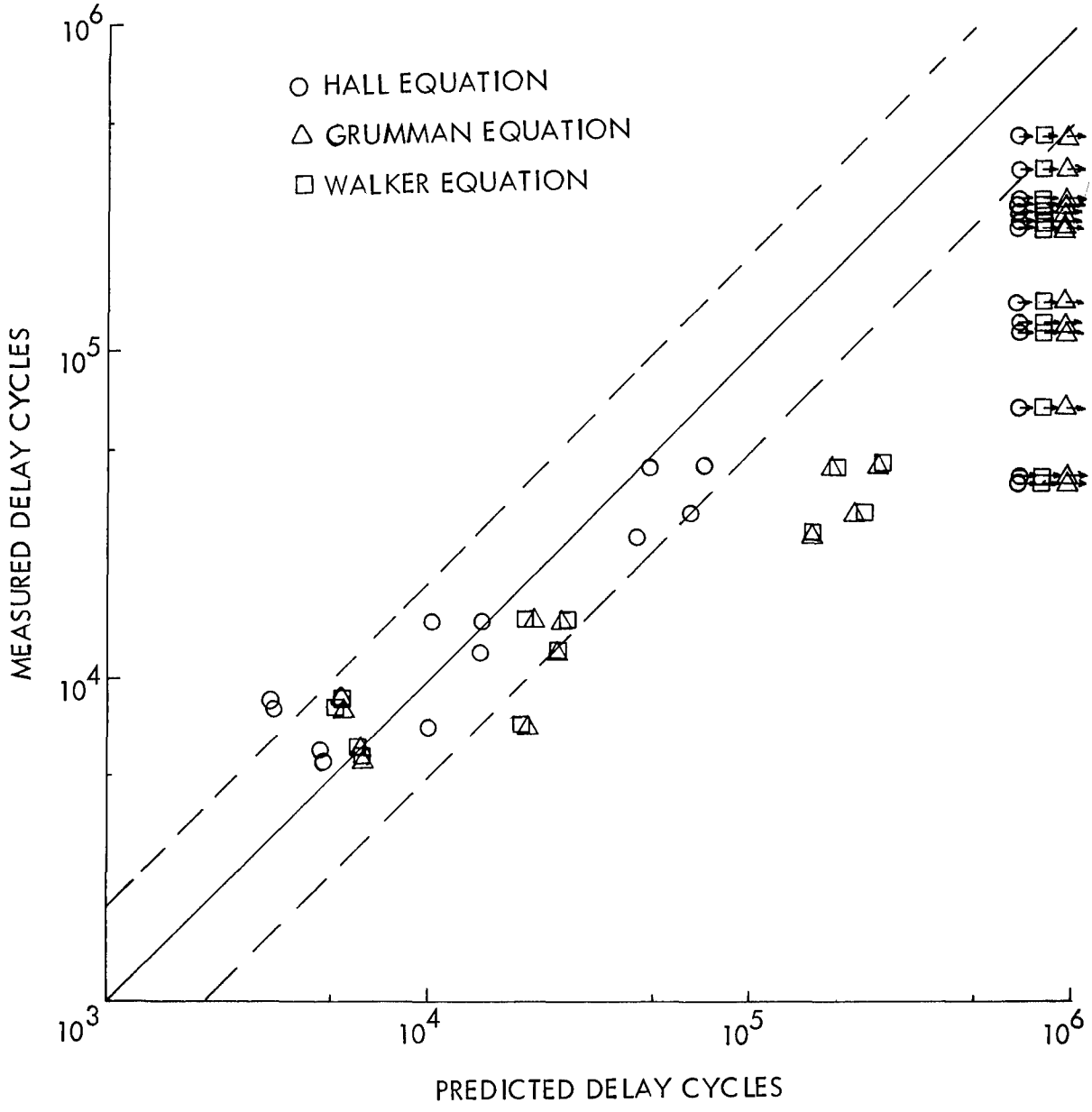

Figure 77 . Correlations of Measured and Predicted Delay Cycles Using the Closure Model and Various Crack Growth Rate Equations for 2219-T851 Aluminum Alloy Plates Subjected to Tension-Compression Overloads and K_2 = 14 and 7.78 Ksi $\sqrt{\text{in.}}$

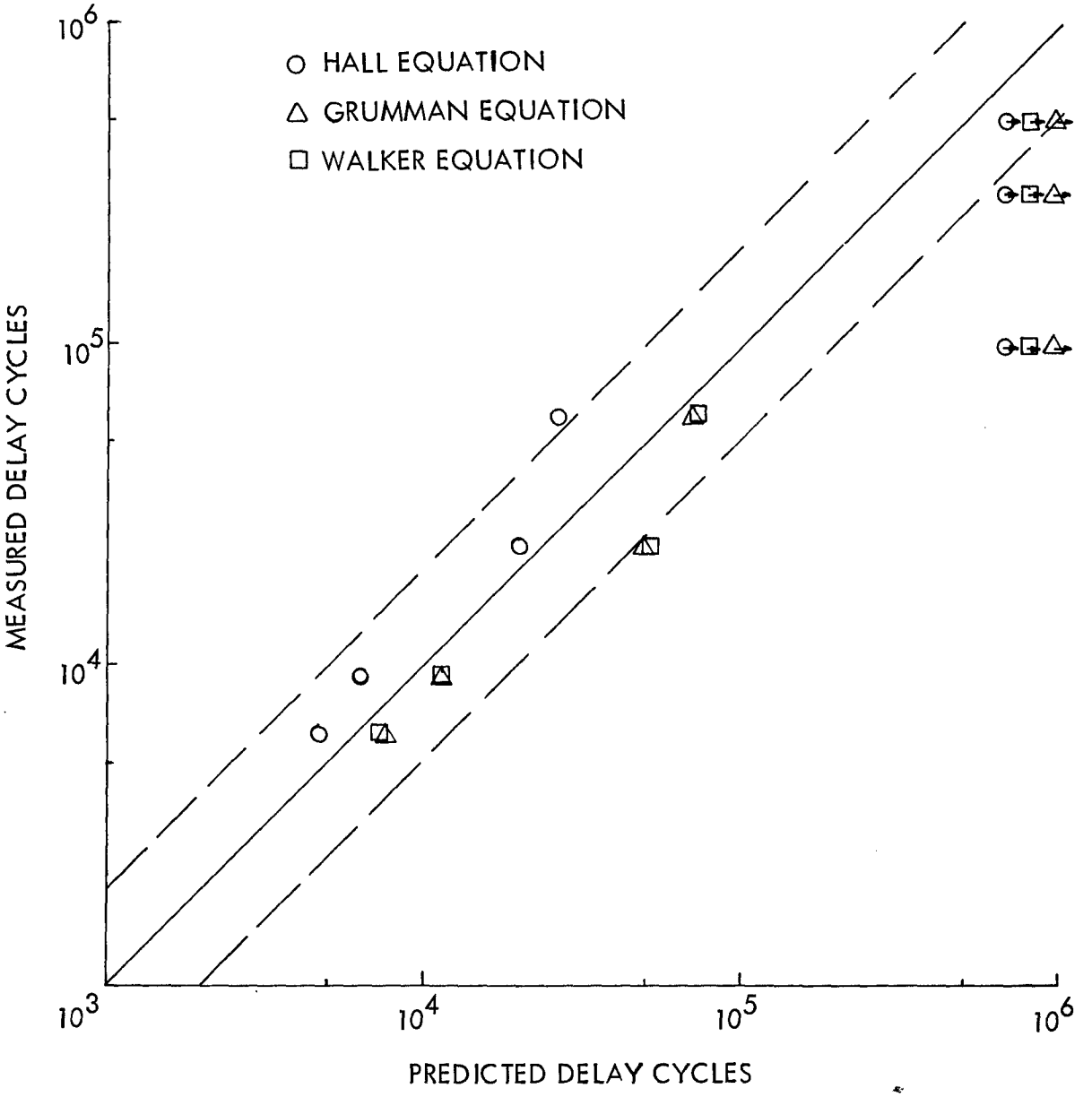

Figure 78 . Correlations of Measured and Predicted Delay Cycles Using the Closure Model and Various Crack Growth Rate Equations for 2219-T851 Aluminum Alloy Plates Subjected to Zero-Tension Overloads

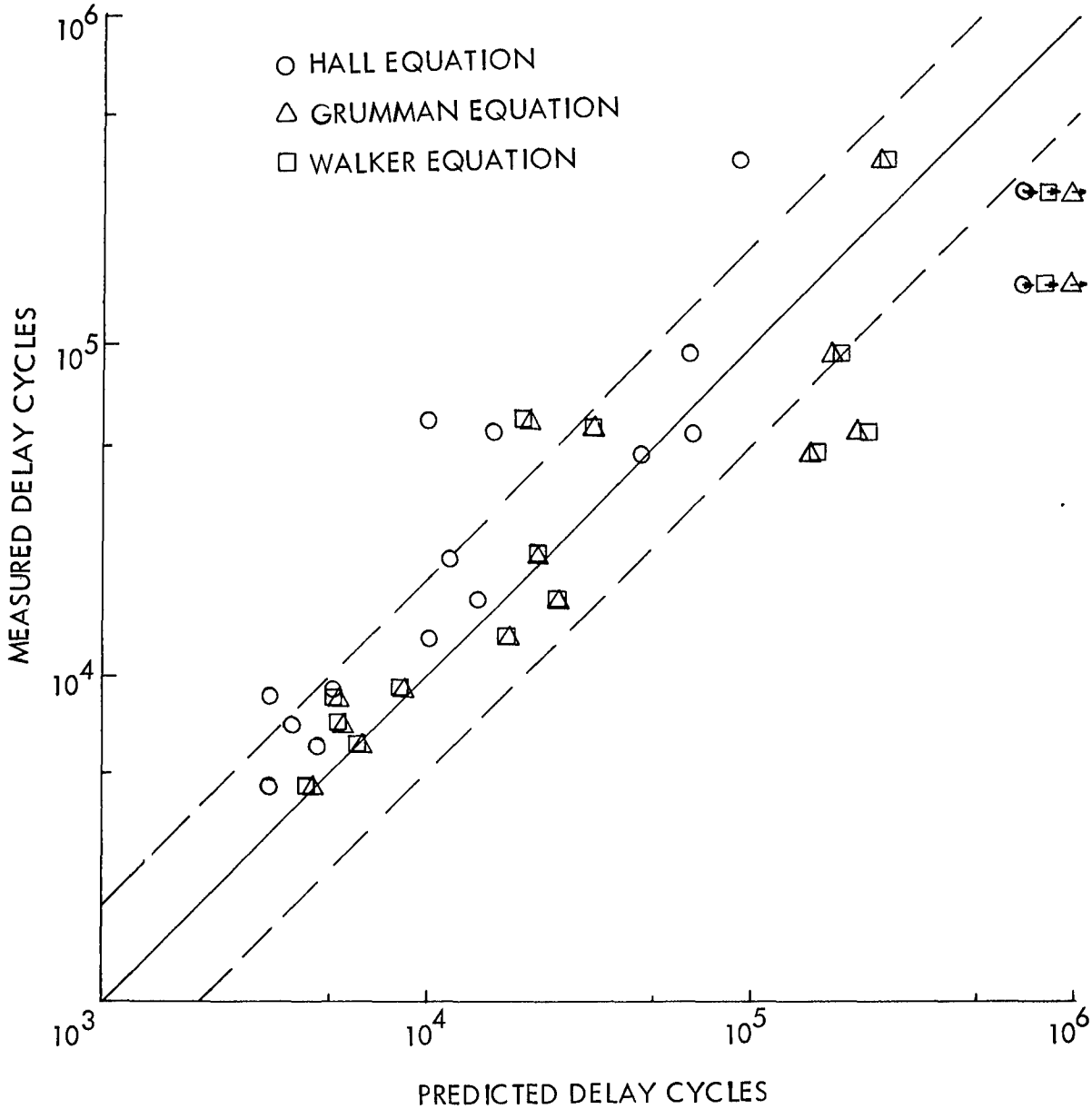

Figure 79 . Correlations of Measured and Predicted Delay Cycles Using the Closure Model and Various Crack Growth Rate Equations for 2219-T851 Aluminum Alloy Plates Subjected to Compression-Tension Overloads

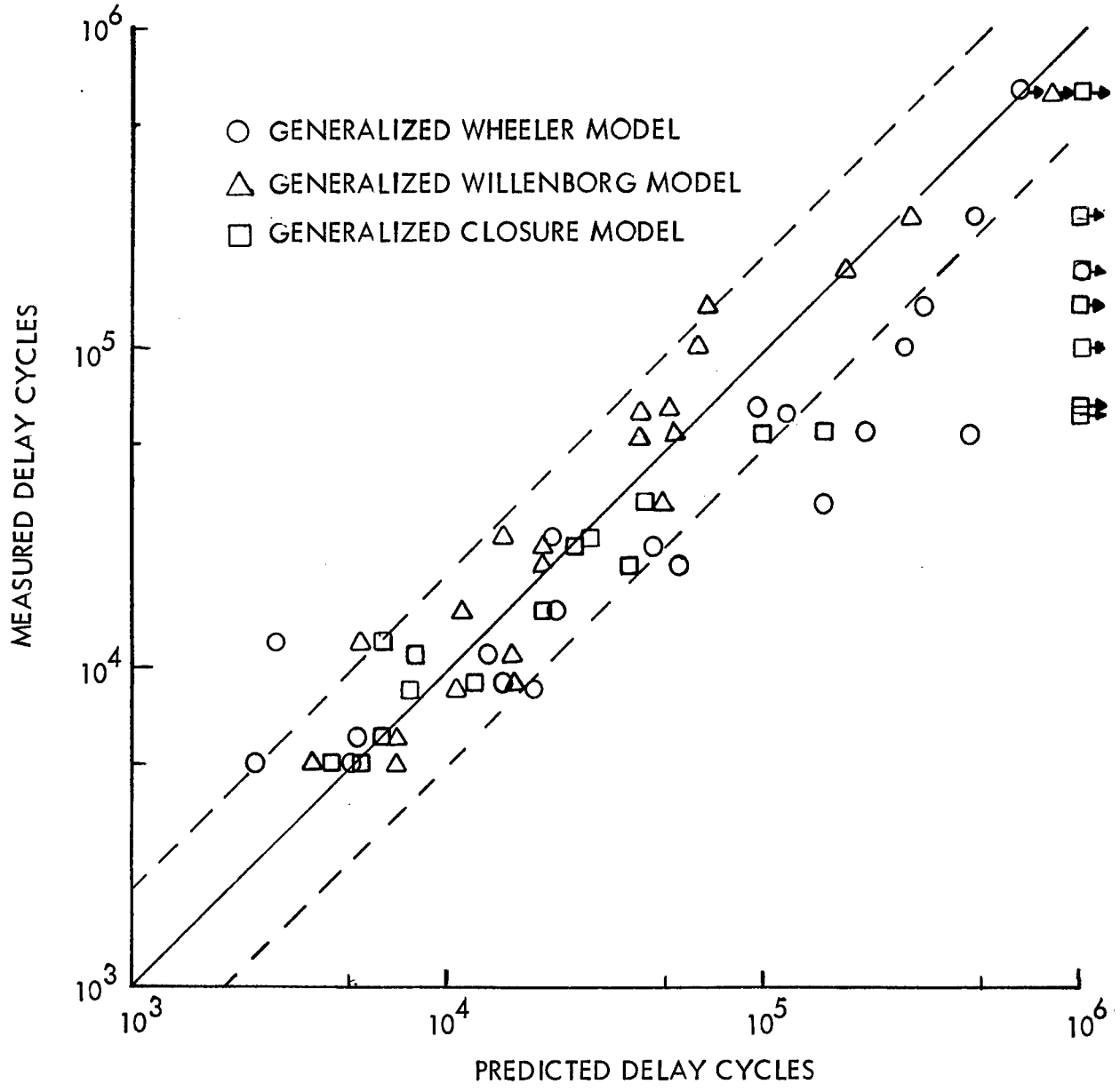

Figure 80 . Correlations of Predicted and Measured Delay Cycles Using the Hall Crack Growth Rate Equation and Various Retardation Models for 2219-T851 Aluminum Alloy Plates Subjected to Tension-Tension Overloads

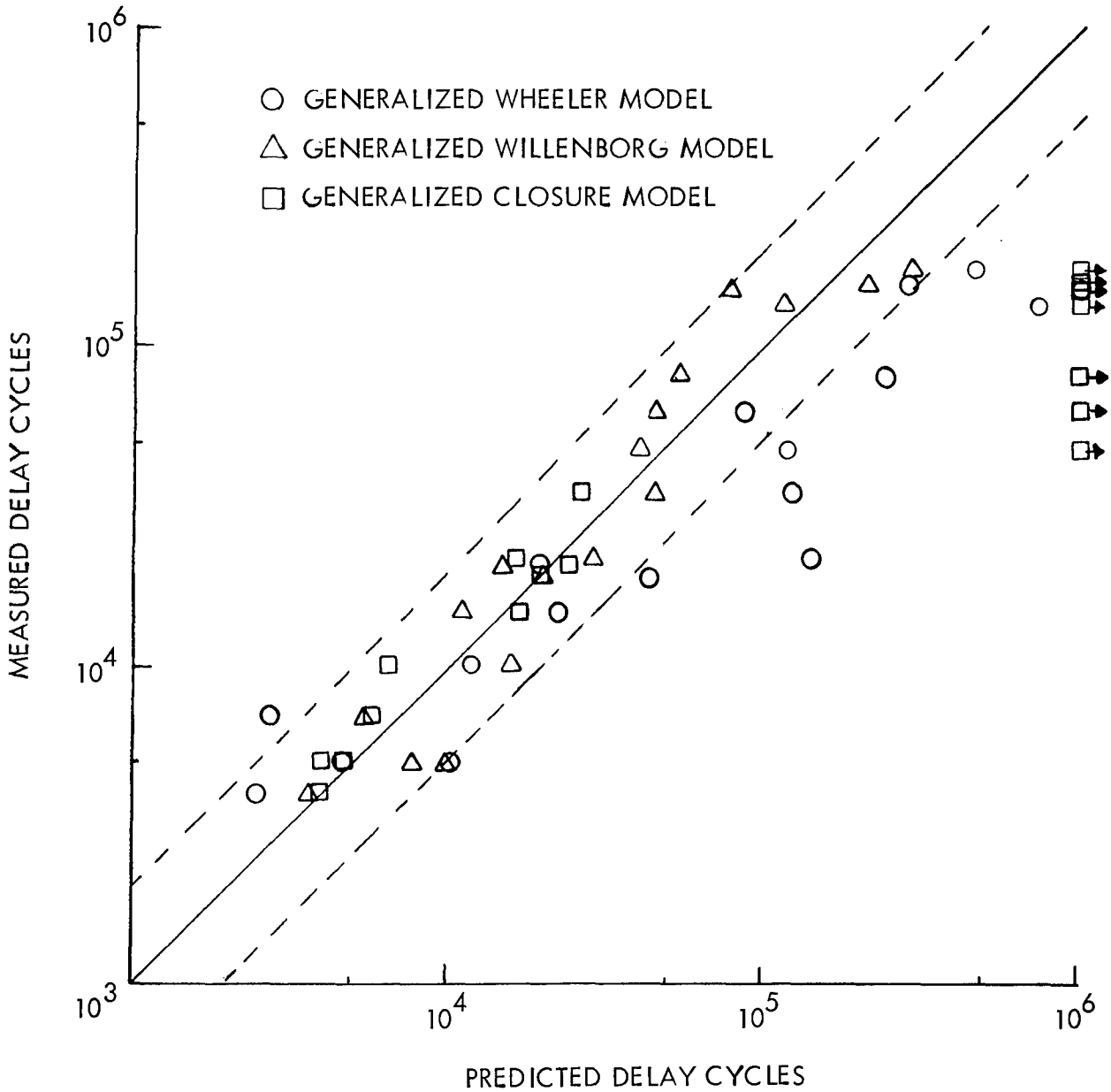

Figure 81 . Correlations of Predicted and Measured Delay Cycles Using the Hall Crack Growth Rate Equation and Various Retardation Models for 2219-T851 Aluminum Alloy Plates Subjected to Tension-Zero Overloads

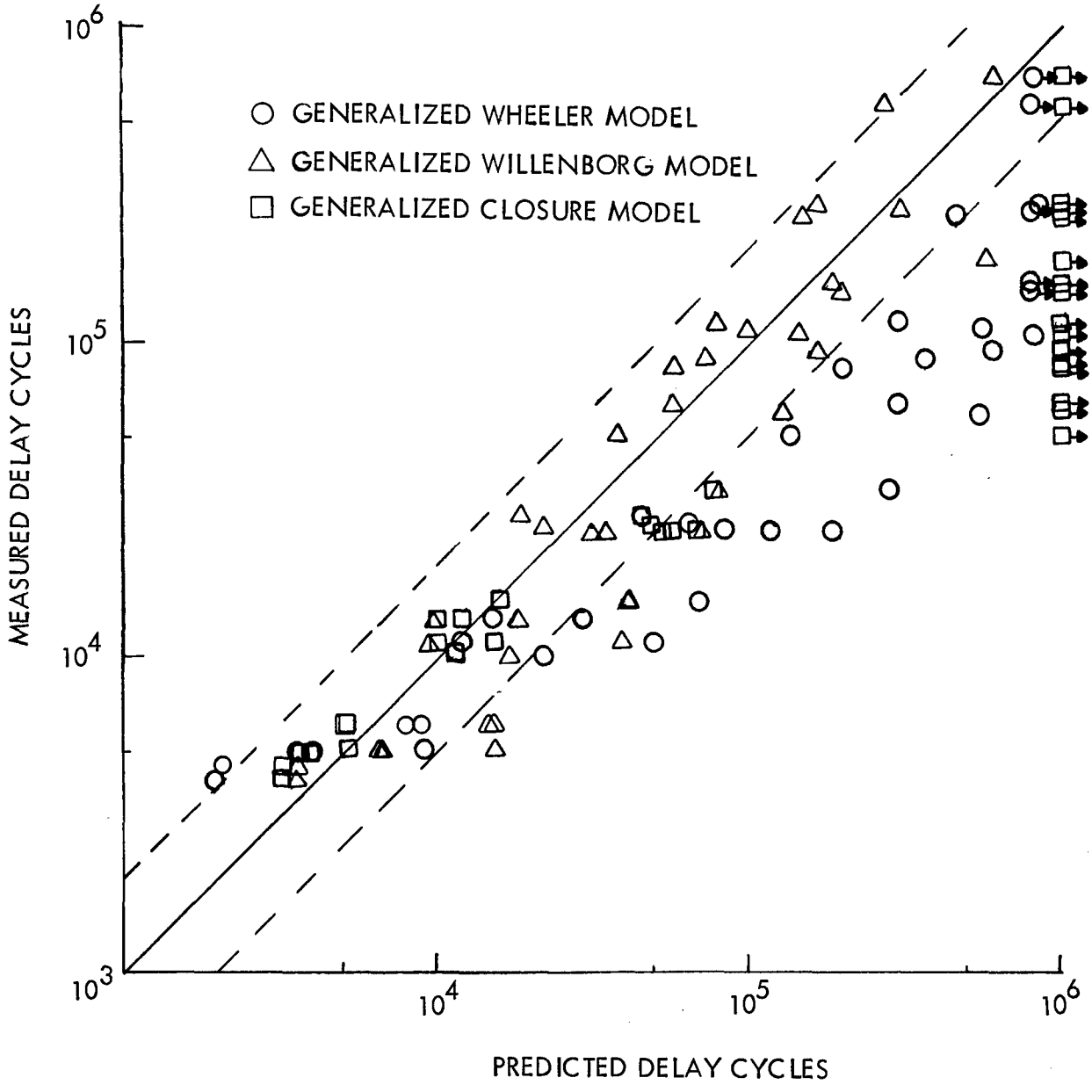

Figure 82 . Correlations of Predicted and Measured Delay Cycles Using the Hall Crack Growth Rate Equation and Various Retardation Models for 2219-T851 Aluminum Alloy Plates Subjected to Tension-Compression Overloads and $K_2 = 10$ Ksi $\sqrt{\text{In}}$

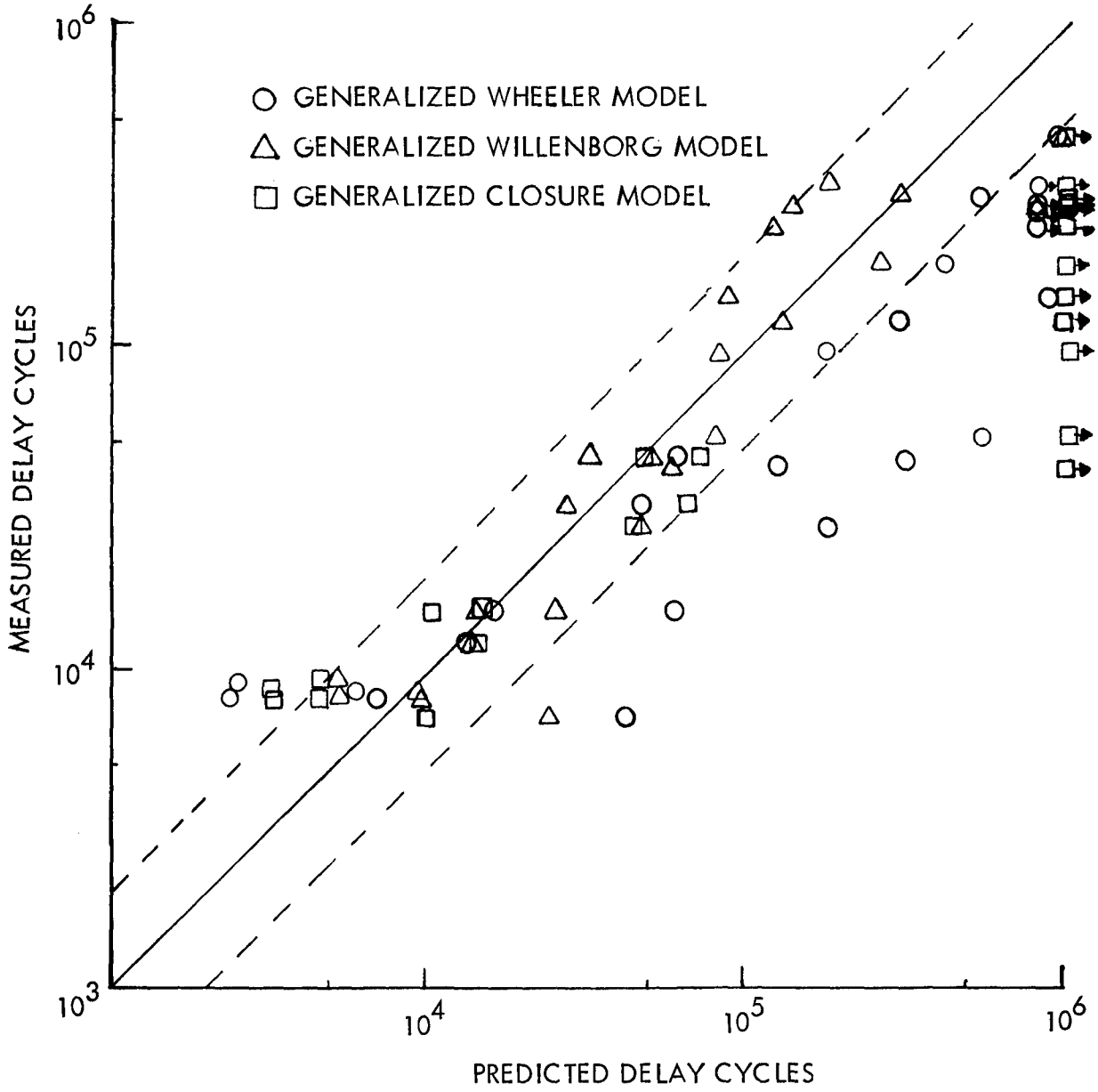

Figure 83 . Correlations of Predicted and Measured Delay Cycles Using the Hall Crack Growth Rate Equation and Various Retardation Models for 2219-T851 Aluminum Alloy Plates Subjected to Tension-Compression Overloads and K_2 = 7.78 and 14 Ksi$\sqrt{\text{In}}$

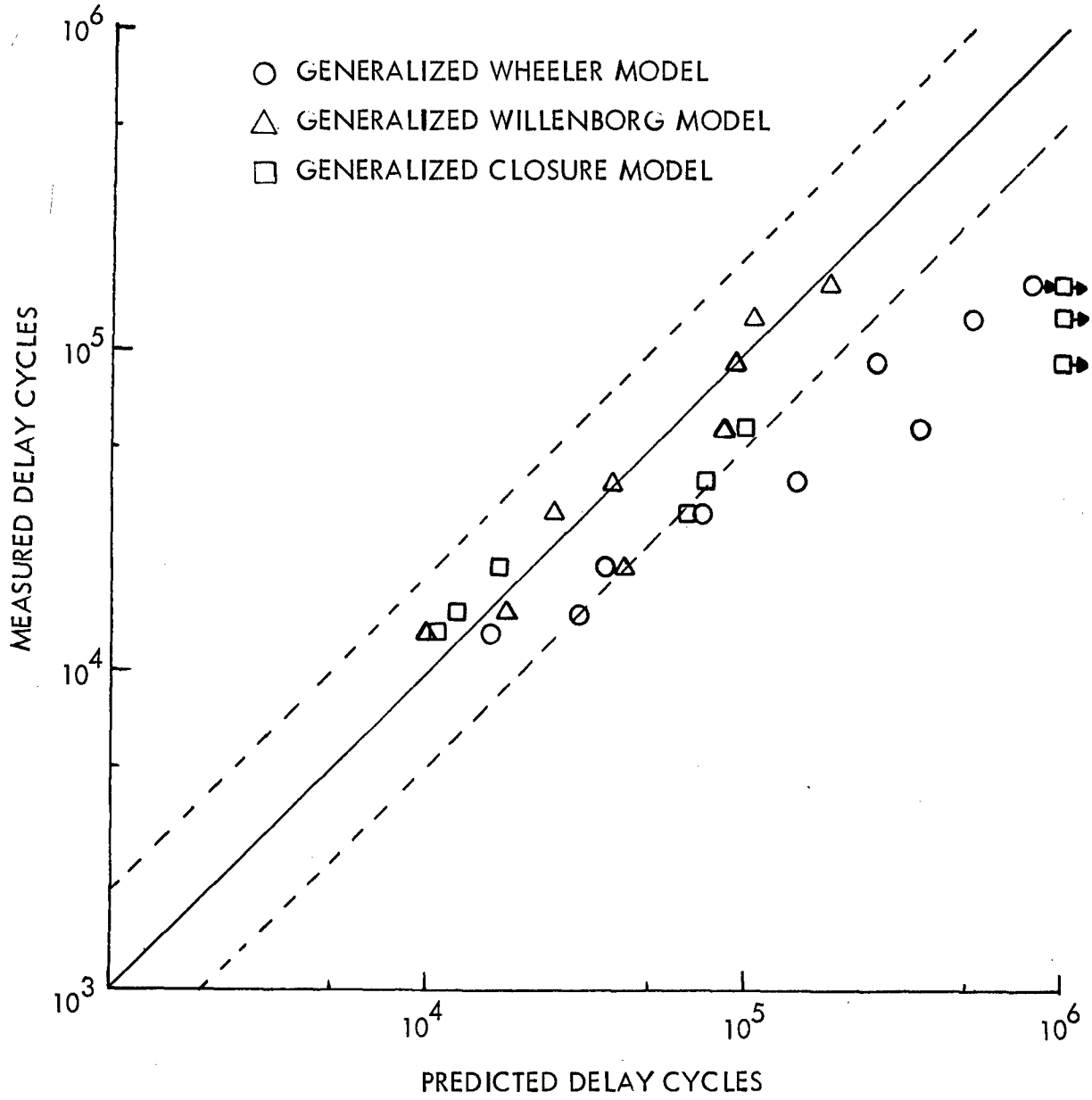

Figure 84 . Correlations of Predicted and Measured Delay Cycles Using the Hall Crack Growth Rate Equation and Various Retardation Models for 2219-T851 Aluminum Alloy Plates Subjected to Tension-Compression Overloads and $K_2 = 10$ and $K_5 = -7.5$ Ksi$\sqrt{\text{In}}$

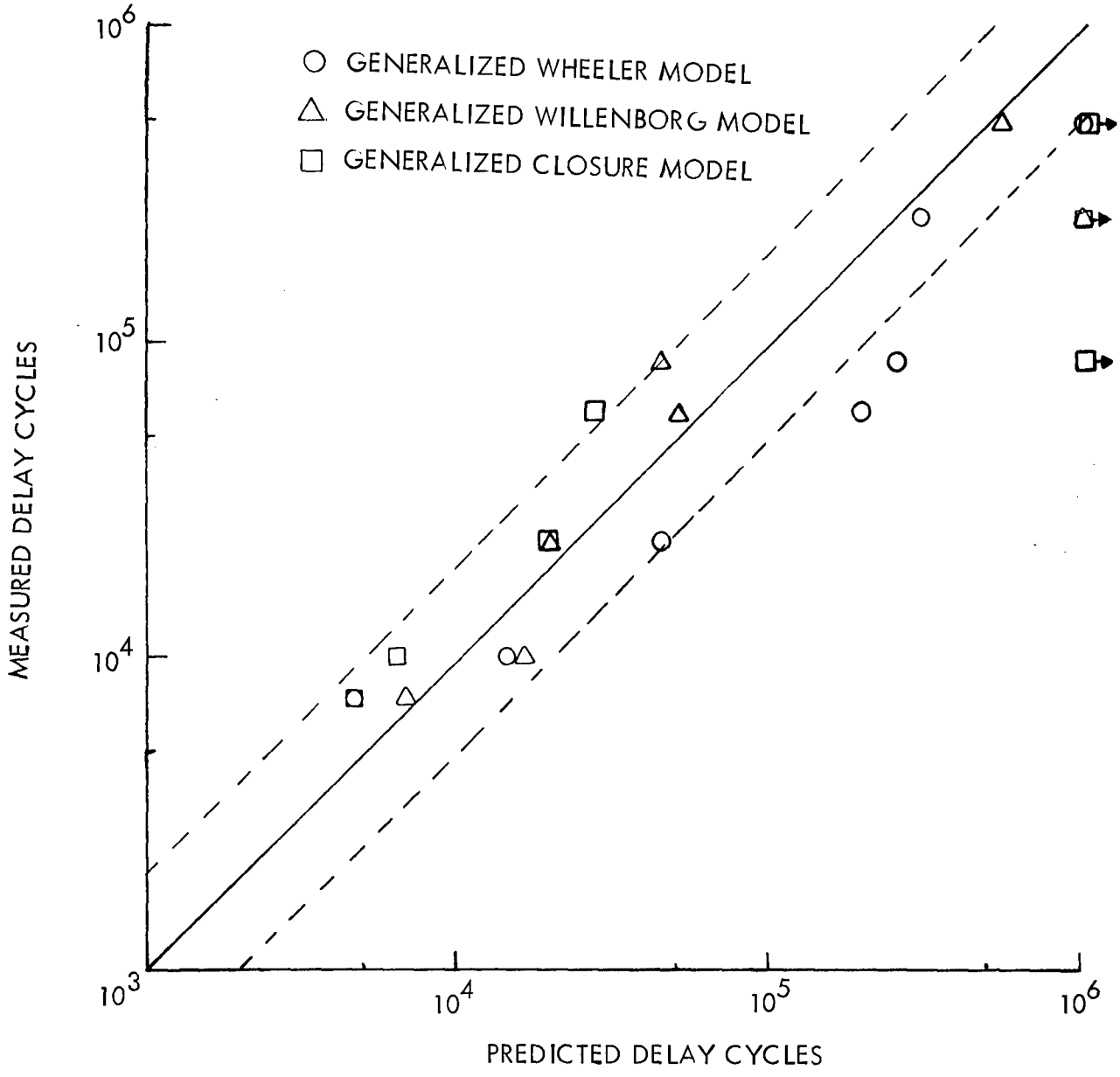

Figure 85 . Correlations of Predicted and Measured Delay Cycles Using the Hall Crack Growth Rate Equation and Various Retardation Models for 2219-T851 Aluminum Alloy Plates Subjected to Zero-Tension Overloads

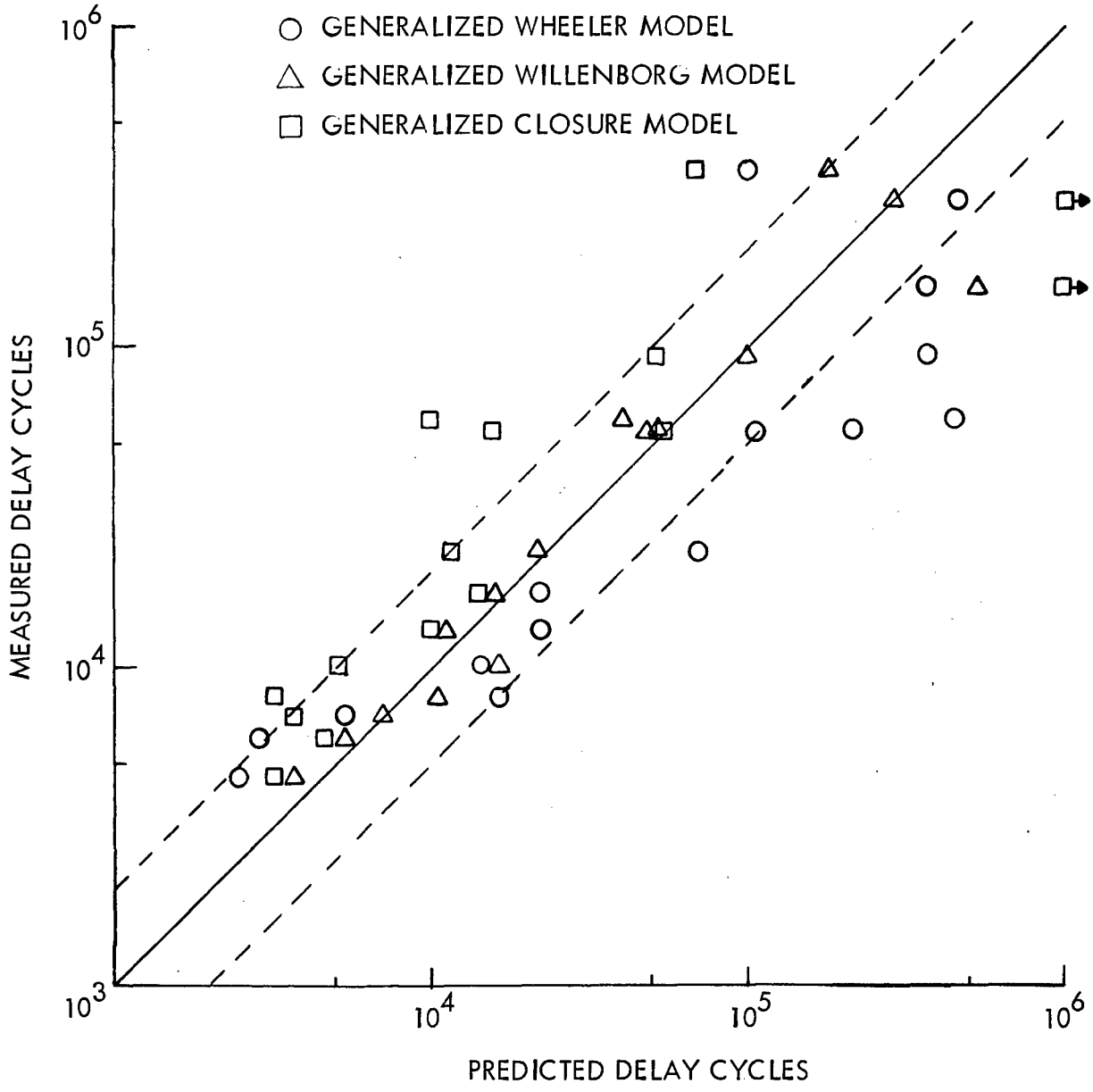

Figure 86 . Correlations of Predicted and Measured Delay Cycles Using the Hall Crack Growth Rate Equation and Various Retardation Models for 2219-T851 Aluminum Alloy Plates Subjected to Compression-Tension Overloads

TABLE I

BASIC PROGRAM, $K_2 = 10$ KSI$\sqrt{\text{IN.}}$

OVERLOAD STRESS INTENSITY RATIO, $S = \frac{K_1}{K_2}$	CONSTANT AMPLITUDE STRESS INTENSITY RATIO, $R=K_3/K_2$		LOAD CLASSIFICATION				
	R	$\Delta K = K_2-K_3$ (KSI $\sqrt{\text{IN.}}$)	TENSION-TENSION $U = \frac{K_1}{K_4}$	TENSION-ZERO $U^{-1} = \frac{K_4}{K_1}$	ZERO-TENSION $U^{-1} = \frac{K_4}{K_1}$	TENSION-COMPRESSION $U_c = \frac{K_1}{K_5}$	COMPRESSION-TENSION $U_c = \frac{K_1}{K_5}$
	0.1	9				-0.67	
1.0	0.3	7	6.67	0			
	0.5	5	4.0	0		-0.67	
	0.1	9	15.0	0		-2.0, -1.0	-1.0
1.5	0.3	7	10.0, 5.0	0	0	-2.0, -1.0	-1.0
	0.5	5	6.0, 3.0	0	0	-2.0, -1.0	-1.0
	0.1	9	20.0	0		-2.67, -2.0, -1.0	-1.0
2.0	0.3	7	13.33, 6.67	0	0	-2.67, -2.0, -1.0	-1.0
	0.5	5	8.0, 4.0	0	0	-2.67, -2.0, -1.0	-1.0
2.4	0.5	5	4.8				
	0.1	9	25.0	0		-3.35, -2.0, -1.0	-1.0
2.5	0.3	7	16.67, 8.33	0	0	-3.33, -2.0, -1.0	-1.0
	0.5	5	10.0	0	0	-3.33, -2.0, -1.0	-1.0
2.6	0.5	5			0		
2.7	0.5	5	10.8				
2.8	0.3	7					-1.0
2.9	0.3	7	9.67				
	0.5	5		0			
	0.1	9	30.0	0		-4, -2.0, -1.0	-1.0
3.0	0.3	7	20.0	0	0	-4, -2.0, -1.0	
	0.5	5				-4, -2.0, -1.0	
3.1	0.3	7	20.67		0		
3.2	0.1	9	32.0	0			
	0.1	9				-2.0, -1.0	
3.5	0.3	7				-2.0, -1.0	
	0.5	5				-4.67, -2.0, -1.0	
3.6	0.3	7				-4.8	
3.7	0.1	9				-4.93	
	0.1	9				-2.0, -1.0	
4.0	0.3	7				-2.0, -1.0	
	0.5	5				-2.0, -1.0	

TABLE II

PROGRAM FOR $K_2 = 7.78$ KSI $\sqrt{\text{IN.}}$

OVERLOAD STRESS INTENSITY RATIO, $S = \frac{K_1}{K_2}$	CONSTANT AMPLITUDE STRESS INTENSITY RATIO, $R = K_3/K_2$		LOAD CLASSIFICATION			
	R	$\Delta K = K_2 - K_3$ (KSI $\sqrt{\text{IN.}}$)	TENSION-TENSION $U = \frac{K_1}{K_4}$	TENSION-ZERO $U^{-1} = \frac{K_4}{K_1}$	TENSION-COMPRESSION $U_c = \frac{K_1}{K_5}$	COMPRESSION-TENSION $U_c = \frac{K_1}{K_5}$
1.5	0.1	7	15.0	0	-2.0, -1.0	-1.0
2.0	0.1	7	20.0	0	-2.0, -1.0	-1.0
2.5	0.1	7	25.0	0	-2.0, -1.0	-1.0
3.0	0.1	7	30.0	0	-2.0, -1.0	-1.0
3.1	0.1	7				-1.0
3.4	0.1	7		0		
3.5	0.1	7			-2.0, -1.0	
4.0	0.1	7			-2.0, -1.0	
4.1	0.1	7			-2.0	
4.5	0.1	7			-1.0	
5.0	0.1	7			-1.0	

TABLE III

PROGRAM FOR K_2 = 14 KSI $\sqrt{IN.}$

OVERLOAD STRESS INTENSITY RATIO, $S = \frac{K_1}{K_2}$	CONSTANT AMPLITUDE STRESS INTENSITY RATIO, $R = K_3/K_2$		LOAD CLASSIFICATION			
	R	$\Delta K = K_2 - K_3$ (KSI $\sqrt{IN.}$)	TENSION-TENSION $U = \frac{K_1}{K_4}$	TENSION-ZERO $U^{-1} = \frac{K_4}{K_1}$	TENSION-COMPRESSION $U_c = \frac{K_1}{K_5}$	COMPRESSION-TENSION $U_c = \frac{K_1}{K_5}$
1.5	0.5	7	3.0	0	-2.0, -1.0	-1.0
2.0	0.5	7	4.0	0	-2.0, -1.0	-1.0
2.3	0.5	7	4.6			-1.0
2.5	0.5	7		0	-2.0, -1.0	
3.0	0.5	7		0	-2.0, -1.0	
3.5	0.5	7			-2.0, -1.0	
4.0	0.5	7			-1.0	

TABLE IV

PROGRAM FOR HOLD TIME EVALUATIONS

OVERLOAD STRESS INTENSITY RATIO	CONSTANT AMPLITUDE STRESS INTENSITY RATIO, $R=K_3/K_2$		LOAD CLASSIFICATION									
			TENSION-TENSION WITH HOLD AT K_1 $U = K_1/K_4$ AT TIME						TENSION-COMPRESSION WITH HOLD AT K_5 $U_c = K_1/K_5$ AT TIME			
$S = K_1/K_2$	R	K_2, $KSI\sqrt{In.}$	0	5 Sec.	0.25 Hr.	1.0 Hr.	4.0 Hr.	24.0 Hr.	0	0.25 Hr.	1.0 Hr.	24.0 Hr.
2.0	0.1	10	20	20	20	20		20	-0.8	-0.8	-0.8	-0.8
2.57	0.13	7.78	20		20	20	20	20				
2.0	0.5	10	4,20	4,20	4,20	4,20	4,20	4,20				
2.5	0.1	10	25		25	25	25	25	-1,-2	-1,-2	-1,-2	-1,-2
2.5	0.5	10							-1	-1	-1	-1
3.21	0.13	7.78							-1	-1	-1	-1

TABLE V

RETARDATION PARAMETER DATA FOR 2219-T851 ALUMINUM ALLOY PLATE IN ROOM TEMPERATURE DESICCATED AIR FOR TENSION-TENSION LOAD CLASS

K_2=10

Specimen No.	S	R	ΔK	U	K_1	K_2	K_3	K_4	N_D	a*, Inch
1-L-10	1.0	0.3	7	6.67	10	10	3	1.5	0	0
1-L-10	1.0	0.5	5	4	10	10	5	2.5	0	0
1-L-6	1.5	0.1	9	15	15	10	1	1	5500	0.017
1-L-18	1.5	0.3	7	10	15	10	3	1.5	5500	0.014
1-L-10	1.5	0.3	7	5	15	10	3	3	6500	0.016
1-L-2	1.5	0.5	5	6	15	10	5	2.5	12000	0.010
1-L-6	1.5	0.5	5	3	15	10	5	5	10000	0.006
3-L-13	2.0	0.1	9	20	20	10	1	1	16000	0.049
1-L-18	2.0	0.3	7	13.33	20	10	3	1.5	23000	0.035
1-L-10	2.0	0.3	7	6.67	20	10	3	3	23000	0.028
1-L-2	2.0	0.5	5	8	20	10	5	2.5	34000	0.014
1-L-6	2.0	0.5	5	4	20	10	5	5	58000	0.013
1-L-16	2.5	0.1	9	25	25	10	1	1	63000	0.087
1-L-2	2.5	0.3	7	16.67	25	10	3	1.5	100000	0.091
3-L-8	2.5	0.3	7	8.33	25	10	3	3	139000	0.059
5-L-6	2.9	0.3	7	9.67	29	10	3	3	(1)	
2-L-14	2.5	0.5	5	10	25	10	5	2.5	174000	0.024
4-L-4	2.4	0.5	5	4.8	24	10	5	5	(1)	
4-L-4	2.7	0.5	5	10.8	27	10	5	2.5	(1)	
4-L-8	3.0	0.1	9	30	30	10	1	1	255000	0.164 (2)
5-L-6	3.2	0.1	9	32	32	10	1	1	(1)	
1-L-13	3.0	0.3	7	20	30	10	3	1.5	668000	0.202 (2)
2-L-8	3.1	0.3	7	20.67	31	10	3	1.5	(1)	

(1) Overload shut-off ratio.

(2) Data for one crack tip.

TABLE VI

RETARDATION PARAMETER DATA FOR 2219-T851 ALUMINUM ALLOY PLATE IN ROOM TEMPERATURE DESICCATED AIR FOR TENSION-TENSION LOAD CLASS

K_2=14 and K_2=7.78

Specimen No.	S	R	ΔK	U	K_1	K_2	K_3	K_4	N_D	a*, Inch
6-L-20	1.5	0.5	7	3	21	14	7	7	8500	0.021
2-L-9	2.0	0.5	7	4	28	14	7	7	56000	0.033
3-L-10	2.3	0.5	7	4.6	32.2	14	7	7	(1)	
6-L-21	1.5	0.1	7	15	11.67	7.78	0.78	0.78	12000	0.015
5-L-20	2.0	0.1	7	20	15.56	7.78	0.78	0.78	26000	0.028
3-L-15	2.5	0.1	7	25	19.45	7.78	0.78	0.78	69000	0.039
3-L-10	3.0	0.1	7	30	23.34	7.78	0.78	0.78	(1)	

(1) Overload shut-off ratio.

TABLE VII

RETARDATION PARAMETER DATA FOR 2219-T851 ALUMINUM ALLOY PLATE IN ROOM TEMPERATURE DESICCATED AIR FOR TENSION-ZERO LOAD CLASS

K_2=10

Specimen No.	S	R	ΔK	I/U	K_1	K_2	K_3	K_4	N_D	a*, Inch
3-L-13	1.0	0.3	7	0	10	10	3	0	0	0
2-L-10	1.0	0.5	5	0	10	10	5	0	0	0
6-L-17	1.5	0.1	9	0	15	10	1	0	4500	0.015
3-L-13	1.5	0.3	7	0	15	10	3	0	5500	0.013
6-L-7	1.5	0.5	5	0	15	10	5	0	10000	0.009
6-L-7	2.0	0.1	9	0	20	10	1	0	16000	0.038
6-L-7	2.0	0.3	7	0	20	10	3	0	20000	0.031
6-L-7	2.0	0.5	5	0	20	10	5	0	36000	0.020
2-L-14	2.5	0.1	9	0	25	10	1	0	46000	0.046
3-L-19	2.5	0.3	7	0	25	10	3	0	81000	0.038
4-L-18	2.5	0.5	5	0	25	10	5	0	132000	0.034
3-L-4	3.0	0.3	7	0	30	10	3	0	(1)	
1-L-1	2.9	0.5	5	0	29	10	5	0	(1)	
2-L-16	3.0	0.1	9	0	30	10	1	0	172000	0.069 (2)
1-L-1	3.2	0.1	9	0	32	10	1	0	(1)	

(1) Overload shut-off ratio.
(2) Data for one crack tip.

TABLE VIII

RETARDATION PARAMETER DATA FOR 2219-T851 ALUMINUM ALLOY PLATE IN ROOM TEMPERATURE DESICCATED AIR FOR TENSION-ZERO LOAD CLASS

K_2=14 and K_2=7.78

Specimen No.	S	R	ΔK	I/U	K_1	K_2	K_3	K_4	N_D	a*, Inch
6-L-20	1.5	0.5	7	0	21	14	7	0	3800	0.012
2-L-9	2.0	0.5	7	0	28	14	7	0	22000	0.046
5-L-3	2.5	0.5	7	0	35	14	7	0	127000	0.055 (1)
5-L-10	3.0	0.5	7	0	42	14	7	0	(2)	
5-L-20	1.5	0.1	7	0	11.67	7.78	0.78	0	8000	0.012
5-L-20	2.0	0.1	7	0	15.56	7.78	0.78	0	22000	0.022
5-L-20	2.5	0.1	7	0	19.45	7.78	0.78	0	60000	0.022
6-L-10	3.0	0.1	7	0	23.34	7.78	0.78	0	155000	0.030 (1)
5-L-3	3.4	0.1	7	0	26.45	7.78	0.78	0	(2)	

(1) Data for one crack tip.
(2) Overload shut-off ratio.

TABLE IX

RETARDATION PARAMETER DATA FOR 2219-T851 ALUMINUM ALLOY PLATE IN ROOM TEMPERATURE DESICCATED AIR FOR ZERO-TENSION LOAD CLASS

K_2=10

Specimen No.	S	R	ΔK	I/U	K_1	K_2	K_3	K_4	N_D	a*, Inch	
2-L-10	1.5	0.3	7	0	15	10	3	0	7500	0.018	
2-L-10	1.5	0.5	5	0	15	10	5	0	10000	0.006	
2-L-10	2.0	0.3	7	0	20	10	3	0	24000	0.027	
2-L-10	2.0	0.5	5	0	20	10	5	0	63000	0.022	
1-L-20	2.5	0.3	7	0	25	10	3	0	92000	0.047	
2-L-8	2.5	0.5	5	0	25	10	5	0	247000	0.032	(1)
1-L-1	2.6	0.5	5	0	26	10	5	0	(2)		
1-L-20	3.0	0.3	7	0	30	10	3	0	494000	0.044	
3-L-7	3.1	0.3	7	0	31	10	3	0	(2)		

(1) Average of two runs, one run shut-off.
(2) Overload shut-off ratio.

TABLE X

RETARDATION PARAMETER DATA FOR 2219-T851 ALUMINUM ALLOY PLATE IN ROOM TEMPERATURE DESICCATED AIR FOR COMPRESSION-TENSION LOAD CLASS

K_2=10

Specimen No.	S	R	ΔK	U_c	K_1	K_2	K_3	K_5	N_D	a*, Inch
5-L-17	1.5	0.1	9	-1.0	15	10	1.	-15	4500	0.018
5-L-10	1.5	0.3	7	-1.0	15	10	3	-15	7500	0.019
5-L-17	1.5	0.5	5	-1.0	15	10	5	-15	10000	0.007
5-L-14	2.0	0.1	9	-1.0	20	10	1	-20	14000	0.042
5-L-10	2.0	0.3	7	-1.0	20	10	3	-20	22000	0.023
5-L-17	2.0	0.5	5	-1.0	20	10	5	-20	56000	0.014
3-L-18	2.5	0.1	9	-1.0	25	10	1	-25	48000	0.069
5-L-10	2.5	0.3	7	-1.0	25	10	3	-25	91000	0.020
5-L-12	2.5	0.5	5	-1.0	25	10	5	-25	(1)	
3-L-16	3.0	0.1	9	-1.0	30	10	1	-30	281000	0.061
5-L-2	2.8	0.3	7	-1.0	28	10	3	-28	(1)	
2-L-4	3.2	0.1	9	-1.0	32	10	1	-32	(1)	

(1) Overload shut-off ratio.

TABLE XI

RETARDATION PARAMETER DATA FOR 2219-T851 ALUMINUM ALLOY PLATE IN ROOM TEMPERATURE DESICCATED AIR FOR COMPRESSION-TENSION LOAD CLASS

K_2=14 and K_2=7.78

Specimen No.	S	R	ΔK	U_c	K_1	K_2	K_3	K_5	N_D	a*, Inch
6-L-20	1.5	0.5	7	-1	21	14	7	-21	8500	0.018
3-L-14	2.0	0.5	7	-1	28	14	7	-28	60000	0.032
1-L-1	2.3	0.5	7	-1	32.2	14	7	-32.2	(1)	
6-L-21	1.5	0.1	7	-1	11.67	7.78	0.78	-11.67	6000	0.009
5-L-20	2.0	0.1	7	-1	15.56	7.78	0.78	-15.56	18000	0.013
3-L-15	2.5	0.1	7	-1	19.45	7.78	0.78	-19.45	55000	0.028
1-L-21	3.0	0.1	7	-1	23.34	7.78	0.78	-23.34	152000	0.043
4-L-21	3.1	0.1	7	-1	24.12	7.78	0.78	-24.12	(1)	

(1) Overload shut-off ratio.

TABLE XII

RETARDATION PARAMETER DATA FOR 2219-T851 ALUMINUM ALLOY PLATE IN ROOM TEMPERATURE DESICCATED AIR FOR TENSION-COMPRESSION LOAD CLASS

K_2=10

Specimen No.	S	R	ΔK	U_c	K_1	K_2	K_3	K_5	N_D	a*, Inch
2-L-7	1.0	0.1	9	-.67	10	10	1	-15	0	0
2-L-7	1.0	0.5	5	-.67	10	10	5	-15	0	0
4-L-14	1.5	0.1	9	-1.0	15	10	1	-15	4500	0.017
4-L-14	1.5	0.1	9	-2.0	15	10	1	-7.5	4500	0.016
6-L-3	1.5	0.3	7	-1.0	15	10	3	-15	5500	0.015
6-L-3	1.5	0.3	7	-2.0	15	10	3	-7.5	6500	0.017
2-L-12	1.5	0.5	5	-1.0	15	10	5	-15	6000	0.007
5-L-2	1.5	0.5	5	-2.0	15	10	5	-7.5	6000	0.007
2-L-7	2.0	0.1	9	-1.0	20	10	1	-20	14000	0.048
2-L-7	2.0	0.1	9	-2.0	20	10	1	-10	16000	0.050
3-L-3	2.0	0.3	7	-1.0	20	10	3	-20	12000	0.029
5-L-17	2.0	0.3	7	-2.0	20	10	3	-10	14000	0.026
1-L-19	2.0	0.5	5	-1.0	20	10	5	-20	12000	0.012
3-L-18	2.0	0.5	5	-2.0	20	10	5	-10	16000	0.013
4-L-14	2.5	0.1	9	-1.0	25	10	1	-25	26000	0.051
6-L-13	2.5	0.1	9	-2.0	25	10	1	-12.5	29000	0.056
1-L-19	2.5	0.3	7	-1.0	25	10	3	-25	28000	0.057
6-L-12	2.5	0.3	7	-2.0	25	10	3	-12.5	26000	0.050
1-L-19	2.5	0.5	5	-1.0	25	10	5	-25	24000	0.015
6-L-12	2.5	0.5	5	-2.0	25	10	5	-12.5	37000	0.023
4-L-11	3.0	0.1	9	-1.0	30	10	1	-30	51000	0.103
2-L-12	3.0	0.1	9	-2.0	30	10	1	-15	83000	0.091
4-L-11	3.0	0.3	7	-1.0	30	10	3	-30	66000	0.077
5-L-7	3.0	0.3	7	-2.0	30	10	3	-15	88000	0.090
5-L-7	3.0	0.5	5	-1.0	30	10	5	-30	60000	0.041
5-L-14	3.0	0.5	5	-2.0	30	10	5	-15	111000	0.043
3-L-7	3.5	0.1	9	-1.0	35	10	1	-35	116000	0.174
3-L-7	3.5	0.1	9	-2.0	35	10	1	-17.5	251000	0.127 (1)
6-L-15	3.5	0.3	7	-1.0	35	10	3	-35	111000	0.169
2-L-3	3.5	0.3	7	-2.0	35	10	3	-17.5	272000	0.211 (1)
6-L-15	3.5	0.5	5	-1.0	35	10	5	-35	147000	0.096 (1)
2-L-3	3.5	0.5	5	-2.0	35	10	5	-17.5	635000	0.261
2-L-17	4.0	0.1	9	-1.0	40	10	1	-40	95000	0.206
1-L-5	4.0	0.1	9	-2.0	40	10	1	-20	187000	0.321
5-L-21	4.0	0.3	7	-1.0	40	10	3	-40	165000	0.224 (1)
5-L-21	4.0	0.3	7	-2.0	40	10	3	-20	707000	0.319 (1)
5-L-21	4.0	0.5	5	-1.0	40	10	5	-40	326000	0.240
2-L-6	4.0	0.5	5	-2.0	40	10	5	-20	1430000	0.303 (1)

(1) Data for one crack tip.

TABLE XIII

RETARDATION PARAMETER DATA FOR 2219-T851 ALUMINUM ALLOY PLATE IN ROOM TEMPERATURE DESICCATED AIR FOR TENSION-COMPRESSION LOAD CLASS

K_2=14 and K_2=7.78

Specimen No.	S	R	ΔK	U_c	K_1	K_2	K_3	K_5	N_D	a*, Inch
6-L-20	1.5	0.5	7	-1	21	14	7	-21	8500	0.032
6-L-20	1.5	0.5	7	-2	21	14	7	-10.5	7500	0.027
3-L-14	2.0	0.5	7	-1	28	14	7	-28	6500	0.018
2-L-9	2.0	0.5	7	-2	28	14	7	-14	14000	0.034
3-L-14	2.5	0.5	7	-1	35	14	7	-35	28000	0.063
3-L-17	2.5	0.5	7	-2	35	14	7	-17.5	45000	0.092
6-L-1	3.0	0.5	7	-1	42	14	7	-42	50000	0.110
5-L-3	3.0	0.5	7	-2	42	14	7	-21	151000	0.180 (1)
6-L-1	3.5	0.5	7	-1	49	14	7	-49	246000	0.533 (1)
1-L-5	3.5	0.5	7	-2	49	14	7	-24.5	276000	0.490
2-L-17	4.0	0.5	7	-1	56	14	7	-56	316000	0.703
6-L-21	1.5	0.1	7	-1	11.67	7.78	0.78	-11.67	8000	0.012
6-L-21	1.5	0.1	7	-2	11.67	7.78	0.78	-5.84	9000	0.012
5-L-20	2.0	0.1	7	-1	15.56	7.78	0.78	-15.56	14000	0.016
5-L-20	2.0	0.1	7	-2	15.56	7.78	0.78	-7.78	16000	0.015
3-L-15	2.5	0.1	7	-1	19.45	7.78	0.78	-19.45	36000	0.034
3-L-15	2.5	0.1	7	-2	19.45	7.78	0.78	-9.72	40000	0.024
2-L-19	3.0	0.1	7	-1	23.34	7.78	0.78	-23.34	42000	0.049
4-L-21	3.0	0.1	7	-2	23.34	7.78	0.78	-11.67	92000	0.047
2-L-19	3.5	0.1	7	-1	27.23	7.78	0.78	-27.23	102000	0.037
2-L-16	3.5	0.1	7	-2	27.23	7.78	0.78	-13.62	172000	0.108 (1)
2-L-19	4.0	0.1	7	-1	31.12	7.78	0.78	-31.12	266000	0.061 (1)
6-L-1	4.0	0.1	7	-2	31.12	7.78	0.78	-15.56	246000	0.109 (1)
6-L-1	4.5	0.1	7	-1	35.01	7.78	0.78	-35.01	452000	0.107 (1)
4-L-7	4.1	0.1	7	-2	31.90	7.78	0.78	-15.95	(2)	
4-L-7	5.0	0.1	7	-1	38.90	7.78	0.78	-38.90	(2)	

(1) Data for one crack tip.
(2) Overload shut-off ratio.

TABLE XIV

RETARDATION PARAMETER DATA FOR 2219-T851 ALUMINUM ALLOY PLATE IN ROOM TEMPERATURE DESICCATED AIR FOR TENSION-COMPRESSION LOAD CLASS

K_2=10 and K_5= -7.5

Specimen No.	S	R	ΔK	U_c	K_1	K_2	K_3	K_5	N_D	a*, Inch
4-L-14	1.5	0.1	9	-2	15	10	1	-7.5	4500	0.016 (1)
6-L-3	1.5	0.3	7	-2	15	10	3	-7.5	6500	0.017 (1)
5-L-2	1.5	0.5	5	-2	15	10	5	-7.5	6000	0.007 (1)
6-L-18	2.0	0.1	9	-2.67	20	10	1	-7.5	14000	0.043
6-L-18	2.0	0.3	7	-2.67	20	10	3	-7.5	20000	0.043
6-L-18	2.0	0.5	5	-2.67	20	10	5	-7.5	28000	0.020
6-L-6	2.5	0.1	9	-3.33	25	10	1	-7.5	36000	0.066
6-L-6	2.5	0.3	7	-3.33	25	10	3	-7.5	42000	0.054
2-L-2	2.5	0.5	5	-3.33	25	10	5	-7.5	68000	0.047
2-L-2	3.0	0.1	9	-4	30	10	1	-7.5	92000	0.091
6-L-16	3.0	0.3	7	-4	30	10	3	-7.5	142000	0.125
4-L-8	3.0	0.5	5	-4	30	10	5	-7.5	171000	0.090
4-L-1	3.7	0.1	9	-4.93	37	10	1	-7.5	(2)	
3-L-5	3.6	0.3	7	-4.8	36	10	3	-7.5	(2)	
3-L-5	3.5	0.5	5	-4.67	35	10	5	-7.5	(2)	

(1) Data from basic program.
(2) Overload shut-off ratio.

TABLE XV

RETARDATION PARAMETER DATA FOR 2219-T851 ALUMINUM ALLOY PLATE IN ROOM TEMPERATURE DESICCATED AIR FOR TENSION-TENSION LOAD CLASS

HOLD TIME EFFECTS

Specimen No.	S	R	ΔK	U	K_1	K_2	K_3	K_4	Time K_1, Hours	N_D	a*, Inch
6-L-14	2.0	0.1	9	20	20	10	1	1	0	16000	0.042
6-L-14	2.0	0.1	9	20	20	10	1	1	0.0014	16000	0.033
6-L-14	2.0	0.1	9	20	20	10	1	1	0.25	22000	0.042
6-L-14	2.0	0.1	9	20	20	10	1	1	1.0	22000	0.035
5-L-11	2.0	0.1	9	20	20	10	1	1	24	28000	0.038
6-L-14	2.5	0.1	0	25	25	10	1	1	0	43000	0.043
6-L-14	2.5	0.1	9	25	25	10	1	1	0.25	70000	0.044
6-L-14	2.5	0.1	9	25	25	10	1	1	1.0	89000	0.029
6-L-14	2.5	0.1	9	25	25	10	1	1	4.0	102000	0.048 (1)
2-L-6	2.5	0.1	9	25	25	10	1	1	24	127000	0.032
2-L-4	2.57	0.13	6.78	20	25.7	7.78	1	1	0	72000	0.027
2-L-4	2.57	0.13	6.78	20	25.7	7.78	1	1	0.25	102000	0.017 (1)
2-L-4	2.57	0.13	6.78	20	25.7	7.78	1	1	1.0	106000	0.018 (1)
2-L-4	2.57	0.13	6.78	20	25.7	7.78	1	1	4.0	138000	0.015 (1)
2-L-4	2.57	0.13	6.78	20	25.7	7.78	1	1	24	178000	0.019 (1)
5-L-11	2.0	0.5	5	20	20	10	5	1	0	24000	0.014
5-L-11	2.0	0.5	5	20	20	10	5	1	0.25	48000	0.017
5-L-11	2.0	0.5	5	20	20	10	5	1	1.0	42000	0.021
5-L-11	2.0	0.5	5	20	20	10	5	1	4.0	52000	0.018
5-L-11	2.0	0.5	5	20	20	10	5	1	24	68000	0.022
3-L-16	2.0	0.5	5	4	20	10	5	5	0	48000	0.016
3-L-16	2.0	0.5	5	4	20	10	5	5	0.25	87000	0.010
3-L-16	2.0	0.5	5	4	20	10	5	5	1.0	103000	0.017
3-L-16	2.0	0.5	5	4	20	10	5	5	4.0	139000	0.029
5-L-11	2.0	0.5	5	4	20	10	5	5	24	568000	0.012 (1)

(1) Data for one crack tip.

TABLE XVI

RETARDATION PARAMETER DATA FOR 2219-T851 ALUMINUM ALLOY PLATE IN ROOM TEMPERATURE DESICCATED AIR FOR TENSION-COMPRESSION LOAD CLASS

HOLD TIME EFFECTS

Specimen No.	S	R	ΔK	U_c	K_1	K_2	K_3	K_5	Time @ $K_{5'}$ Hours	N_D	a*, Inch
4-L-1	2.0	0.1	9	-0.8	20	10	1	-25	0	8500	0.029
4-L-1	2.0	0.1	9	-0.8	20	10	1	-25	0.25	6500	0.024
4-L-1	2.0	0.1	9	-0.8	20	10	1	-25	1.0	7500	0.029
4-L-1	2.0	0.1	9	-0.8	20	10	1	-25	24	8500	0.036
4-L-14	2.5	0.1	9	-1.0	25	10	1	-25	0	26000	0.051 (1)
5-L-11	2.5	0.1	9	-1.0	25	10	1	-25	0.25	14000	0.041
5-L-11	2.5	0.1	9	-1.0	25	10	1	-25	1.0	14000	0.040
5-L-11	2.5	0.1	9	-1.0	25	10	1	-25	24	12000	0.038
2-L-6	3.21	0.13	6.78	-1.0	25	7.78	1	-25	0	52000	0.024
2-L-6	3.21	0.13	6.78	-1.0	25	7.78	1	-25	0.25	45000	0.042
2-L-6	3.21	0.13	6.78	-1.0	25	7.78	1	-25	1.0	40000	0.042
2-L-6	3.21	0.13	6.78	-1.0	25	7.78	1	-25	24	54000	0.057
1-L-19	2.5	0.5	5	-1.0	25	10	5	-25	0	24000	0.015 (1)
4-L-1	2.5	0.5	5	-1.0	25	10	5	-25	0.25	24000	0.016
4-L-1	2.5	0.5	5	-1.0	25	10	5	-25	1.0	24000	0.016
4-L-1	2.5	0.5	5	-1.0	25	10	5	-25	24	24000	0.026
6-L-13	2.5	0.1	9	-2.0	25	10	1	-12.5	0	29000	0.056 (1)
1-L-9	2.5	0.1	9	-2.0	25	10	1	-12.5	0.25	24000	0.050
1-L-9	2.5	0.1	9	-2.0	25	10	1	-12.5	1.0	22000	0.053
1-L-9	2.5	0.1	9	-2.0	25	10	1	-12.5	24	20000	0.060

(1) Data from basic program.

TABLE XVII

PREDICTED DELAY CYCLES USING DIFFERENT NUMERICAL INTEGRATION STEPS FOR K_1=15, K_2=10, K_3=1 AND K_4=1 KSI $\sqrt{IN.}$

NUMBER OF INTEGRATION STEPS	PREDICTED DELAY CYCLES		
	G. WHEELER	G. WILLENBORG	G. CLOSURE
25	7405	2391	4895
50	7411	2391	4895
100	7413	2391	4896
250	7413	2391	4896

TABLE XVIII

MEASURED AND PREDICTED DELAY CYCLES USING VARIOUS RETARDATION MODELS FOR 2219-T851 ALUMINUM ALLOY PLATES SUBJECTED TO TENSION-TENSION OVERLOADS AND $K_2 = 10$ KSI$\sqrt{IN}$

SPECIMEN NO.	S	R	K_1	K_4	MEASURED N_D	PREDICTED N_D		
						G. WHEELER	G. WILLENBORG	CLOSURE
1-L-6	1.5	0.1	15	1	5500	2504	3774	4353
1-L-18	1.5	0.3	15	1.5	5500	5028	6986	5311
1-L-10	1.5	0.3	15	3	6500	5310	7039	6300
1-L-2	1.5	0.5	15	2.5	12000	13533	16071	7940
1-L-6	1.5	0.5	15	5	10000	15919	16459	12326
3-L-13	2.0	0.1	20	1	16000	22373	11101	20002
1-L-18	2.0	0.3	20	1.5	23000	49026	20029	25458
1-L-10	2.0	0.3	20	3.0	23000	54440	20473	37500
1-L-2	2.0	0.5	20	2.5	34000	156119	48540	42619
1-L-6	2.0	0.5	20	5	58000	213097	52633	155256
1-L-16	2.5	0.1	25	1	63000	118754	39151	∞
1-L-2	2.5	0.3	25	1.5	100000	279295	62684	∞
3-L-8	2.5	0.3	25	3	139000	323002	76321	∞
2-L-14	2.5	0.5	25	2.5	174000	1018536	180484	∞
4-L-8	3.0	0.1	30	1	255000	463096	293627	∞
1-L-13	3.0	0.3	30	1.5	668000	1154512	$>10^9$	∞

TABLE XIX

MEASURED AND PREDICTED DELAY CYCLES USING VARIOUS RETARDATION MODELS FOR 2219-T851 ALUMINUM ALLOY PLATES SUBJECTED TO TENSION-ZERO OVERLOADS AND $K_2 = 10$ KSI $\sqrt{IN}$

SPECIMEN NO.	S	R	K_1	K_2	K_4	MEASURED N_D	PREDICTED N_D		
							G. WHEELER	G. WILLENBORG	CLOSURE
6-L-20	1.5	0.5	21	14	7	8500	19099	10754	7793
2-L-9	2.0	0.5	28	14	7	56000	455033	40517	98153
6-L-21	1.5	0.1	11.67	0.78	0.78	12000	2888	5384	6208
5-L-20	2.0	0.1	15.56	0.78	0.78	26000	21175	15521	28536
3-L-15	2.5	0.1	19.45	0.78	0.78	69000	95628	50860	∞

TABLE XX

MEASURED AND PREDICTED DELAY CYCLES USING VARIOUS RETARDATION MODELS FOR 2219-T851 ALUMINUM ALLOY PLATES SUBJECTED TO TENSION-ZERO OVERLOADS AND $K_2 = 10\ KSI\sqrt{IN}$

SPECIMEN NO.	S	R	K_1	MEASURED N_D	PREDICTED N_D		
					G. WHEELER	G. WILLENBORG	CLOSURE
6-L-17	1.5	0.1	15	4500	2504	3774	4047
3-L-13	1.5	0.3	15	5500	4786	6939	4731
6-L-7	1.5	0.5	15	10000	11906	15783	6384
6-L-7	2.0	0.1	20	16000	22373	11101	17173
6-L-7	2.0	0.3	20	20000	44587	19650	19935
6-L-7	2.0	0.5	20	36000	122074	45909	26545
2-L-14	2.5	0.1	25	46000	118754	39151	$>10^7$
3-L-19	2.5	0.3	25	81000	244790	54098	$>10^7$
4-L-18	2.5	0.5	25	132000	724290	115302	$>10^7$
2-L-16	3.0	0.1	30	172000	463096	293627	∞

TABLE XXI

MEASURED AND PREDICTED DELAY CYCLES USING VARIOUS RETARDATION MODELS FOR 2219-T851 ALUMINUM ALLOY PLATES SUBJECTED TO TENSION-ZERO OVERLOADS AND K_2 = 14 AND 7.78 KSI$\sqrt{IN}$

SPECIMEN NO.	S	R	K_1	K_2	MEASURED N_D	PREDICTED N_D		
						G. WHEELER	G. WILLENBORG	CLOSURE
6-L-20	1.5	0.5	21	14	3800	10365	9978	4036
2-L-9	2.0	0.5	28	14	22000	142523	29024	16782
5-L-10	2.5	0.5	35	14	127000	1070120	78013	$>10^7$
5-L-20	1.5	0.1	11.67	7.78	8000	2790	5355	5771
5-L-20	2.0	0.1	15.56	7.78	22000	19804	15094	24487
5-L-20	2.5	0.1	19.45	7.78	60000	87090	45510	∞
6-L-10	3.0	0.1	23.34	7.78	155000	290671	226127	∞

TABLE XXII

MEASURED AND PREDICTED DELAY CYCLES USING VARIOUS RETARDATION MODELS FOR 2219-T851 ALUMINUM ALLOY PLATES SUBJECTED TO TENSION-COMPRESSION OVERLOADS AND $K_2 = 10$ KSI$\sqrt{IN}$

SPECIMEN NO.	S	R	K_1	K_5	MEASURED N_D	PREDICTED N_D		
						G. WHEELER	G. WILLENBORG	CLOSURE
4-L-14	1.5	0.1	15	-15	4500	1944	3653	3243
4-L-14	1.5	0.1	15	- 7.5	4500	2101	3689	3287
6-L-3	1.5	0.3	15	-15	5500	3553	6678	3798
6-L-3	1.5	0.3	15	- 7.5	6500	3957	6768	3848
2-L-12	1.5	0.5	15	-15	6000	8163	15018	5144
5-L-2	1.5	0.5	15	- 7.5	6000	9162	15239	5211
2-L-7	2.0	0.1	20	-20	14000	12123	9523	10028
2-L-7	2.0	0.1	20	-10	16000	15121	9863	10321
3-L-3	2.0	0.3	20	-20	12000	22160	17408	11689
5-L-17	2.0	0.3	20	-10	14000	29160	18189	12027
1-L-19	2.0	0.5	20	-20	12000	49691	39034	15691
3-L-18	2.0	0.5	20	-10	16000	69259	41186	16138
4-L-14	2.5	0.1	25	-25	26000	45707	18787	45694
6-L-13	2.5	0.1	25	-12.5	29000	64150	22486	49933
1-L-19	2.5	0.3	25	-25	28000	83546	33406	52861
6-L-12	2.5	0.3	25	-12.5	26000	117258	35885	57735
1-L-19	2.5	0.5	25	-25	24000	187341	74908	69893
6-L-12	2.5	0.5	25	-12.5	37000	281955	81784	76255
4-L-11	3.0	0.1	30	-30	51000	134545	38508	∞
2-L-12	3.0	0.1	30	-15	83000	199807	57163	∞
4-L-11	3.0	0.3	30	-30	66000	245931	57083	∞
5-L-7	3.0	0.3	30	-15	88000	365223	71401	∞
5-L-7	3.0	0.5	30	-30	60000	551468	127857	∞
5-L-14	3.0	0.5	30	-15	111000	818965	143713	∞
3-L-7	3.5	0.1	35	-35	116000	307775	78760	∞
3-L-7	3.5	0.1	35	-17.5	251000	464547	147444	∞
6-L-15	3.5	0.3	35	-35	111000	562575	98894	∞
2-L-3	3.5	0.3	35	-17.5	272000	849134	163074	∞
6-L-15	3.5	0.5	35	-35	147000	1261501	201558	∞
2-L-3	3.5	0.5	35	-17.5	635000	2068882	269037	∞
2-L-17	4.0	0.1	40	-40	95000	609146	166295	∞
1-L-5	4.0	0.1	40	-20	187000	1003666	579266	∞
5-L-21	4.0	0.3	40	-40	165000	1113443	188042	∞
5-L-21	4.0	0.3	40	-20	707000	1834576	595616	∞
5-L-21	4.0	0.5	40	-40	326000	2496750	307985	∞
2-L-6	4.0	0.5	40	-20	1430000	4113799	684155	∞

TABLE XXIII

MEASURED AND PREDICTED DELAY CYCLES USING VARIOUS RETARDATION MODELS FOR 2219-T851 ALUMINUM ALLOY PLATES SUBJECTED TO TENSION-COMPRESSION OVERLOADS AND K_2 = 14 AND 7.78 KSI$\sqrt{IN}$

SPECIMEN NO.	S	R	K_1	K_5	K_2	MEASURED N_D	PREDICTED N_D		
							G. WHEELER	G. WILLENBORG	CLOSURE
6-L-20	1.5	0.5	21	-21	14	8500	5894	9393	3252
6-L-20	1.5	0.5	21	-10.5	14	7500	6999	9559	3295
3-L-14	2.0	0.5	28	-28	14	6500	42472	24296	9920
2-L-9	2.0	0.5	28	-14	14	14000	59220	25349	10202
3-L-14	2.5	0.5	35	-35	14	28000	180026	46188	44186
3-L-17	2.5	0.5	35	-17.5	14	45000	316959	50872	48209
6-L-1	3.0	0.5	42	-42	14	50000	523362	76099	∞
5-L-3	3.0	0.5	42	-21	14	151000	873423	84967	∞
6-L-1	3.5	0.5	49	-49	14	246000	1362948	118938	∞
1-L-5	3.5	0.5	49	-24.5	14	276000	2207104	137702	∞
2-L-17	4.0	0.5	56	-56	14	316000	3061702	179767	∞
6-L-21	1.5	0.1	11.67	-11.67	7.78	8000	2380	5228	∞
6-L-21	1.5	0.1	11.67	- 5.84	7.78	9000	2554	5283	4686
5-L-20	2.0	0.1	15.56	-15.56	7.78	14000	13491	13756	14299
5-L-20	2.0	0.1	15.56	- 7.78	7.78	16000	15903	14197	14716
3-L-15	2.5	0.1	19.45	-19.45	7.78	36000	46263	27419	65156
3-L-15	2.5	0.1	19.45	- 9.72	7.78	40000	60134	32219	71213
2-L-19	3.0	0.1	23.34	-23.34	7.78	42000	125822	57243	∞
4-L-21	3.0	0.1	23.34	-11.67	7.78	92000	170805	81697	∞
2-L-19	3.5	0.1	27.23	-27.23	7.78	102000	286048	129864	∞
2-L-16	3.5	0.1	27.23	-13.62	7.78	172000	400119	249844	∞
2-L-19	4.0	0.1	31.12	-31.12	7.78	266000	537750	292947	∞
6-L-1	4.0	0.1	31.12	-15.56	7.78	246000	815540	1357031	∞
6-L-1	4.5	0.1	35.01	-35.01	7.78	452000	970926	935252	∞

TABLE XXIV

MEASURED AND PREDICTED DELAY CYCLES USING VARIOUS RETARDATION MODELS FOR 2219-T851 ALUMINUM ALLOY PLATES SUBJECTED TO TENSION-COMPRESSION OVERLOADS AND $K_2 = 10$ AND $K_5 = -7.5$ KSI$\sqrt{\text{IN}}$

SPECIMEN NO.	S	R	K_1	K_5	MEASURED N_D	PREDICTED N_D		
						G. WHEELER	G. WILLENBORG	CLOSURE
4-L-14	1.5	0.1	15	-7.5	4500	2101	3689	3287
6-L-3	1.5	0.3	15	-7.5	6500	3957	6768	3848
5-L-2	1.5	0.5	15	-7.5	6000	9162	15239	5211
6-L-18	2.0	0.1	20	-7.5	14000	15953	9955	10759
6-L-18	2.0	0.3	20	-7.5	20000	30887	18367	12533
6-L-18	2.0	0.5	20	-7.5	28000	73687	41632	16806
6-L-6	2.5	0.1	25	-7.5	36000	74131	24920	66222
6-L-6	2.5	0.3	25	-7.5	42000	146827	38186	76452
2-L-2	2.5	0.5	25	-7.5	68000	358958	86906	100656
2-L-2	3.0	0.1	30	-7.5	92000	258989	81272	∞
6-L-16	3.0	0.3	30	-7.5	142000	522709	106991	∞
4-L-8	3.0	0.5	30	-7.5	171000	1304003	184621	∞

TABLE XXV

MEASURED AND PREDICTED DELAY CYCLES USING VARIOUS RETARDATION MODELS FOR 2219-T851 ALUMINUM ALLOY PLATES SUBJECTED TO ZERO-TENSION OVERLOADS AND $K_2 = 10\ KSI\sqrt{IN}$

SPECIMEN NO.	S	R	K_1	MEASURED N_D	PREDICTED N_D		
					G. WHEELER	G. WILLENBORG	CLOSURE
2-L-10	1.5	0.3	15	7500	4786	6939	4731
2-L-10	1.5	0.5	15	10000	14603	16249	6384
2-L-10	2.0	0.3	20	24000	44587	19650	19935
2-L-10	2.0	0.5	20	63000	180637	50334	26545
1-L-20	2.5	0.3	25	92000	244790	54098	$>10^7$
2-L-8	2.5	0.5	25	247000	1246335	301886	$>10^7$
1-L-20	3.0	0.3	30	494000	981532	536532	∞

TABLE XXVI

MEASURED AND PREDICTED DELAY CYCLES USING VARIOUS RETARDATION MODELS FOR 2219-T851 ALUMINUM ALLOY PLATES SUBJECTED TO COMPRESSION-TENSION OVERLOADS AND $K_2 = 10$ KSI $\sqrt{IN}$

SPECIMEN NO.	S	R	K_1	K_5	MEASURED N_D	PREDICTED N_D		
						G. WHEELER	G. WILLENBORG	CLOSURE
5-L-17	1.5	0.1	15	-15	4500	2504	5774	3243
5-L-10	1.5	0.3	15	-15	7500	5310	7039	3798
5-L-17	1.5	0.5	15	-15	10000	14603	16249	5144
5-L-14	2.0	0.1	20	-20	14000	22373	11101	10028
5-L-10	2.0	0.3	20	-20	22000	69622	21932	11689
5-L-17	2.0	0.5	20	-20	56000	213097	52633	15691
3-L-18	2.5	0.1	25	-25	48000	118754	39151	45694
5-L-10	2.5	0.3	25	-25	91000	379492	99946	52861
3-L-16	3.0	0.1	30	-30	281000	463096	293627	∞

TABLE XXVII

MEASURED AND PREDICTED DELAY CYCLES USING VARIOUS RETARDATION MODELS FOR 2219-T851 ALUMINUM ALLOY PLATES SUBJECTED TO COMPRESSION-TENSION OVERLOADS AND K_2 = 14 AND 7.78 KSI $\sqrt{IN}$

SPECIMEN NO.	S	R	ΔK	U_c	K_1	K_2	K_5	MEASURED N_D	PREDICTED N_D		
									G. WHEELER	G. WILLENBORG	CLOSURE
6-L-20	1.5	0.5	7	-1	21	14	-21	8500	16624	10563	3252
3-L-14	2.0	0.5	7	-1	28	14	-28	60000	455033	40517	9920
6-L-21	1.5	0.1	7	-1	11.67	7.78	-11.67	6000	2888	5384	4625
5-L-20	2.0	0.1	7	-1	15.56	7.78	-15.56	18000	22783	16076	14299
3-L-15	2.5	0.1	7	-1	19.45	7.78	-19.45	55000	105914	58171	65156
1-L-21	3.0	0.1	7	-1	23.34	7.78	-23.34	152000	370153	535835	∞

REFERENCES

1) Bell, P. D., and Creager, M., "Crack Growth Analysis for Arbitrary Spectrum Loading", Air Force Flight Dynamics Report AFFDL-TR-74-129, October 1974.

2) Hsu, T. M., "Extended Flaw Growth at Fastener Holes", Third Quarterly Progress Report on Contract F33615-76-C-3099, April 1976.

3) Probst, E. P. and Hillberry, B. M., "Fatigue Crack Delay and Arrest Due to Peak Tensile Overloads", AIAA Paper No. 73-325, presented at AIAA Dynamics Specialists Conference, March 1973.

4) Hall, L. R., Shah, R. C., and Engstrom, W. L., "Fracture Crack Growth Behavior of Surface Flaws and Flaws Originating at Fastener Holes", Air Force Flight Dynamics Report, AFFDL-TR-74-47, May 1974.

5) Walker, K., "The Effect of Stress Ratio During Crack Propagation and Fatigue for 2024-T3 and 7075-T6 Aluminum", Effects of Environment and Complex History on Fatigue Life, ASTM STP 462, American Society for Testing and Materials, 1970.

6) Gray, T. D. and Gallagher, J. P., "Predicting Fatigue Crack Retardation Following a Single Overload Using a Modified Wheeler Model", presented at the 8th National Symposium on Fracture Mechanics, Brown University, Providence, R.I., 26-28 August 1974.

7) Gallagher, J. P. and Hughes, T. F., "Influence of Yield Strength on Overload Affected Fatigue Crack Growth Behavior in 4340 Steel", AFFDL-TR-74-27, July 1974.

8) Von Euw, E. F. J., Hertzberg, R. W. and Roberts, R., "Delay Effects in Fatigue Crack Propagation", Stress Analysis and Growth of Cracks, ASTM STP 513, 1972.

9) Gallagher, J. P., "A Generalized Development of Yield Zone Models", AFFDL-TM-74-28-FBR, January 1974.

APPENDIX A
RETARDATION MODEL FORMULATIONS

APPENDIX A

This appendix contains definition and discussion of the three retardation models used for predicting delay cycles for the cases evaluated experimentally. In order of discussion, the models were: 1) generalized Wheeler model, 2) generalized Willenborg model, and 3) Grumman closure model.

1. GENERALIZED WHEELER MODEL

The first retardation model was proposed by Wheeler (A1) who suggested the use of a reduction factor, C_p, on the steady-state (constant-amplitude) crack-growth rate to obtain the retarded crack-growth rate under spectrum loading as

$$\left(\frac{da}{dN}\right)_{sp} = C_p \left(\frac{da}{dN}\right)_{ss} \tag{A1}$$

and C_p is defined as

$$C_p = \begin{cases} \left(\frac{z_c}{z^*}\right)^m & \text{for } z_c < z^* \\ 1 & \text{for } z_c \geq z^* \end{cases} \tag{A2}$$

In Equation (A2), the quantity z_c, equivalent to R_y in the original Wheeler paper, is the extent of the current load interaction zone caused by the current maximum applied cyclic stress intensity factor, K_{max}. The quantity z*, which is equivalent to $a_p - a$ in Reference (A1), is the difference between the load interaction zone due to a previous overload, z_{OL}, and the current crack growth increment since that overload, Δa, or

$$z^* = z_{OL} - \Delta a \tag{A3}$$

z* is also the load interaction zone that would be necessary to have no retardation.

Wheeler assumed that the load interaction zone, z, was equal to the plastic zone radius created under plain-strain condition, i.e.

$$z = \frac{1}{4\sqrt{2\pi}} \left(\frac{K_{max}}{\sigma_{ys}}\right)^2 \tag{A4}$$

where σ_{ys} is the yield strength of the material.

For any given load interaction zone, z*, there always exists a K^*_{max} such that Equation (A4) is satisfied. By substituting Equation (A4) into Equation (A3) and rearranging the results, one obtains

$$K^*_{max} = K^{OL}_{max} \left[1 - \frac{\Delta a}{z_{OL}}\right]^{1/2} \tag{A5}$$

where K^{OL}_{max} is the maximum stress intensity factor generated by the overload.

The steady-state and spectrum crack-growth rates can be written in the following general forms:

$$\left(\frac{da}{dN}\right)_{ss} = c\left[f(\Delta K, R)\right]^n \tag{A6}$$

and

$$\left(\frac{da}{dN}\right)_{sp} = c\left[\Delta K_{eff}\right]^n \tag{A7}$$

respectively. In the above equations, c and n are constants for a given stress ratio, R, $f(\Delta K,R)$ is the controlling stress intensity function, and ΔK_{eff} is an effective stress intensity range under variable-amplitude loading. The function $f(\Delta K,R)$ has different forms, depending upon the growth rate equation used, e.g.,

$$f(\Delta K,R) = \Delta K \tag{A8}$$

if Paris' Equation (A2) is used;

$$f(\Delta K,R) = (K_{max} - K_{th}) \frac{m_H}{n_H \cdot \Delta K} \tag{A9}$$

if the Hall Equation (A3) is used;

$$f(\Delta K,R) = (1 + 0.6R)\Delta K \tag{A10}$$

if the Grumman Equation (A4) is used; and

$$f(\Delta K, R) = K_{max}\,(1-R)^{m} W \tag{A11}$$

if Walker's Equation (A5) is used.

Substitution of Equations (A2) through (A7) into Equation (A1) and after some simplification lead to

$$\Delta K_{eff} = \left[\frac{K_{max}}{K_{max}^{OL}\left(1 - \frac{\Delta a}{z_{OL}}\right)^{1/2}}\right]^{2m/n} f(\Delta K, R) \qquad \text{if } K^{*}_{max} > K_{max}$$
$$= f(\Delta K, R) \qquad \text{if } K^{*}_{max} \leqq K_{max} \tag{A12}$$

Experiments involving single overloads in 2024-T3 aluminum and Ti-6Aℓ-4V (A6) indicate that there is a particular value of overload ratio, say S_{so}, such that when $K_{max}^{OL}/K_{max} \geqq S_{so}$, crack arrest occurs. This particular value, S_{so}, is called the "overload shut-off ratio" and its corresponding overload is called the "shut-off overload."

By assuming that the shut-off overload level develops the local stress state such that the effective stress intensity range just equals the threshold stress intensity range, ΔK_{th}, the point below which no measurable fatigue crack growth occurs, then, from Equation (A12), one obtains

$$\Delta K_{th} = \left(\frac{1}{S_{so}}\right)^{2m/n} \cdot f(\Delta K, R) \tag{A13}$$

from which yields the exponent m as

$$m = \frac{n}{2}\left[\frac{\log\left\{\frac{\Delta K_{th}}{f(\Delta K, R)}\right\}}{\log\left(\frac{1}{S_{so}}\right)}\right] \qquad \text{or} \qquad m = \frac{n}{2}\left[\frac{\log\left\{\frac{f(\Delta K, R)}{\Delta K_{th}}\right\}}{\log S_{so}}\right] \tag{A14}$$

It is clear that the exponent m depends not only on the specific material being used, but also on the loading subsequent to the overload.

For any load cycle subsequent to the overload, having crack growth increment since the overload, Δa, one can calculate its effective stress intensity range, ΔK_{eff}, from Equations (A12) and (A14), and its corresponding crack growth rate from Equation (A7).

2. GENERALIZED WILLENBORG MODEL

Since the rate of propagation of a fatigue crack is controlled by the stress intensity factor at the crack tip, the magnitude of the stress intensity factor is a good indicative of the extent of crack tip deformation. Willenborg, Engle, and Wood (A7) then proposed a model using an "effective stress" concept to reduce the applied stress, and hence the crack tip stress intensity factor. To help identify the physical implications, Gallagher (A8) reformulated the Willenborg et al. model by using a residual stress intensity factor concept which suggests that the local or effective stress intensity factor, K_{eff}, be calculated from the equation

$$K_{eff} = K - K_R \tag{A15}$$

where K is the stress intensity factor associated with far-field applied load, and K_R is the residual stress intensity factor which has the following general form:

$$K_R = f(K^{OL}_{max}, K^{OL}_{min}, N_{OL}, K_{max}, R, \sigma_{ys}, N, \ldots) \tag{A16}$$

The undefined parameters in the above equation are

K^{OL}_{min} = minimum K generated by the overload

N_{OL} = number of overloads applied

N = number of cycles of K_{max}

The equivalent residual stress intensity factor for the Willenborg et al. model is

$$K^W_R = K^{OL}_{max}\left(1 - \frac{\Delta a}{z_{OL}}\right)^{1/2} - K_{max} = K^*_{max} - K_{max} \tag{A17}$$

where z_{OL} is the overload created load interaction zone, which is approximately equal to the overload plane stress plastic zone radius

$$z_{OL} \cong r_{y_{OL}} = \frac{1}{2\pi}\left(\frac{K^{OL}_{max}}{\sigma_{ys}}\right)^2 \tag{A18}$$

and Δa is an increment of crack growth into the overload load interaction zone since the application of overload. Following an overload, Δa is approximately zero and the residual stress intensity factor is maximum.

Equation (A17) has been found in error, since crack growths have been observed after single overload application where the overload ratio, which is defined as

$$S = \frac{K^{OL}_{max}}{K_{max}} \tag{A19}$$

is greater than or equal to 2.0, the condition for which the Willenborg et al. model predicts zero crack tip effective stress intensity factors. Gallagher and Hughes (A9) suggested that the actual residual stress intensity factor K_R may be proportional to the Willenborg et al. residual stress intensity factor, K^W_R, and introduced the factor ϕ such that

$$K_R = \phi K^W_R \tag{A20}$$

Using Equations (A17) and (A20), the effective maximum and minimum stress intensity factors can be written as

$$(K_{max})_{eff} \; K_{max} - \phi\left[K^{OL}_{max}\left(1 - \frac{\Delta a}{z_{OL}}\right)^{1/2} - K_{max}\right] \tag{A21}$$

and

$$(K_{min})_{eff} = K_{min} - \phi\left[K^{OL}_{max}\left(1 - \frac{\Delta a}{z_{OL}}\right)^{1/2} - K_{max}\right] \tag{A22}$$

$$\text{or } (K_{min})_{eff_{cf}}, \text{ whichever is larger,}$$

where $(K_{min})_{eff_{cf}}$ is the cut-off value of the minimum effective stress intensity factor. Normally, $(K_{min_{eff_{cf}}})$ is set equal to zero. When the overload ratio is greater than 3.0, it has been found that $(K_{min})_{eff_{cf}} = -0.3\,(K_{max})_{eff}$ will give a better prediction.

The effective stress intensity range and effective stress ratio are then calculated from the following equations:

$$(\Delta K)_{eff} = (K_{max})_{eff} - (K_{min})_{eff} \tag{A23}$$

and

$$R_{eff} = \frac{(K_{min})_{eff}}{(K_{max})_{eff}} \tag{A24}$$

By assuming that the shut-off overload level develops a local (effective) stress intensity factor condition such that no growth is induced, Gallagher et al. (A9) set the maximum local stress intensity factor, $(K_{max})_{eff}$, equal to the maximum fatigue threshold stress intensity factor, $(K_{max})_{TH}$, since $(K_{max})_{TH}$ is approximately constant for negative stress ratios. (A10) Immediately following the shut-off overload which produces no growth, $\Delta a = 0$ and $(K_{max})_{eff} = (K_{max})_{TH}$, and they solve Equation (A21) for ϕ subjected to these assumptions as

$$\phi = \frac{1 - (K_{max})_{TH}/K_{max}}{S_{so} - 1} \tag{A25}$$

For any load cycle subsequent to the overload, one can calculate its effective stress intensity range, ΔK_{eff}, from Equations (A21) through (A25), and its corresponding crack growth rate from any crack growth rate equation by setting $\Delta K = \Delta K_{eff}$ and $R = R_{eff}$.

3. GENERALIZED CLOSURE MODEL

In 1968, Elber (A11) observed that the surface of the fatigue crack closed during fatigue crack propagation tests under cyclic tension loading (tension-tension load cycle) on aluminum alloy sheet specimens. Based on results of tests, he suggested that the tip of a fatigue crack closes while specimens were still subjected to a tension loading, and that the fatigue crack propagates only during that portion of the load cycle in which it was fully open. Assuming that the crack closure stress is not different from the crack open stress, then according to Elber's hypothesis, the effective stress range, $\Delta\sigma_{eff}$, is equal to the difference between maximum stress, σ_{max}, and the closure stress, σ_c, i.e.,

$$\Delta\sigma_{eff} = \sigma_{max} - \sigma_c$$

or (A26)

$$\Delta\sigma_{eff} = \sigma_{max}\,(1 - C_f)$$

where C_f is the closure factor defined as

$$C_f = \frac{\sigma_c}{\sigma_{max}} \tag{A27}$$

The closure stress, σ_c, in general is a function of applied stress ratio, previous applied load history and any other pertinent parameters.

Bell, et al., (A4) uses the Elber crack-closure concept and modifies the Paris equation as

$$\frac{da}{dN} = c\left[\frac{\sigma_{max} - \sigma_c}{(1 - C_{f_o})}\sqrt{\pi a}\right]^n \tag{A28}$$

for the case of a through-crack in an infinite sheet. The coefficients c and n in Equation (A28) have the same values that would be determined by using the Paris equation to fit crack-growth rate data plotted against the actual applied stress intensity range. C_{f_o} is the closure factor at $R = 0$.

Equation (A28) can be modified for any other geometric configuration by introducing the total correction factor β_T to account for all the appropriate stress intensity magnification factors, as

$$\frac{da}{dN} = c\left[\frac{\sigma_{max} - \sigma_c}{(1 - C_{f_o})}\sqrt{\pi a \beta_T}\right]^n \tag{A29}$$

Equation (A29) can also be expressed in terms of stress intensity factors as

$$\frac{da}{dN} = c\left[\frac{K_{max} - K_c}{1 - C_{f_o}}\right]^n \tag{A30}$$

where K_c is the closure stress intensity factor.

Following a similar approach, the Hall and Walker crack growth rate equations may be written in the closure form as

$$\frac{da}{dN} = c_H (K_{max} - K_{th})^{m_H} \left[\frac{K_{max} - K_c}{1 - C_{f_o}}\right]^{n_H} \tag{A31}$$

and

$$\frac{da}{dN} = c_W \left[\frac{K_{max} - K_c}{1 - C_{f_o}}\right]^{n_W} \tag{A32}$$

respectively.

a. Closure Model for Constant Amplitude

The constant-amplitude crack growth rate equation for 2219-T851 aluminum was given as (A4)

$$\frac{da}{dN} = 1.96 \times 10^{-9} [(1 + 0.6R)\,\Delta K]^{3.34}, \text{ for } 0 \leq R \leq 0.5 \tag{A33}$$

by letting $c = 1.96 \times 10^{-9}$ and $n = 3.34$ in Equation (A30), and solving Equations (A30) and (A33) for the closure factor leads to

$$C_f = \frac{K_c}{K_{max}} = 1 - (1 - C_{f_o})(1 + 0.6R)(1 - R) \tag{A34}$$

However, based on the test data generated under various constant stress ratio ($-1 \leq R \leq 0.7$), the closure factor was later chosen as (A4)

$$C_f = C_{f_{-1}} + (C_{f_o} - C_{f_{-1}})(1 + R)^P \tag{A35}$$

For 2219-T851 aluminum, $C_{f_{-1}} = 0.347$, $C_{f_o} = 0.40$, and $P = 3.93$.

Equation (A35) was also proposed to account for the effects of negative stress ratios and compressive stresses.

For constant-amplitude load cycles, Equation (A35) is used to calculate the closure factor C_f. The corresponding closure stress and its crack growth rate are computed from

Equations (A27) and (A30), respectively, where in Equation (A30) $c = 1.96 \times 10^{-9}$, $n = 3.34$, and $C_{f_o} = 0.40$.

b. Closure Model for High-Low Loading Sequence Having Constant Minimum

Let σ_{c_1} and σ_{c_2} be the constant-amplitude closure stresses of high stress cycles, σ_1, and lower stress cycles, σ_2, respectively. Then, for a high-low loading sequence having a constant minimum stress level, the crack growth during the lower loading cycles will be retarded before it changes to the steady-state growth. During the retarded period, the closure model assumes that the closure stress, σ_c, varied according to the following equation:

$$\sigma_c = \sigma_{c_1} - (\sigma_{c_1} - \sigma_{c_2})\left(\frac{\Delta a}{z}\right)^B \quad \text{for } 0 \leq \Delta a \leq z \tag{A36}$$

where Δa is the crack growth since the stress change, z is the load interaction zone caused by σ_1, and B is an empirical exponent. A process of trial and error was used to obtain the values of the parameters for 2219-T851 aluminum as

$C_{f_o} = 0.4$

$z \cong$ plane stress plastic zone radius

$B \simeq 1.0$

c. Effect of Minimum Stress on Closure

If the minimum stress of applied load cycles decreases from one load level to the second load level, regardless of the maximum stresses, the closure model assumes that step-wise change in closure stress level occurs during the first load cycle after the load change. The closure factor immediately after the application of the new lower minimum stress, σ_{min_2}, is calculated as C'_f from Equation (A35) using $R = \sigma_{min_2}/\sigma_1$ and its corresponding closure stress is calculated from Equation (A27) as $\sigma'_{c_1} = \sigma_1 C'_f$. Starting from this value, the closure stress varies as described by Equation (A36). The same concept can be extended to the case where the minimum stress is negative, i.e. $\sigma_{min_2} < 0$. For the case where $R < -1$, the current closure model treats it the same as $R = -1$.

d. Increasing and Decreasing Closure Level

To use the closure model, it is necessary to define whether the closure level is increasing or decreasing during variable-amplitude loading. The current closure stress, which is defined in the value which existed prior to a load change, may be modified by overload or minimum stress consideration immediately after the application of the new loading. If the current closure stress is greater than the expected closure stress, which is defined as the stabilized value associated with the new loading, a decreassing closure situation exists, and the behavior of the closure stress is defined by Equation (A36).

Conversely, when the closure level is increasing, i.e. the current closure stress is less than the expected closure stress, say σ_{c_2}, then the closure stress is calculated from the following equation for 2219-T851 aluminum:

$$\sigma_c = \left[\frac{2}{3} + \frac{1}{3}\left(\frac{N_{OL} - 1}{12}\right)\right]\sigma_{c_2} \qquad \text{(A37)}$$

or 1 whichever is smaller

where N_{OL} is the number of consecutive overload cycles after a load change. According to Equation (A37), 13 cycles of the new loading are required to regain a stabilized closure value for 2219-T851 aluminum.

APPENDIX A - REFERENCES

(A1) Wheeler, O. E., "Spectrum Loading and Crack Growth," Transaction of the ASME, J. of Basic Engineering, March 1972, pp. 181-186.

(A2) Paris, P. and Erdogan, F., "A Critical Analysis of Crack Propagation Laws," Journal of Basic Engineering, December 1963, p. 528.

(A3) Hall, L. R., Shah, R. C., and Engstrom, W. L., "Fracture and Fatigue Crack Growth Behavior of Surface Flaws and Flaws Originating at Fastener Holes," Air Force Flight Dynamics Report, AFFDL-TR-74-47, May 1974.

(A4) Bell, P. D., and Creager, M., "Crack Growth Analysis for Arbitrary Spectrum Loading," Air Force Flight Dynamics Report AFFDL-TR-74-129, October 1974.

(A5) Walker, K., "The Effect of Stress Ratio During Crack Propagation and Fatigue for 2024-T3 and 7075-T6 Aluminum," Effects of Environment and Complex History on Fatigue Life, ASTM STP 462, American Society for Testing and Materials, 1970.

(A6) Wei, R. P., Shih, T. T. and Fitzgerald, J. H., "Load Interaction Effects on Fatigue Crack Growth in Ti-6Aℓ-4V Alloy," NASA CR-2239, April 1973.

(A7) Willenborg, J., Engle, R. M., and Wood, H. A., "A Crack Growth Retardation Model Using an Effective Stress Concept," AFFDL-TM-71-1-FER, January 1971.

(A8) Gallagher, J. P., "A Generalized Development of Yield Zone Models," AFFDL-TM-74-28 -FBR, January 1974.

(A9) Gallagher, J. P. and Hughes, T. F., "Influence of Yield Strength on Overload Affected Fatigue Crack Growth Behavior in 4340 Steel," AFFDL-TR-74-27, July 1974.

(A10) Pook, L. P., "Fatigue Crack Growth Data for Various Materials Deduced From the Fatigue Lives of Precracked Plate," Stress Analysis and Growth of Cracks, ASTM STP 513, 1972, p. 106.

(A11) Elber, W., "The Significance of Fatigue Crack Closure," Damage Tolerance in Aircraft Structures, ASTM STP 486, 1971, p. 230.

☆ U. S. GOVERNMENT PRINTING OFFICE: 1977 — 757-001/543